3-23-2021 2:00 PM

Cellulose biodegradability and its impact on enhanced biological phosphorus removal

Moustafa Ibrahim Elbahrawi, *The University of Western Ontario*

Supervisor: Dr. George Nakhla, *The University of Western Ontario*

A thesis submitted in partial fulfillment of the requirements for the Master of Science degree in Civil and Environmental Engineering

Abstract

Cellulose from toilet paper contributes approximately one third of the influent organic suspended solids (TSS) to wastewater treatment plants and is a key target for resources recovery. Cellulose recovery is beneficial as it reduces the required energy for treatment and biosolids treatment cost. Hence, understanding the hydrolysis of cellulose in wastewater which is mainly affected by temperature and the solids retention time (SRT), is a major key to determine the optimum location for its recovery. In order to assess the impact of temperature and SRT on cellulose degradation, this study investigated the biological aerobic degradation of cellulose in four laboratory-scale sequencing batch reactors (SBR) at four different temperatures (10-33°C) and two different sludge retention times (SRT of 15 days and 3 days). The degradation efficiency of cellulose was observed to increase with temperature and was slightly dependent on sludge retention time (80%-90% at an SRT of 15 days, and 78%-85% at an SRT of 3 days). A set of respirometry tests and modelling work was done using sludge samples from the four SBRs, tested and verified this value for fibrous cellulose, but alpha cellulose hydrolyzed significantly faster (approximately 3 times), indicating it is not an effective biochemical proxy for fibrous cellulose.

In wastewater treatment plants (WWTP), the influent carbon limitations negatively affect biological nutrient removal (BNR) performance. With increasing emphasis on resource recovery, wastewater treatment plants (WWTPs) supplement internal extra readily biodegradable carbon in the form of volatile fatty acids (VFA) produced from the fermentation of primary clarification biosolids to enhance BNR processes. Despite significant work on the fermentation of primary clarification biosolids, emerging technologies like rotating belt filters (RBF) which can selectively capture cellulose leading to potentially higher VFA yields and better BNR performance, have not been investigated. In this study, the fermentability of the cellulose-rich rotating belt filter (RBF) biosolids and its impact on enhancing biological phosphorus removal (EBPR) was studied and compared to the addition of fermented primary sludge in two lab-scale SBRs operated at a solids retention time (SRT) of 10 days. PE-SBR treated primary effluent and RBF-SBR treated RBF effluent. Allylthiourea (ATU) was added at 50 mg/L concentration to both SBRs to inhibit the nitrification and focus on the biological phosphorus removal. After the addition of fermented PS to PE-SBR and fermented RBF sludge

to RBF-SBR, the total phosphorus (TP) removal efficiencies increased from 69% and 72% to 91% and 93% for PE-SBR and RBF-SBR, respectively. Effluent soluble phosphorus (SP) concentrations averaged 0.1 mg/L and 0.3 mg/L for PE-SBR and RBF-SBR, respectively.

Keywords

Cellulose degradation, temperature correction factor, cellulose hydrolysis rate, temperature, SRT, kinetics, phosphorus removal, fermentation, rotating belt filter, enhanced biological phosphorus removal with fermentation, sludge fermentation products.

Summary for Lay Audience

Achieving a lower cost for wastewater treatment by minimizing the different treatment processes energy and solids resulting from the treatment different processes is the main focus of municipal wastewater treatment plants (WWTPs).

The estimated daily consumption of toilet paper in the United States is 18,000 tons. Cellulose originates mainly from toilet paper in the municipal wastewater entering the sewer systems and reaching wastewater treatment plants. The cellulose that can be recovered using physical treatment units located in most of the treatment plants, can be reused as a carbon source for treatment which reduce the treatment costs and energy.

In this study, the main focus was on understanding the different factors that affect cellulose fate in wastewater treatment plants bioreactors in order to identify its recovery opportunities.

Fermentation of two types of primary treatment biosolids for the recovery of volatile fatty acids, required to improve the removal of phosphorous biologically, was also assessed and compared in this study.

Co-Authorship Statement

The content of this master's thesis is either published or under review as listed below:

Chapter 4: Aerobic Cellulose Degradation in Sequencing Batch Reactors (Paper under the tittle of Kinetics of Aerobic Cellulose Degradation in Raw Municipal Wastewater.)

Authors: Min Gu Kim, Moustafa Elbahrawi, Azardokht Aryaei, Domenico Santoro, Damien Batstone and George Nakhla

Journal: Science of the Total Environment

Authors contribution:

Moustafa Elbahrawi: Conducted all experimental work, data collection and data analysis.

Min Gu Kim: Contributed to the experimental work, data analysis and drafted the manuscript.

Azardokht Aryaei: Helped in the analysis of the samples for the study.

George Nakhla and Domenico Santoro: Were involved in the conception and design of the study. They also reviewed and evaluated the manuscript in terms of quality and novelty.

Damien Batstone: Methodology, Software, Writing - Review & Editing of an additional part that is not used in the content of this thesis.

Status: Published.

Chapter 5: Respirometry experimental and modelling work.

Authors: Moustafa Elbahrawi, Min Gu Kim and George Nakhla

Authors contribution:

Moustafa Elbahrawi: Conducted the experimental work, data collection, data analysis, writing the chapter in the thesis and the modelling work.

Min Gu Kim: Contributed to the experimental work, data analysis and conducted the respirometry design conditions.

George Nakhla: he was involved in the conception and design of the study. They also reviewed and evaluated the work in terms of quality and novelty.

Chapter 6: Enhancing Phosphorus Removal Using Fermentation. (Paper under the tittle of Biological nutrient removal enhancement using fermented primary and rotating belt filter biosolids.)

Authors: Gholamreza Bahreini, Moustafa Elbahrawi, Elsayed Elbeshbishy, Domenico Santoro and George Nakhla

Journal: Science of The Total Environment

Authors contribution:

Moustafa Elbahrawi: Conducted all the experimental work, data collection and data analysis, content writing of the work.

Gholamreza Bahreini: Was involved in the experimental work, data collection and data analysis and drafted the manuscript.

George Nakhla, Elsayed Elbeshbishy and Domenico Santoro: Was involved in the conception and design of the study. They also reviewed and evaluated the manuscript in terms of quality and novelty.

Status: Published.

Acknowledgments

First of all, I would like to thank God for making me what I am today, without his mercy and blessing, I would not achieve anything in life.

I would like to express my deepest appreciation to my supervisor Dr. George Nakhla, for his great assistance, practical suggestions and excellent guidance. He has always pushed me to give the best quality of work and get the best version of myself during my master's degree. His approach to teaching and his passion for his work has influenced my point of view to work and my life goals. I have learnt a lot from his extensive knowledge not only in science but in the professional aspects. From the first time I met him, I started to learn.

I would like to especially thank my colleague, Dr. Mingu Kim, for helping me making my first experimental experience interesting through giving me the required trainings and tips that made my experimental skills relevant to my work during the two years of my degree. Moreover, his help whenever I faced any issues or challenges.

I would also like to thank my research group, Amr Ismail, Bassem Haroun, Mohammad Chowdhury, Masuduz Zaman. A special thanks to Ahmed Ahmed, Ahmed Khalil and Niema Afroze for their support and their presence whenever I face any challenges or issues. Another special thanks for Gholamreza Bahreini as he was my partner for the last experiment, and we faced a lot of challenges together.

I want to acknowledge the support of my father who passed away three years ago but his soul was my main source of inspiration to continue whenever I feel down. My mother, my sister and my brother presence were always a huge motive for me. They always taught me how to keep struggling for success against all odds in life.

I also want to thank my friends who I met in Canada for making it a second home and for their support and help.

Finally, I must acknowledge Marjam Ewes for her presence and for handling my stressful times. She made me happy throughout my difficult times and she was one of the main supports to continue and reach this level.

Table of Contents

List of Tables

List of Figures

List of Abbreviations and Symbols

WWTP	Wastewater treatment plant
BOD	Biochemical oxygen demand (mg/L)
BOD5	5-day biochemical oxygen demand (mg/L)
COD	Chemical oxygen demand (mg/L)
DO	Dissolved oxygen (mg/L)
HRT	Hydraulic retention time (h)
EBNR	Enhanced biological nutrients removal
EBPR	Enhanced biological phosphorus removal
K	Maximum specific substrate utilization rate (gCOD/gVSS-d)
Kd	Endogenous decay coefficicent (d-1)
Ks	Half-velocity constant (mgCOD/L)
θ	Temperature correction coefficient
OUR	Oxygen uptake rate (mg/L.hr)
SBR	Sequence batch reactor
MBR	Membrane bioreactor
nbCOD	Non-biodegradable COD (mg/L)
nbsCOD	Non-biodegradable COD (mg/L)
nbVSS	Non-biodegradable votatile suspended solids
NH4-N	Ammonium nitrogen (mg/L)
NO2-N	Nitirte nitrogen (mg/L)
NO3-N	Nitrate nitrogen (mg/L)
rbCOD	Readily biodegradable COD (mg/L)
rbsCOD	Readily biodegradable soluble COD (mg/L)

SCOD	Soluble chemical oxygen demand (mg/L)
VFA	Volatile fatty acids (mg/L)
SRT	Sludge retention time (d)
PS	Primary sludge
RBF	Rotating belt filter
PE	Primary effluent
RBFE	Rotating belt filter effluent
TCOD	Total chemical oxygen demand (mg/L)
TKN	Total Kjeldahl nitrogen (mg/L)
TN	Total nitrogen (mg/L)
SN	Soluble Nitrogen (mg/L)
TP	Total phosphorous (mg/L)
SP	Soluble phosphorus (mg/L)
TS	Total solids (mg/L)
TSS	Total suspended solids (mg/L)
VSS	Volatile suspended solids (mg/L)
Y	True yield coefficient (mgVSS/mgCOD)
μ	Specific growth rate (d^{-1})
μmax	Maximum specific growth rate (d^{-1})

Chapter 1

Introduction

1.1 Rationale

Nutrients removal has always been one of the main objectives of wastewater treatment. Lately wastewater treatment technologies have been focusing on improving sustainability by resources recovery and energy minimization and hence treatment cost reduction to achieve a circular economy (Ruiken et al., 2013a).

Cellulose in the form of toilet paper is a major constituent of municipal wastewaters (Gupta et al., 2018b). Cellulose can be captured and recovered by primary treatment technologies such as primary clarifiers that rely on settling, and emerging technologies such as the rotating belt filter (RBF) that uses sieving, among others. Successful diversion of cellulose from biological treatment reduces aeration energy, biological sludge production, and hence the overall treatment cost (Ruiken et al., 2013a). Moreover, recovered cellulose can be reused for many industrial purposes such as biofuels, building materials, and asphalt (Honda et al., 2000a; Mansouri et al., 2017a).

Hence, recent research studies have targeted cellulose for a better understanding of its fate and behavior in wastewater. Cellulose quantification, recovery, and degradation in wastewater have been previously discussed in the literature (Ahmed et al., 2019a; Gupta et al., 2018b). Despite that, many knowledge gaps are still exist as described in the literature review chapter.

Wastewater treatment modeling is a useful tool for design and optimization of wastewater treatment plants (WWTP). However, cellulose is not currently considered in activated sludge models (ASM) as a separate state variable (Reijken et al., 2018b). Moreover, cellulose kinetics are yet to be accurately specified. For a better understanding of cellulose, a combination of experimental and modeling work should be implemented (Ahmed et al., 2019a). In this thesis, cellulose was introduced to ASM1 as a separate state variable

describing its hydrolysis as an extra slowly process to differentiate it from the hydrolysis of slowly biodegradable particulates.

The satisfactory performance of biological nutrients removal (BNR) in wastewater treatment plants (WWTPs) rely on influent carbon. Due to the limitation of influent carbon in most of WWTPs, the whole process is dependent on supplementing extra source of readily biodegradable carbon (Tong and Chen, 2007a). Fermentation of primary biosolids to produce volatile fatty acids (VFAs) during the acidogenic phase of the fermentation was proved to be effective to enhance the BNR process (Ji and Chen, 2010; Tong and Chen, 2007b). Rotating belt filters (RBF) is one of the emerging primary treatment technologies which selectively capture cellulose, that can thus impact biological treatment yields, BNR performance, oxygen demand and hence the overall treatment cost (Chakraborty, 2015; Ruiken et al., 2013b). Despite the significant work on the fermentation of primary clarification biosolids to produce volatile fatty acids (VFA) for the enhancement of BNR processes, the fermentability of the cellulose-rich RBF biosolids and impact on BNR, both for nitrogen and phosphorous removal, has been sparsely studied in the literature.

1.2 Research objectives

The specific objectives of the aerobic cellulose degradation in sequencing batch reactors study are:

1- Assessment of the effect of temperature and solids retention times (SRT) on cellulose degradation in sequencing batch reactors (SBRs).
2- Determination of cellulose degradation rates at different operational conditions.
3- Estimation of cellulose hydrolysis rates and temperature correction factors.
4- Comparison of the hydrolysis rates for both fibrous and alpha cellulose.
5- Incorporation of cellulose hydrolysis and degradation kinetics in ASM1 as a separate state variable from the slowly biodegradable organics (X_S).

The second study focusing on the enhancement of phosphorus removal using fermentation had the following specific objectives:

1- Assessment of the effect of the addition of fermented RBF sludge on biological phosphorus removal efficiencies.
2- Comparison of the effects of fermented primary sludge (PS) and RBF sludge on enhanced biological phosphorus removal (EBPR) efficiency.

1.3 Thesis organization

Chapter 1 presents an overview of the thesis, provides a background on the significance of cellulose degradation and recovery, and identifies the knowledge gaps both with respect to experimental and modeling studies. Chapter 2 presents a detailed literature review on cellulose recovery, reuse, and discusses its biodegradation and kinetics, and discusses the current limitations of ASM models with respect to cellulose modeling. Furthermore, the RBF technology which selectively removes cellulose is discussed with respect to performance and sludge characteristics, with particular emphasis on the fermentability of the RBF sludges for EBPR. Chapter 3 presents the materials and methods used during the overall thesis work which includes all the experimental conditions, operational and startup conditions, and analytical methods of the four lab scaled SBRs complemented by a set of respirometric tests on different sludge samples from the SBRs system with the addition of microcrystalline α-cellulose as a model cellulosic substrate, and the cellulose-rich RBF sludge. Moreover, it includes the description, configuration, and objectives of the cellulose simulation work in a modified activated sludge model (ASM1) with cellulose as a separate state variable. Chapter 4 includes detailed discussion on the sequencing batch reactors experimental work with respect to aerobic cellulose degradation rates in raw wastewater, effect of temperature and SRT on cellulose degradation. Chapter 5 includes the respirometry tests results that was used in calibrating the modified ASM1 models developed on SUMO and the modeling work results in matching the various oxygen uptake rates (OUR) of the respirometric tests to estimate cellulose hydrolysis kinetics. Chapter 6 discusses the experimental results of two SBRs fed with the fermented primary sludges to enhance the removal of total phosphorus (TP). Chapter 7 presents the conclusion of the overall thesis work and the recommendations for future research work.

1.4 Thesis Format

This thesis follows the requirements stated by the School of Graduate and Postdoctoral Studies (SGPS), Western University. Chapter 4 study is under review in Science of the Total Environment journal. Chapter 6 study is accepted and currently in the process of being published in Science of the Total Environment journal. The overall thesis references are stated at the end of the thesis after chapter 7.

Chapter 2

Literature Review

2.1 Cellulose in wastewater

New wastewater treatment technologies are developed to improve sustainability and reduce cost mainly through minimizing energy costs and resource recovery. This has become one of the priorities along with the normal standards of successful management of the environmental and health impacts of wastewater disposal (Ruiken et al., 2013a).

Cellulose in municipal wastewater mostly originates from toilet paper. A study by Ruiken et al., (2013) reported that per capita annual consumption of toilet paper was 23 kg for North America and 13.8 kg for Western Europe. In the United States, the same study of (Li et al., 2019a) estimated the daily consumption of toilet paper is 18,000 tons with a substantial fraction of approximately 50% entering the sewer systems and hence the raw municipal wastewater contains about 158 mg/L of toilet paper based on a water consumption per capita of 400 L/day (Tchobanoglous et al., 2003a). Based on the above estimate cellulose in the influent is about 40% of the mass of solids and about 20%-30% of the influent total COD (Ruiken et al., 2013, 2018).

However, cellulose fibers have received little attention in the activated sludge process (Ruiken et al., 2013a) with a few reports on the fate of cellulose and its conversion in wastewater treatment processes, especially in activated sludge processes (Verachtertk and Bevers, 1982a).

2.2 Cellulose quantification

Finding a consistent, reliable, and accurate method for cellulose quantification in wastewater is a significant step to understand the behavior of cellulose in wastewater treatment (Ahmed et al., 2019a). Several approaches have been developed to measure cellulose in wastewater to track its fate in different treatment processes (Gupta et al., 2018).

Of the several methods proposed in the literature; enzymatic hydrolysis and acid hydrolysis were the most focused on. The two methods quantify the cellulose by the hydrolysis of

cellulose to monosaccharides and the glucose yield is the cellulose content index (Gupta et al., 2018b).

DuBois et al., (1956) used the method of phenol-sulfuric acid, Honda et al., 2000 followed the same method to quantify cellulose using NaOH and H2SO4 for pretreatment. The aforementioned authors reported that 7% and 17% of the TSS were the cellulose content in both raw wastewater and primary sludge for combined and separate sewer systems, respectively and 1% of TSS for biological sludge. Honda et al., (2002) proposed conventional autoclaving treatment after sludge hydrolysis with diluted sulfuric acid in order to separate cellulose fibers from sludge. Moreover, Hofsten and Edberg, (1972) who investigated the cellulose degradation rate, quantified cellulose content by H2SO4 hydrolysis followed by the anthrone method in which carbohydrate derivatives are determined by a colorimetric method.

Gupta et al., (2018) assessed four methods of measuring cellulose in both wastewater and sludge. Out of 4 cellulose quantification methods, three methods were based on hydrolysis either with one or two steps then the determination of soluble product, and the fourth method is a gravimetric measurement. Acid hydrolysis using sulfuric acid, National Renewable Energy Laboratory (NREL), enzymatic hydrolysis, and Schweitzer methods were the methods evaluated by the aforementioned authors. It was concluded that the Schweitzer method is the most accurate and reliable method of measurement of cellulose having the advantages of full recovery, efficiency, temperature dependency, and reproducibility compared with the other methods, which even with using pure cellulose were not reproducible. Hurwitz et al., (1961) quantified cellulose in sludge using the Schweitzer reagent method at 4.5%-13.5% of total TSS in raw, 2%-10% of in primary sludge (PS), and 1%-3.55% in waste activated sludge (WAS).

2.3 Cellulose Recovery and Energy

Cellulose is a complex carbohydrate which is known that it is a linear polymer of β-1,4-glycosidic bond linked D-glucopyranose units (Olsson and Westm, 2013a). Cellulose is used in several industrial processes such as food, clothing, paper, fuel, and shelter industries, and is the most abundant organic polymer on earth (Bauer and Ibáñez, 2014a; Harris et al., 2010a; Olsson and Westm, 2013a; Thoorens et al., 2014a).

Cellulose recovery helps reduce oxygen consumption and energy requirements, and decreases sludge disposal costs (Honda et al., 2002a). Hence, cellulose recovery is significantly beneficial for achieving a circular economy and lowering overall treatment costs (Reijken et al., 2018a), as the recovered cellulose can be used for industrial purposes such as asphalt, biofuels or additives in building materials (Boztas, 2017; Honda et al., 2000b), bioplastic bottles (Boztas, 2017).

Moreover, cellulose can pose challenges to selected treatment processes such as membrane bioreactors as it can loop around the membrane bundle, which requires proper screening of influent or recirculation of mixed liquor (Li et al., 2011).

Furthermore, an investigation on performance of rotating belt filter (RBF) using several water qualities from several WWTP showed that, 80% removal of total suspended solids (TSS), and 60% removal of COD can be achieved with the decreased flux to the filter mesh and increased TSS and COD removal due to formation of filter cake (Chakraborty, 2015).

2.4 Cellulose Degradation

Influent cellulose concentrations for raw wastewater constitute approximately 1/3 of the influential total suspended solids (TSS), as indicated by the plant surveys performed in two full-scale water recovery facilities situated in Canada (33%) and the Netherlands (31%) (Ahmed et al., 2019a).

Solids disposal is one of the major problems faced at wastewater treatment plants, particularly with the diminishing availability of landfills. Cellulose can contribute to the formation of bulky solids rather than a granular which can lead to several problems with physical solids separation (Hurwitz et al., 1961a) In addition, cellulose degradation also results in reduced sludge production and associated biosolids processing costs (Li et al., 2011).

Understanding the fate of cellulose in WWTP at different treatment conditions such as temperature and SRT is essential to identify the best location in WWTP for efficient recovery of cellulose. Furthermore, while aerobic cellulose degradation consumes energy, its anaerobic degradation produces energy and hence its fate can significantly impact the potential for energy neutrality at a given plant (Ahmed et al., 2019a).

Hurwitz et al., (1961), showed that in a plant-scale experiment that used mixed liquors of 2000 to 2500 mg/L, 2500 to 3000 mg/L and 3500-4000 mg/L for cellulose reduction, the MLSS concentration of 3500-4000 mg/L provided better reduction of cellulose and cellulose reduction is proportional to the MLSS concentration in the aeration tank, however, could hardly be achieved in winter because of the reduction of microbial activity.

Cellulose degradation is strongly dependent on temperature and solid retention time (SRT). (Verachtertk and Bevers, 1982a) reported that in 4 weeks, 60% of the cellulose was degraded in activated sludge process under aerobic conditions. Moreover, In pilot scale studies at 15^{o}C, the degradation rate and COD removal of influent very slowly biodegradable organics has proportionally increased with increasing solids retention time (Nowak et al., 1999a). Cellulose aerobic degradation organisms are temperature sensitive. A batch experiment done by Ruiken et al., (2013), found that temperature has a strong effect on cellulose degradation by showing that 10% of cellulose was degraded in 20 days at a temperature of 9°C (representing winter season) compared to 12 days for full removal of cellulose at a temperature of 24°C (representing summer season). Reijken et al., (2018) assumed a temperature correction factor through the Arrhenius relationship of 1.1098 °C^{-1}.

Edberg and Hofsten (1975) tested degradation of cellulose and reported 40% degradation under anaerobic conditions. On the other hand, Verachtertk and Bevers, (1982) reported 60% cellulose degradation under aerobic conditions and 50%-60% cellulose degradation under anaerobic conditions after 15 days of operation.

Furthermore, biodegradation of 50% calculated based on AENOR, (2003) was reported by (Alvarez et al., 2009a) of toilet paper under aerobic conditions. However, an anaerobic degradation rate for cellulose sieved sludge (fine mesh less than 0.35mm) were 62% and 57% for thermophilic and mesophilic conditions was reported by (Ghasimi et al., 2016a).

Reported cellulose degradation efficiency in wastewater treatment varied. Hurwitz et al., (1961) who studied the aerobic degradation of cellulose using laboratory batch experiments reported that cellulose degradation after 72 hours was 6.7% at 12-13°C and 87% at 23°C, indicating a significant temperature impact. A recent study by Ahmed et al., (2019) analyzed cellulose in two water resource recovery facilities (WRRFs) operated at SRT of 7-14 days and temperatures of 14 °C -25 °C and reported that the influent cellulose concentration in raw municipal wastewater was one-third of the influent total suspended solids, and cellulose in primary effluent degraded at an efficiency of 70%-90%, with secondary effluent cellulose concentrations of 2-3 mg/L. Furthermore, the aforementioned study highlighted the selective removal of cellulose by RBF and emphasized that irrespective of the presence or lack of primary treatment, secondary effluent cellulose concentrations were independent of primary treatment, Cellulose degradation rates increased with MLSS concentrations and SRT.

Benneouala et al. (2017) studied the hydrolysis of four different particulates of toilet papers with different particulate settable COD contents (15220 mg/L, 8180 mg/L, 11300 mg/L and 10001 mg/L) using respirometric tests at 20 °C and reported that the hydrolysis rate coefficients of particulate settleable solids collected before primary clarification, particulates at the outlet of residential buildings which was considered as the upstream part of the sewage networks, toilet paper, and cellulose were 0.4, 3.2, 1.3, and 1.2 d-1, respectively. The aforementioned studies by (Benneouala et al., 2017a), and (Reijken et al., 2018a) indicated that the hydrolysis of particles was primarily influenced by the active

biomass which colonized particles and thus increase of biomass by adding more inoculum, beyond what is required for colonization, did not necessarily affect hydrolysis rates.

The discrepancy in hydrolysis rates of cellulose in the previous studies could be related to testing conditions i.e. continuous-flow reactor operation and batch respirometry tests. Moreover, the cellulose to mixed liquor volatile suspended solids (MLVSS) mass ratio mg/g was 450-490 mg/g in Li et al. (2011), much higher than the 8 mg/g in Benneouala et al. (2017) and 12-30 mg/g in Ahmed et al. (2019). This could have impacted the estimated hydrolysis rate coefficients as discussed above. Temperature also is also known to affect hydrolysis rate in a microbially-mediated enzymatic process. However, the previous studies tested at near 20 °C, and the impact of temperature on hydrolysis of cellulose was not thoroughly addressed in the literature. Ruiken et al. (2013) who conducted batch anaerobic degradation of cellulose reported 10% cellulose degradation at 9 °C and a contact time of 20 days and 100% degradation at 24 °C and a contact time of 12 days under anaerobic conditions. Similarly, Ghasimi et al. (2016) also reported that cellulose anaerobic degradation efficiency was 57% at mesophilic conditions and 62% at thermophilic conditions at 15 days of contact time for both cases.

Ahmed et al., (2019) investigated full-scale gravity settling and micro-sieving primary processes with cellulose capture rate > 80%. The cellulose content of the RBF sludge was almost twice high as primary clarifier sludge i.e. 35% versus 17% by TSS weight, respectively. Cellulose was effectively biodegraded under the experiment operational conditions and temperature ranges from 13.7 to 24.8 °C, with all systems achieving secondary effluent cellulose of 2–3 mg/L within an SRT range of 7-14 days.

Comprehensive systematic studies delineating the impacts of temperature and SRT on cellulose are not available in the literature. Thus, the temperature correction factor for cellulose degradation is still unclear. In addition, the studies by Ruiken et al., (2013) and Ghasimi et al., (2016b) were conducted anaerobically; thus, the impact of different operational conditions on aerobic cellulose degradation has not been investigated to date.

2.5 Cellulose kinetics and modeling in wastewater

Activated sludge models (ASM) i.e. ASM1, ASM2, and ASM3 are the most popular models for the design and optimization of wastewater treatment processes. In these models, respirometric techniques are the basis of the influent fractionation (Reijken et al., 2018a). There are many uses for respirometry, including characterizing wastewater streams, assessing the toxicity and inhibitory effects on biomass and calibrating mathematical models (figure 2.1)

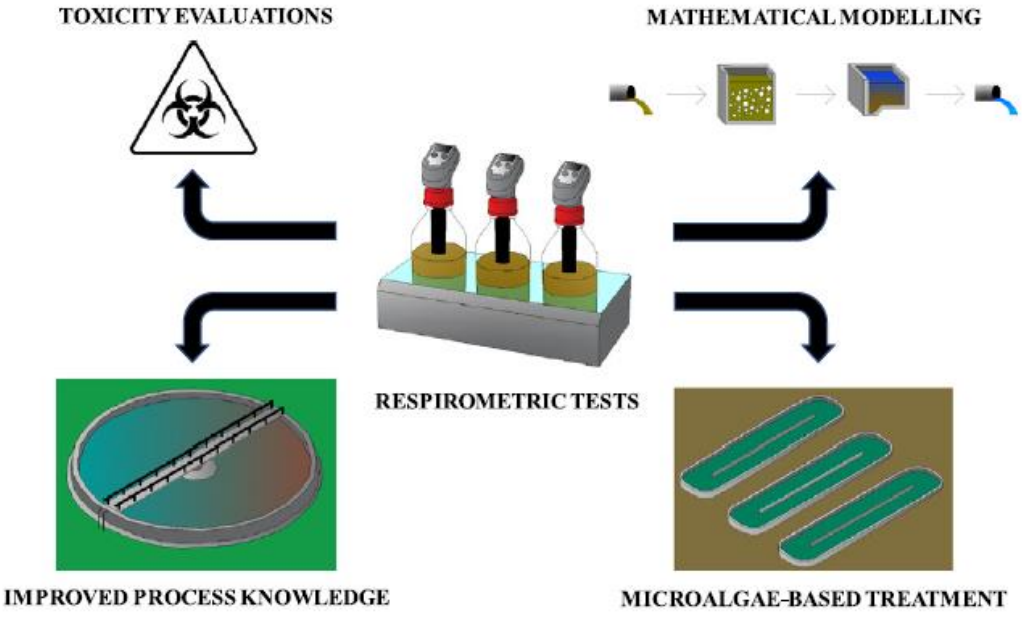

Figure 2.1 Uses of respirometry tests (Rossi et al., 2020)

Cellulose is not described as a state variable separately in ASM models. (Reijken et al., 2018a). Hence, cellulose should be implemented differently from slowly biodegradable organic to be a separate state variable having a slower hydrolysis rate (Reijken et al., 2018a).

Cellulose hydrolysis process can be described with different kinetics, first order (Weimer, 1992a), Monod (Mino et al., 1995a), and Contois (von Munch et al. 1999). Reijken et al., (2018) described the cellulose hydrolysis in the modified model of ASM1 as first order for simplicity and for the complexity of describing cellulose hydrolysis process which is not

well defined. The hydrolysis factor in the proposed model was introduced to be dependent on temperature with temperature correction factor of 1.1098 d^{-1}. However, knowing that hydrolysis of cellulose happens at the particle surface, the rate of degradation is dependent on the particular surface which will result in a power of 2/3 in cellulose concentration rate kinetics.

Surprisingly, the traditional activated sludge models do not include a significant fraction of domestic wastewater (Henze et al., 2000a), which is extra slowly biodegradable COD. However, several modifications to ASM were proposed. One of the early modifications to ASM1, was developed by Nowak et al., (1999), describing the extra slowly biodegradable organic matter as X_v without specifying its nature, at 10%-15% of the COD of the influent. The implementation of this new variable was based on the finding that the difference between inert and slowly biodegradable particulate content appeared to depend on the wastewater treatment plant's temperature and sludge age. It was the first model to differentiate slowly biodegradable from the extra slowly biodegradable component in ASM1.

Cellulose as mentioned earlier is described as very slowly biodegradable and also part of it is inert, is affected mainly by temperature (more degradable in high temperature than low temperature), and solids retention time (SRT) in biological reactors (Ruiken et al., 2013a). Hence, introducing cellulose into ASM1 is challenging due to its complicated degradation behavior and degradability dependency on temperature and SRT.

Reijken et al., (2018) developed a modified ASM1 model incorporating the cellulose as a separate state variable and describing its hydrolysis behavior with a first-order hydrolysis rate aiming to monitor the effect of cellulose sieving on the performance of a plant. In the model inputs, cellulose was considered 20% of the total COD. Aerobic hydrolysis rate coefficients of cellulose in the literature were estimated using the first-order model (Benneouala et al. 2017, Li et al. 2019, Reijken et al., 2018) while activated sludge model 1 (ASM1) uses the Contois model (equation 1) for particulates which explicitly considers the food to microorganisms (F/M) ratio, and oxygen availability (Henze et al. 2006). It was shown by Reijken et al., (2018) that at an SRT of 16 days, cellulose mostly is degraded

although part of it has been found in the sludge produced of the sieves which were around 5-15% at a hydrolysis rate of 0.2 d^{-1}.

Furthermore, (Revilla et al., a and b) developed an integrated activated sludge model including cellulose as a state variable, simulating industrial waste generated from a cellulose company.

However, cellulose degradation is an exocellular enzymatic process, influenced by solid substrate concentrations and active biomass (Benneouala et al. 2017). Common kinetic expressions for particulate hydrolysis are first order and Contois in particulate concentration are indicated in equations 2.1 and 2.2, respectively.

$$r = k_{H,C} X \quad (2.1)$$

$$r = k_{H,c} \frac{X}{K_{x+\frac{X}{X_H}}} \quad (2.2)$$

Where X is the particulate concentration (mg/L), k_H is the first order hydrolysis coefficient (d^{-1}), $k_{H,C}$ is the Contois rate coefficient (d^{-1}), Kx is the Contois saturation coefficient, and X_H is the biomass (normally heterotrophic biomass).

Contois kinetics are the default in activated sludge models (ASM) (Henze et al. 2006), with modification factors for oxygen availability etc. When biomass is in excess, the Contois equation approximates to first order in particulate, with $k_H \sim k_{H,c}/K_X$. When cellulose is in excess, the Contois equation approximates to zero order in particulate with $r \sim k_{H,c} X_H$, and hence $k_{H,c}$ is the biomass specific cellulose hydrolysis rate.

Cellulose is considered as slowly biodegradable with rate coefficients varying widely in the literature. Reijken et al., (2018a) who estimated the hydrolysis rate of cellulose using first-order kinetics in a modeling study reporting that cellulose is slowly biodegradable with a hydrolysis rate coefficient of 0.11 d-1, lower than 3 d-1 of particulates in activated sludge models (Henze et al. 2006). Li et al. (2019) who operated four SBR systems fed with toilet paper containing 56% (w/w) of cellulose at different SRTs of 5, 10, 20, and 40

days estimated that the hydrolysis rate coefficient at 22°C using first-order kinetics was as low as 0.03-0.12 d-1 for toilet paper and 0.03-0.07 d-1 for cellulose.

2.6 Rotating Belt Filter (RBF)

A suitable alternative to primary clarification (PC) is the rotating belt filter (RBF), among others such as rotary drum filters, disk filters, rotary circular filters etc... The RBF performance depends on the mesh pore size of the filters (typically 50 to 500 µm), influent particulate size distribution. Lema and Suarez, (2017) showed that larger influent particles separated by the mesh. Although smaller particles can be retained when the mesh pore size becomes smaller by the cake formations, however, decrease the permeability and flow through the filters.

While the COD fractionation of primary effluents has been well documented in the literature (Henze et al., 2000a), COD fractionation of RBF effluent were examined in few studies which investigated its denitrification kinetics.

Also, routine analysis of RBF samples from a full-scale RBF pilot done by Gupta et al., (2018b) found that the efficiencies of TSS and TCOD removal of 28±1% and 17±2% respectively. Moreover, measured TCOD was found to be, 61±5% of which 54±3% was found to be XCOD.

The aforementioned author also showed that the RBF has no impact on the SCOD fractions. The SCOD/TCOD fraction of 46% for RBF effluent was higher than raw wastewater's fraction of 39%. The ratio of components in wastewater from RWW and RBFE from literature had been presented in Table 2.1.

Table 2.1 Raw wastewater and RBF components ratios

Reference	$\frac{TSS}{VSS}$	$\frac{XCOD}{VSS}$	$\frac{rbSS}{TCOD}$	SI or SH	XI	YH	Standard ratio
(Tchobanoglous et al., 2003a)	0.78±0.03, 0.74±0.05	-					0.6-0.8
(Henze et al., 2008)	-	1.82±0.40, 1.95±0.44					1.5
(Gupta et al., 2018a)						0.65±0.004	
Henze et al., (2010)			0.22-0.24			0.63-0.67	
(Tas et al., 2009)				14±0.7 (5% of SCOD, 2% of TCOD) SH=13-39% of TCOD	COD(XI) and slowly biod. COD (XI)=24% & 27% respectively.		

XCOD=Particulate COD, rbSS=Readily biodegradable suspended solids, SI=Soluble Inert, SH=Soluble Hydrolysable, XI=Inert, YH=Heterotrophic yield.

The effect of organic carbon recovery which includes cellulose on the aeration energy and biogas production was monitored by Behera et al., (2018). Influent cellulose was estimated to be 25%-40% of the influent COD and cellulose degradation under anaerobic and aerobic conditions was estimated at 50%-70% and 15%-35%, respectively in 9-14 days of operation. Recovering cellulose using RBF technology with thick mat formation increased methane production from the sludge by 10% and decreased aeration energy by 8% based on the results of the model compared to primary clarification; without mat formation the corresponding values are 20% increase in methane production and 2% energy reduction.

2.7 Enhanced biological phosphorus removal (EBPR).

Effluent phosphorus concentrations in wastewater treatment plants effluents typically range within 0.1-1 mg/L (Zhao, 2017), although effluents as lows as 0.01 mg/L are sometimes required. The removal of phosphorus in wastewater is either achieved biologically or chemically and in some cases, both biological and chemical treatments are used (Tchobanoglous et al., 2003a).

EBPR processes involve anaerobic/aerobic phases. The anaerobic phase (fermentation step) is primarily for P release and uptake of short-chain volatile fatty acids by phosphorous accumulating bacteria (PAOs) (Comeau et al., 1986). PAOs which are responsible for phosphorus removal, store phosphates in intercellular granules for energy, which is produced from glycogen breakdown and the hydrolysis of polyphosphate cells which is a chain rich of energy. PAOs store VFA it in the form of carbon deposits – polyhydroxyalcanoates – PHA under anaerobic conditions. The phosphate concentration in the anaerobic phase increases when polyphosphates are broken to ortho-phosphate to release energy. In the aerobic phase, PHA is oxidized for the growth of cells, P storage, and glycogen regeneration (Seviour et al., 2003).

Biological P-removal primarily occurs via the accumulation of P as polyphosphate, by microorganisms which is termed luxury phosphorus uptake (D. et al., 1979). Although PAOs seem to outcompete other microorganisms under several conditions, exception lies

in the presence of Glycogen Accumulating Organisms (GAO) that metabolize volatile fatty acids (VFAs) or other carbon compounds as PAO without accumulating P (Cydzik-Kwiatkowska and Zielińska, 2016) which is detrimental for phosphorus uptake. While acetate is the dominant carbon source in the wastewater system, propionate could be added to the acetate to achieve better EBPR performance (Thomas et al., 2003).

2.8 Anaerobic Fermentation

Carbon shortage has always been a challenge for biological nutrients removal (BNR) from domestic wastewater. In order to enhance the treatment process, either external sources of carbon are added to the processes such as acetate and methanol (Hwang et al., 2016) or the VFA-rich supernatant from fermented primary and waste activated sludges. The chemical oxygen demand (COD) to the microorganism through cell synthesis i.e. to the waste activated sludge (WAS) happens in the biological process and that needs to be treated further (Yuan et al., 2016a). Anaerobic fermentation is an intermediate process in the anaerobic digestion of organics, whereby complex organic substrates are broken down by facultative bacteria to volatile fatty acids (Cuevas-Rodríguez et al., 1998). However, after the anaerobic fermentation process, mechanical centrifugation is typically needed for the separation of the fermented sludge solids from the fermentation supernatant due to the change in particles characteristics (Liu et al., 2017) and poor filterability of the supernatant (Zheng et al., 2009).

Furthermore, during the WAS fermentation, nitrogen and phosphorus are released from sludge particles to liquid (Ahn and Speece, 2006a; Jiang et al., 2007a; Yuan et al., 2006a), thereby increasing the nutrients loadings to BNR systems (Tong and Chen, 2009a, 2007a).

Yuan et al. (2015) reported that 31.65 mg COD/L which produced short chain fatty acids (SCFAs) of 17.21 mg COD/L that added to the influent from fermentation products which, showed the potential and feasibility of recovering and using organic carbon produced in the fermentation products without any nitrogen or phosphorus removal.

2.9 Synopsis of literature review

Based on the literature review, there has always been a debate on the estimation of cellulose degradation kinetics under WWTPs common cellulose affecting operational conditions such as temperature and SRT. Moreover, introducing cellulose as a separate state variable to ASM1 and using the modification in validating experimental calculated cellulose hydrolysis rate (Khcl) with simulated models using Contois model has not been introduced to the literature yet. In this thesis, the first experimental work targeted assessing the effect of temperature and SRT on cellulose degradation and estimating cellulose hydrolysis rates at different operational conditions. In Incorporating cellulose kinetics in ASM1 model separately from slowly biodegradable organics (Xs) was a comparison of hydrolysis rates of fibrous and alpha cellulose as well.

Studying the effect of the addition of fermented sludges on enhancing nutrients removal has been always been a main research topic in enhancing biological phosphorus removal (EBPR) process. However, with the several emerging treatment technologies introduced recently, studying the fermentability of RBF technology sludges and its effect improving nutrients removal efficiencies has been a knowledge gap in the literature. The second part of this thesis focused on studying the fermentability of RBF sludge and checking its effect on EBPR process. Furthermore, the experiment mentioned the latter was a comparison of using primary treatment sludges of primary sludge versus RBF sludge as an extra carbon source.

Chapter 3

Materials and Methods

3.1 Aerobic Cellulose Degradation in Sequencing Batch Reactors

3.1.1 SBR Set-up and Operation

Four lab-scale SBR systems with a working volume of 2 L were operated at four different temperatures i.e. 10 °C (R1), 17 °C (R2), 25 °C (R3), and 33 °C (R4) (Figure 3.1). Temperatures were controlled using a chiller (PolySciences Heated Circulating Bath, 1 SD07R-20-A11B, Polysciences, Inc., Warrington, PA 18976) and hot plate (Corning® Digital Hot Plates, VWR). A total of 160 days of operation was monitored with phase 1 (day 1-100) at an SRT of 15 days and phase 2 (101-160 days) at an SRT of 3 days. The systems were inoculated with activated sludge taken from the nitrifying Greenway WWTP (London, Ontario, Canada) with 5000 mg/L of MLSS and 4000 mg/L of MLVSS and fed with de-gritted wastewater. Dissolved oxygen levels during the aerobic phase were 5-7 mg/L. For chemical P removal, $FeCl_3$ solution was also added to the feed at a ratio of 5 mg Fe per 1 L wastewater.

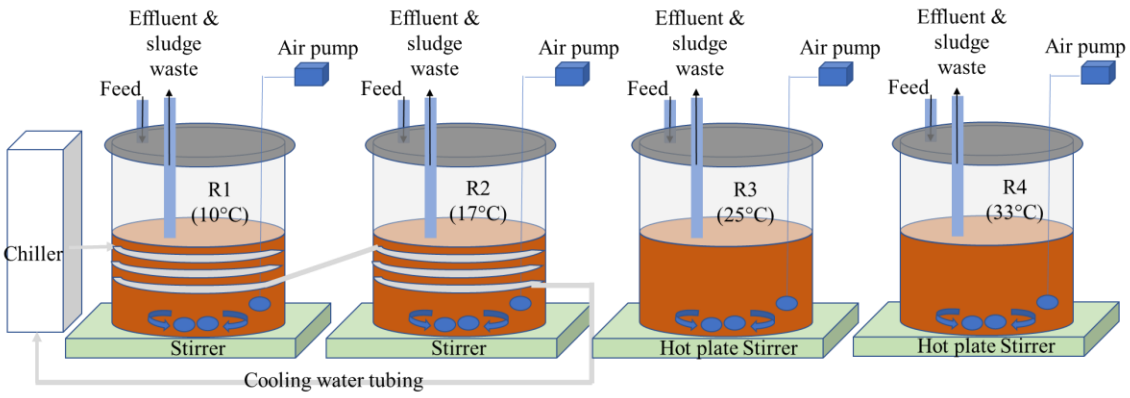

Figure 3.1 Lab-scale SBR system

The SBR systems, operated with three cycles a day, and treated 3 L/d of municipal wastewater with 1 L in each cycle and each 8-hr cycle consisting of filling (0.5 hr), anoxic phase (1.5 hr), aerobic phase (4.5 hr), settling (1 hr), and decanting (0.5 hr) (Figure 3.2). Dissolved oxygen levels during the aerobic phase were in the range of 5-7 mgO_2/L.

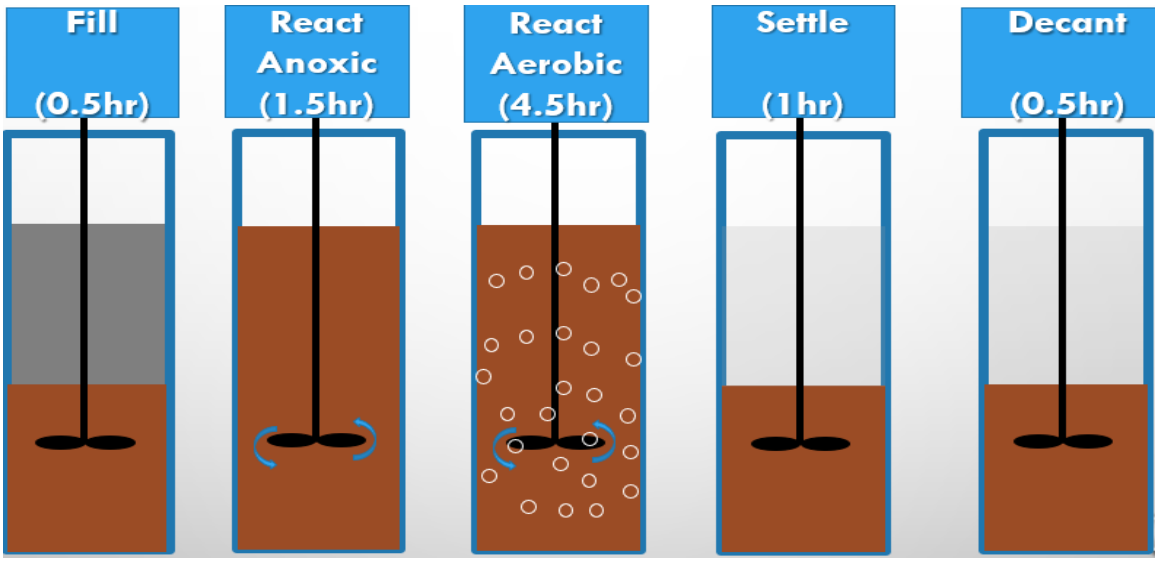

Figure 3.2 SBR cycle operation

3.1.2 Analytical methods

Table 3.1 presents the raw influent wastewater from Greenway characteristics. Samples were collected twice a week for analysis of total COD, soluble COD, total nitrogen (TN), soluble nitrogen (SN), ammonium (NH4), nitrate (NO3), nitrite (NO2), total phosphorus (TP), soluble phosphorus (SP) according to Hach Methods and suspended solids and alkalinity according to Standard Methods (APHA, 1998). A 0.45 μm membrane filter was used to differentiate between soluble and particulate fractions.

Table 3.1 Raw Wastewater characteristics

Parameter	Phase 1 (Day 37-100) (n=19) Influent	Phase 2 (Day 110-160) (n=14) Influent
pH	7.5±0.3	7.4±0.3
Alkalinity (mgCaCO3/L)	375±35	368±32
TSS (mg/L)	208±72	346±79
VSS (mg/L)	144±47	233±55
TCOD (mg/L)	359±104	447±132
SCOD (mg/L)	142±41	138±36
TN (mgN/L)	37±8	45±8
SN (mgN/L)	28±4	34±5
Amm-N (mgN/L)	25±4.3	25±5
NO3 (mgN/L)	0.4±0.1	0.5±0
NO2 (mgN/L)	0.0±0.0	0.1±0
TP (mgP/L)	7.6±4.1	7.4±2
SP (mgP/L)	2.5±1.3	1.2±1

Cellulose in the influent, effluent, and mixed liquor samples was also determined once a week using the Schweitzer method (Gupta et al., 2018c; Hurwitz et al., 1961b). Briefly, this method involved several steps to capture cellulose through reaction with cupric hydroxide in alkaline solution to form copper complexes from which cellulose was precipitated with dilute acids or alcohol, and gravimetrically measured. The chemicals used for this analysis included sodium hydroxide (50%), Schweitzer reagent, ethyl alcohol (80%) and hydrochloric acid (1.25%). The Schweitzer reagent, prepared by adding 5.5 g of cupric hydroxide to 1 L of 28% to 29 % ammonium hydroxide, was used as a solvent for cellulose.

3.2 Respirometry tests

3.2.1 Experimental work

Respirometry is the tool to measure the respiration rate of living microorganisms in activated sludge. As discussed in the literature review chapter, one of the main uses of respirometry tests is calibrating wastewater models. A series of respirometry tests using an 8-cell Challenge Respirometer (Respirometer Systems and Application, Fayetteville, Arkansas, USA) were conducted on SBR sludges samples with the addition of microcrystalline α-cellulose (Sigma Aldrich, Ontario) and cellulose-rich RBF sludges at a low substrate to biomass (S/X) ratio of 0.2 (gCOD/gVSS) and high S/X of 2,4 and 8 (gCOD/gVSS) in order to investigate the impact of cellulose type on degradation rates. The respirometry tests design conditions are summarized in appendix A1.

Microcrystalline α-cellulose has been used as standard cellulose in cellulose degradation studies (Ghasimi et al., 2016b). The working volume was 500 mL. Allylthiourea was added at 20 mg/L to inhibit nitrification. Ammonia was also added at 20 mg/L ensuring that the system was not ammonia limited. For the high S/X tests with α-cellulose, as presented in appendix A1, α-cellulose in the range of 58-120 mgCOD/L were added to the respirometry bottes. The high α-cellulose bottles were conducted at 27°C using R1 and R2 sludges. However, for the low S/X tests with α-cellulose supplemented at 120 mgCOD/L were conducted at 14 °C using R1 and R2 sludges and at 29 °C using R3 and R4 sludges.

Similarly, the two high and low S/X tests with RBF sludge containing 100 mg COD/L of fibrous cellulose was run at 20 °C using the mixed biomass of the four reactors (R1-R4) during phase 2. The quantified cellulose content of the RBF sludge was 19% of particulate COD. The seed control bottles were also monitored to estimate the endogenous respiration rate.

3.2.2 Respirometry simulation

The main purpose of the respirometry tests was to calibrate the modified ASM1 models in order to describe the cellulose degradation. Data from the respirometry tests were processed using SUMO software (Dynamita, Nyons, France) to estimate kinetic parameters such as the maximum specific growth rate, the half-saturation concentration, cellulose

hydrolysis rate coefficients. The respirometry tests data were simulated using a Contois model to describe the cellulose hydrolysis process. The kinetic parameters were determined through closely matching SUMO simulated oxygen uptake rates with experimental OUR.

The ASM1 in stock format was used with a modification of describing the cellulose hydrolysis rate by separate hydrolysis kinetics. The only process added and modified was the cellulose as X_C and the parameters used to calibrate the models are the maximum growth rate of heterotrophs (μmax), decay rate for heterotrophs (b_H), and cellulose hydrolysis factor ($K_{H,CL}$).

3.2.2.1 Modelling objectives and novelty

The main modeling objectives were to introduce a new separate state variable which is cellulose to ASM1 model to differentiate it from the slowly biodegradable organics as an extra slowly biodegradable organic. Moreover, the model was built with the aim of estimating the hydrolysis rate coefficient of cellulose at different food- to-microorganisms ratios based on a Contois model for the first time in the literature.

3.2.2.2 Modelling procedures

Data Collection

The sludge data used for both respirometry tests and the models are sludge collected from the SBRs (R1-R4) and only two runs used RBF sludge with a mixture of the SBRs sludges.

ASM1 Modification

In order to modify any activated sludge model which is originally a mathematical model based on differential equations describing the rate of hydrolysis of particulates and biodegradation of soluble organics of each parameter presented in the Gujer matrix. It also describes the rate of growth and decay of microorganisms in wastewater. The rate of change of each parameter is stochiometric based. Hence, to introduce any parameter to ASM, which is the cellulose in this case, the rate of its hydrolysis should be inputted as well as the stochiometric coefficients.

As shown in Figure 3.3, ASM1 Gujer matrix, (i) represents the different components in wastewater and (j) represent the different processes.

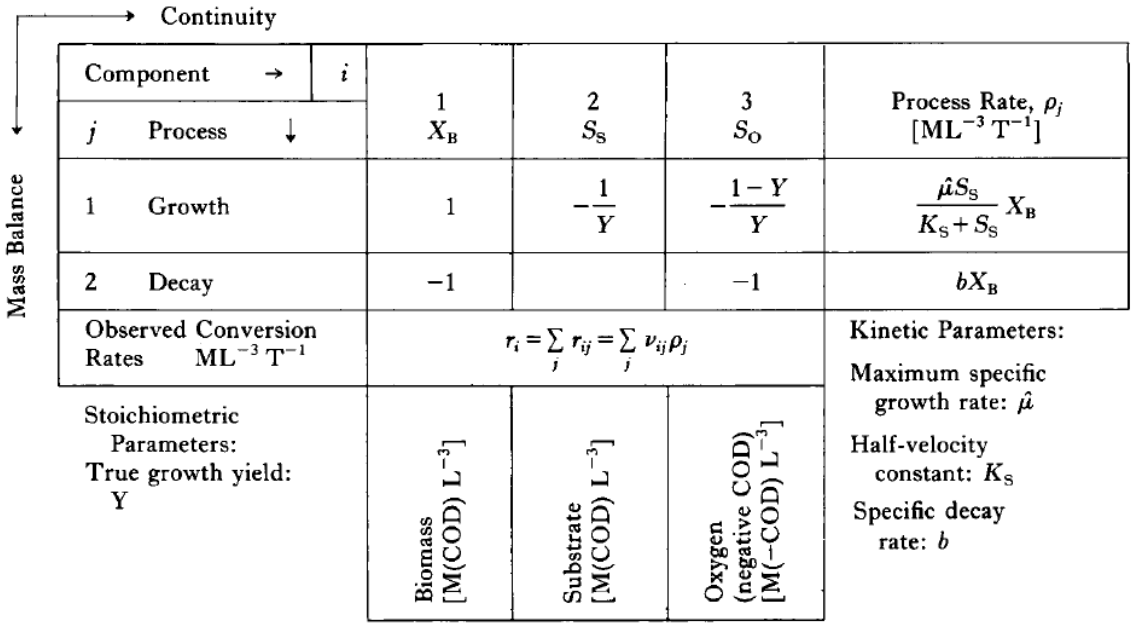

Figure 3.3 ASM1 Gujer Matrix description (Henze et al., 2000a)

Gujer Matrix Components

Table 3.2 presents the different soluble and particulate components of ASM1 model stated in the Gujer matrix (*SUMO, Dynamita, Nyons, France*, 2019). The cellulose as shown in the mentioned table is added as a separate particulate component (Xcl).

Table 3.2 ASM1 components description (*SUMO, Dynamita, Nyons, France*, 2019)

Symbol	Name	Unit	Particle size
S_I	Soluble undegradable organics	g COD.m^{-3}	S
S_S	Soluble biodegradable organics	g COD.m^{-3}	S
X_I	Particulate unbiodegradable organics from the influent	g COD.m^{-3}	X
X_S	Particulate biodegradable organics	g COD.m^{-3}	X
$X_{B,H}$	Ordinary heterotrophic organisms (OHO)	g COD.m^{-3}	X
$X_{B,A}$	Autotrophic nitrifying organisms ($NH4^+$ to $NO3^-$)	g COD.m^{-3}	X
X_P	Particulate undegradable endogenous products	g COD.m^{-3}	X
S_O	Dissolved oxygen (O_2)	g O_2.m^{-3}	S
S_{NO}	Nitrate and nitrite (NO_3 + NO_2)	g N.m^{-3}	S
S_{NH}	Ammonia ($NH4^+$ + NH3)	g N.m^{-3}	S
S_{ND}	Soluble biodegradable organic N	g N.m^{-3}	S
X_{ND}	Particulate biodegradable organic N	g N.m^{-3}	X
S_{ALK}	Alkalinity (ALK)	eq ALK.L^{-1}	S
S_{N2}	Dissolved nitrogen (N_2)	g N.m^{-3}	S
X_{INORG}	Inorganic suspended solids	g TSS.m^{-3}	X
Xcl	Slowly biodegradable cellulose	g Cl.m^{-3}	X

ASM1 model was modified by adding cellulose to the Gujer kinetics (Henze et al., 2000b) matrix as a separate state variable (Xcl) with a stoichiometric coefficient of -1 and 1 for the Xcl and S_S components respectively, describing the cellulose conversion as an extra slow hydrolysable particulate to S_S (Table 3.3). The hydrolysis rate for cellulose was described as Contois model (Eq. 3.1) including cellulose hydrolysis factor Kcl and cellulose half-saturation factor of Xcl/XB,H as Kxcl.

$$\frac{dXcl}{dt} = -Kcl \frac{(Xcl/XB,H)}{(Kxcl+Xcl/XB,H)} [(\frac{SO}{(KO,H+SO)})] XB,H \quad (3.1)$$

Where Kcl presents the hydrolysis of Cellulose (d^{-1}), Xcl is the cellulose particulates concentration, $X_{B,H}$ is the heterotrophic biomass concentration and Kxcl represents the half-saturation of $Xcl/X_{B,H}$.

Table 3.3 Modified Gujer Kinetic Matrix (*SUMO, Dynamita, Nyons, France*, 2019)

		Gujer kinetic matrix									
j	**Symbol**	**Process**	*SI*	*SS*	*XI*	*XS*	*XB,H*	*XB,A*	*XP*	*SO*	*SNO*
1	**r1**	**Aerobic growth of heterotrophs**		$-1/Y_H$			1			$-(1-Y_H)/Y_H$	
2	**r2**	**Anoxic growth of heterotrophs**		$-1/Y_H$			1				$-(1-Y_H)/(i_{NO3,N2}*Y_H)$
3	**r3**	**Aerobic growth of autotrophs**						1		$-(-i_{COD,NO3}-Y_A)/Y_A$	$1/Y_A$
4	**r4**	**Decay of heterotrophs**				$1-f_P$	-1		f_P		
5	**r5**	**Decay of autotrophs**				$1-f_P$		-1	f_P		
6	**r6**	**Ammonification of soluble organic nitrogen**									
7	**r7**	**Hydrolysis of entrapped organics**		1		-1					
8	**r8**	**Hydrolysis of entrapped organic nitrogen**									
9	**r9**	**Hydrolysis of Cellulose**		1							

S_{NH}	S_{ND}	X_{ND}	S_{ALK}	S_{N2}	X_{INORG}	Xcl	Rate	Unit
$-i_{XB}$			$-i_{XB}*i_{Charge,SNHx}$				$\mu_H*Msat_{SS,KS}*Msat_{SO,KO,H}*Msat_{SNH,KNH,H}*Msat_{SALK,KALK}*X_{B,H}$	$g.m^{-3}.d^{-1}$
$-i_{XB}$			$-(1-Y_H)/(i_{NO3,N2}*Y_H)*i_{Charge,SNOx}-i_{XB}*i_{Charge,SNHx}$	$(1-Y_H)/(i_{NO3,N2}*Y_H)$			$\mu_H*Msat_{SS,KS}*Minh_{SO,KO,H}*Msat_{SNO,KNO}*Msat_{SNH,KNH,H}*\eta_g*X_{B,H}$	$g.m^{-3}.d^{-1}$
$-i_{XB}-1/Y_A$			$-(i_{XB}+1/Y_A)*i_{Charge,SNHx}+(1/Y_A)*i_{Charge,SNOx}$				$\mu_A*Msat_{SNH,KNH}*Msat_{SO,KO,A}*Msat_{SALK,KALK}*X_{B,A}$	$g.m^{-3}.d^{-1}$
		$i_{XB}-f_P*i_{XP}$					$b_H*X_{B,H}$	$g.m^{-3}.d^{-1}$
		$i_{XB}-f_P*i_{XP}$					$b_A*X_{B,A}$	$g.m^{-3}.d^{-1}$
1	-1		$i_{Charge,SNHx}$				$k_a*S_{ND}*X_{B,H}$	$g.m^{-3}.d^{-1}$
							$k_h*MRsat_{XS,XB,H,KX}*(Msat_{SO,KO,H}+\eta_h*Minh_{SO,KO,H}*Msat_{SNO,KNO})*X_{B,H}$	$g.m^{-3}.d^{-1}$
	1	-1					$k_h*(X_{ND}/X_S)*MRsat_{XS,XB,H,KX}*(Msat_{SO,KO,H}+\eta_h*Minh_{SO,KO,H}*Msat_{SNO,KNO})*X_{B,H}$	$g.m^{-3}.d^{-1}$
						-1	$K_{cl}*MRsat_{Xcl,XB,H,KX}*Msat_{SO,KO,H}*X_{B,H}$	$g.m^{-3}.d^{-1}$

The description of the Gujer Matrix's components is presented in the tables below extracted from the SUMO software ASM1 formation code. Table 3.4 lists the description of autotrophic microorganism's growth, decay and half saturations parameters used in the Gujer matrix of ASM1 earlier.

Table 3.4 Growth and decay of autotrophic nitrifying organisms (*SUMO, Dynamita, Nyons, France,* 2019)

Symbol	Name	Unit
μ_A	Maximum specific growth rate of autotrophs	d^{-1}
b_A	Decay rate of autotrophs	d^{-1}
k_a	Rate of ammonification	$m^3.g\ COD^{-1}.d^{-1}$
$K_{O,A}$	Half-saturation of oxygen	$g\ O_2.m^{-3}$
K_{NH}	Half-saturation of ammonia	$g\ N.m^{-3}$

Table 3.5 lists the description of heterotrophic microorganism's growth, decay and half saturations parameters used in the Gujer matrix of ASM1 earlier.

Table 3.5 Growth and decay of heterotrophic organisms (*SUMO, Dynamita, Nyons, France,* 2019)

Symbol	Name	Unit
μ_H	Maximum specific growth rate of heterotrophs	d^{-1}
η_g	Reduction factor for anoxic growth of heterotrophs	unitless
K_S	Half-saturation of SB	$g\ COD\ m^{-3}$
b_H	Decay rate of heterotrophs	d^{-1}
$K_{O,H}$	Half-saturation of oxygen	$g\ O_2.m^{-3}$
K_{NO}	Half-saturation of nitrate	$g\ N.m^{-3}$
$K_{NH,H}$	Half-saturation of ammonia	$g\ N.m^{-3}$

In table 3.6, the different hydrolysis and half saturation factors used in Gujer matrix are listed. As per contois model hydrolysis equation (3.1), the hydrolysis rate (K_{cl}) and half saturation factor ($X_{cl}/X_{b,H}$) were added to the different hydrolysis parameters of ASM1 to describe the cellulose hydrolysis process.

Table 3.6 Hyrolysis factors of ASM1 (*SUMO, Dynamita, Nyons, France*, 2019)

Symbol	Name	Unit
k_h	Maximum specific hydrolysis rate	g X_S.g $X_{B,H}^{-1}$.d^{-1}
K_X	Half-saturation of $X_B/X_{B,H}$	g X_S.g $X_{B,H}^{-1}$
η_h	Correction factor for hydrolysis under anoxic conditions	unitless
K_{cl}	Hydrolysis of Cellulose	g X_{cl}.g $X_{B,H}^{-1}$.d^{-1}
K_{xcl}	Half-saturation of $X_{cl}/X_{B,H}$	g X_{cl}.g $X_{B,H}^{-1}$

Table 3.7 and 3.8 presents the different yields, alkalinity half-saturation factor, fractions and electron equivalence and charge balance values used in modified ASM1 model. All the mentioned parameters were used as the default values of ASM1.

Table 3.7 Yields coefficients for autotrophic and heterotrophic microorganisms (*SUMO, Dynamita, Nyons, France*, 2019)

Symbol	Name	Default value	Unit
Y_H	Yield for $X_{B,H}$ growth	0.67	g XB,H.g COD^{-1}
Y_A	Yield of $X_{B,A}$ growth per S_{NO3}	0.24	g XB,A.g N^{-1}

Table 3.8 Alkalinity, fractions and electron equivalence and charge balance (*SUMO, Dynamita, Nyons, France*, 2019)

Symbol	Name	Default value	Unit
K_{ALK}	Half-saturation of alkalinity	0.001	eq/L
f_P	Fraction of X_U generated in biomass decay	0.08	unitless
i_{XB}	N content of biomasses	0.086	g N.g COD^{-1}
i_{XP}	N content of products from biomass	0.06	g N.g COD^{-1}
$i_{NO3,N2}$	Conversion factor for NO_3 reduction to N_2	2.86	g COD.g N^{-1}
$i_{COD,NO3}$	Conversion factor for NO_3 into COD	-4.57	g COD.g N^{-1}
$i_{COD,N2}$	Conversion factor for N_2 into COD	-1.71	g COD.g N^{-1}
$i_{Charge,SNHx}$	Conversion factor for NHx into charge	0.00007	kCharge.g N^{-1}
$i_{Charge,SNOx}$	Conversion factor for NO3 into charge	-0.00007	kCharge.g N^{-1}

Table 3.9 presents the calculated variables ratios of ASM1. All default values were used in the simulation processes of all developed models.

Table 3.9 Calculated variables ratios (*SUMO, Dynamita, Nyons, France*, 2019)

Symbol	Name	Default value	Unit
i_{CV}	Particulate COD to VSS ratio	1.48	g COD.g VSS^{-1}
$i_{CV,SS}$	S_S S_{COD}/VS ratio	1.07	g COD.g VS^{-1}
$i_{CV,SI}$	S_I S_{COD}/VS ratio	0.93	g COD.g VS^{-1}
$f_{BOD5,BODult}$	BOD_5 to ultimate BOD ratio	0.65	gCOD.gCOD^{-1}

The saturation and inhibitions terms used in all the rates of different parameters of the modified ASM1 are listed in table 3.10. The saturation factor of cellulose particulates was added to this table following the contois hydrolysis rate equation (3.1).

Table 3.10 Saturation/inhibition terms of modified ASM1 (*SUMO, Dynamita, Nyons, France*, 2019)

Symbol	Name	Expression
$Msat_{SS,KS}$	Saturation term for soluble biodegradable organics	$S_S/(S_S+K_S)$
$Msat_{SO,KO,H}$	Saturation term for dissolved oxygen (heterotrophs)	$S_O/(K_{O,H}+S_O)$
$Msat_{SO,KO,A}$	Saturation term for dissolved oxygen (autotrophs)	$S_O/(K_{O,A}+S_O)$
$Msat_{SNH,KNH,H}$	Saturation term for ammonia (heterotrophs)	$S_{NH}/(K_{NH,H}+S_{NH})$
$Msat_{SNH,KNH}$	Saturation term for ammonia (autotrophs)	$S_{NH}/(K_{NH}+S_{NH})$
$Msat_{SALK,KALK}$	Saturation term for alkalinity	$S_{ALK}/(K_{ALK}+S_{ALK})$
$Msat_{SNO,KNO}$	Saturation term for nitrate and nitrite	$S_{NO}/(K_{NO}+S_{NO})$
$MRsat_{XS,XB,H,KX}$	Saturation term for particulate biodegradable organics (heterotrophs)	$(X_S/X_{B,H})/(K_X+X_S/X_{B,H})$
$Minh_{SO,KO,H}$	Inhibition term for dissolved oxygen	$K_{O,H}/(K_{O,H}+S_O)$
$MRsat_{Xcl,XB,H,KX}$	Saturation term for Cellulose	$(Xcl/X_{B,H})/(K_{xcl}+Xcl/X_{B,H})$

System Configuration

The respirometry experiment was simulated on SUMO software as a batch reactor aerated with a dissolved oxygen (DO) setpoint of 2 mg O_2/L and the reactor volume was set to 500 ml.

Model Inputs and Calibration

For Contois model calibration and parameters estimation on SUMO, the software influent tool was used to check some of the influent ratios listed in table 3.11. Moreover, the kinetics values were used to match the simulated OUR profiles with the experimental profiles from the respirometric test runs. The kinetics values used for calibration were in the reasonable range of the default kinetics values. To describe the temperature effect on kinetics, values were adjusted with temperature correction values from literature (Tchobanoglous et al., 2003b). Different temperature correction factors are shown in appendix A2.

Table 3.11 Influent tool ratios checks (*SUMO, Dynamita, Nyons, France*, 2019)

COD/BOD/TSS/VSS match	Measured data	Calculated from estimated fractions	Verdict
Influent COD	360.0	360.0	good match
Calculated influent filtered COD	150.8	150.8	good match
Calculated Influent filtered flocculated COD	85.0	85.0	good match
Calculated influent BOD5	6.0	6.1	good match
TSS	225.0	202.7	so-so…
VSS	144.6	130.3	so-so…

Due to the nitrification and denitrification inhibition in the respirometric bottles, the allylthiourea addition was incorporated by setting the maximum growth rate (μmax) and decay coefficients for autotrophic microorganisms both as 0 d^{-1}.

Key Calibration Parameters

The key parameters used to estimate the hydrolysis rate of cellulose in the different models were the maximum specific growth rate of heterotrophs (μmax) and the cellulose hydrolysis rate (Kxcl).

The μmax controlled the peak level of OUR on the y-axis (mgO_2/L.h) with time (d) on the x-axis. Figure 3.5 shows the effect of decreasing μmax value from 6 1/d to 3 1/d, which decreased the peak OUR value from 1.1 to 0.65 mg/L.h.

3.3 Enhancing Phosphorus Removal Using Fermented Primary Sludge and RBF sludge

3.3.1 Set-up and Operation

Two lab-scale sequence batch reactors (SBRs) systems, as shown in Figure 3.7, were operated for 75 days. The first reactor treated primary effluent (PE-SBR) and the second reactor treated RBF effluent SBR (RBFE-SBR) collected from Greenway WWTP, London, Ontario, Canada. The working volume was 2 L with a filling ratio of 50% and a flowrate of 3 L/d. The reactors were operated with 3 cycles/day, 8 hours per cycle (480 mins). Each cycle consisted of 0.5hr of filling, 1.5 hr of anoxic phase, 4.5 hr of aerobic phase, 1 hr for settling and 0.5 for decanting (Figure 3.7). During the anaerobic phase, mixing was achieved using mechanical stirring to promote the biological phosphorus release. The seed sludge was collected from Greenway WWTP (London, Ontario, Canada) with a concentration of 1430 mg/L for MLSS and 1080 mg/L for MLVSS. The system was operated at an SRT of 10 days for 75 days. Sludge wasting was performed at the end of the aeration phase before the settling phase. The wastewater samples were collected from Greenway WWTP (London, Ontario, Canada). Dissolved oxygen levels were kept in the range of 4-5 mg/L. Allylthiourea was added starting from day 38 to day 75 at 50 mg/L concentration to inhibit nitrification in both reactors in order to focus on the phosphorus removal.

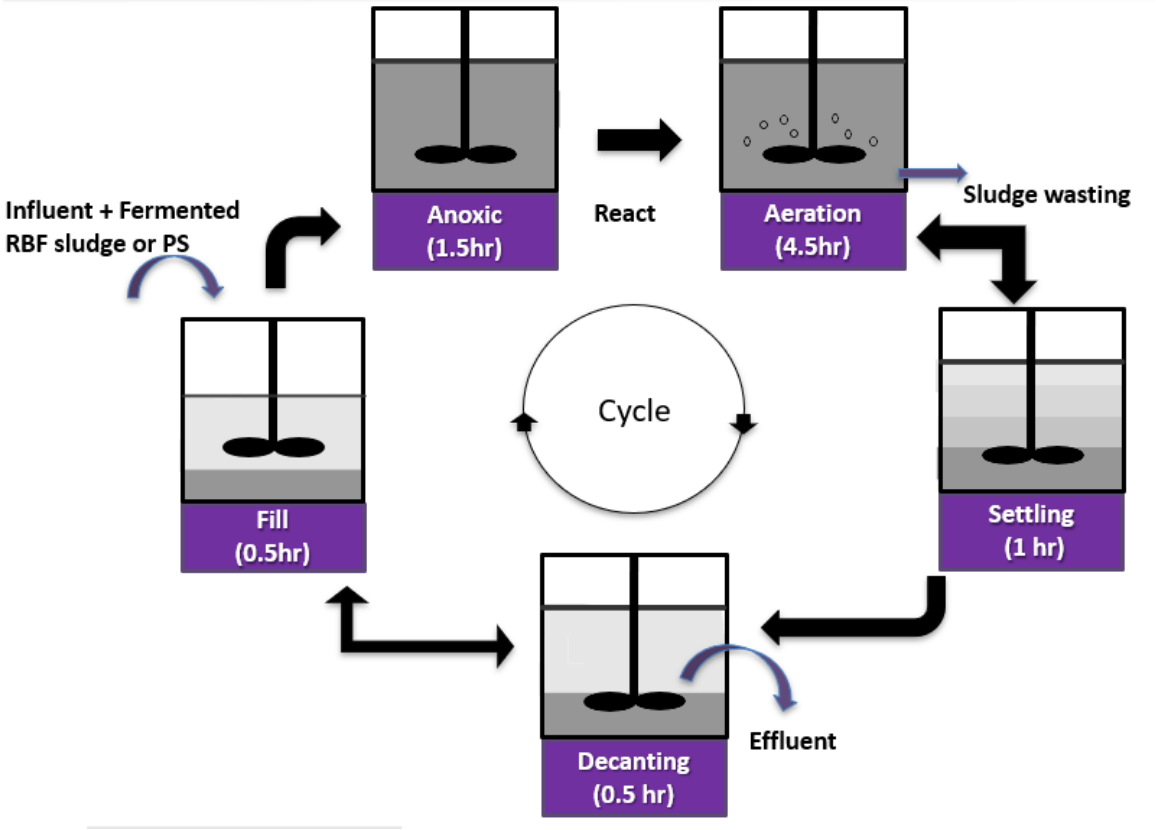

Figure 3.4 SBR cycle operation

The operation comprised three phases: phase 1 (day 1- 42) with both reactors treating primary effluent (PE) without any addition of fermented sludge or allylthiourea to reach the steady-state condition, phase 2 (day 43-53) operation with the supplementation of carbon by addition of fermented primary sludge (PS) to both PE-SBR and RBFE-SBR, and phase 3 (day 54-75) where PE-SBR and RBFE-SBR were supplemented with fermented PS and RBF sludge, respectively. Moreover, phase 2 and 3 included the addition of allylthiourea for nitrification inhibition to focus on the phosphorus removal in both reactors.

Primary sludge (PS) and RBF sludge were collected once a week for the fermentation process from Greenway WWTP (London, Ontario, Canada). Moreover, RBF effluent and sludge were collected from an RBF pilot that was operated in the same treatment plant. Primary and RBF sludges used for fermentation collected from Greenway was characterized as presented in Table 3.12.

Table 3.12 Wastewater and sludge feed characteristics

Parameter	Primary effluent	RBF effluent	Primary sludge feed	RBF sludge feed
PH	7.6 ± 0.3	7.6 ± 0.2	6.2 ±0.3	6.2 ±0.4
Alk	353 ± 23	364 ± 19	1826 ±266	1397 ±210
VFA	-	-	945 ±513	974 ±470
TCOD	230 ± 40	382 ± 46	33331 ±5512	39225 ±14022
SCOD	129 ± 33	149 ± 44	1861 ±925	2042 ±602
TN	29 ± 5	38 ± 5	880 ±275	1383 ±472
SN	23 ± 3	27 ± 5	190 ±108	163 ±79
NH4	21 ± 1	25 ± 3.1	59 ±62	139 ±100
NO3	0.7 ± 0.3	0.6 ± 0.3	16 ±9	17 ±6
NO2	0.02 ± 0.01	0.02 ± 0.01	0.31 ±0.18	0.28 ±0.17
TP	4.7 ± 1.5	9.1 ± 3.2	460 ±202	474 ±170
SP	2.8 ± 0.7	4.1 ± 0.7	38 ±14	50 ±15
TS	-	-	26302 ±4601	50612 ±10841
VS	-	-	19173 ±2869	33083 ±11182
TSS	87 ± 11	257 ± 63	-	-
VSS	64 ± 9	159 ± 42	-	-

Anaerobic fermentation was done continuously for an SRT of 4 days for both sludge types at a temperature of 35°C. The working volume of the fermentation reactors were 400 ml. After the fermentation, the supernatant of both fermented sludges was separated from the solids using a mechanical centrifuge. Two cycles of centrifugation were applied to the sludges after fermentation. The sludges were centrifuged at 2400 g (2500 rpm) for 15 minutes per cycle of centrifugation. The centrifuge process was followed with filtration using double 1.2 μm filters in order to reduce the suspended solids as much as possible not to affect significantly the solids concentration in the reactors. PE-SBR and RBF-SBR were enriched with 120 ml of fermented PS and RBF supernatant at the start of each cycle as a carbon source to enhance the biological phosphorus removal process. The added fermetates volume was calculated based on keeping a minimum SCOD/TN ratio of 6 and SCOD/TP of 20.

3.3.2 Cyclic Tests

Three cyclic tests were done in the third phase of the experiment on three different days for PE-SBR and RBF-SBR to monitor the biological phosphorus removal inside the reactors starting from the feeding phase at t=0 till the end of the reaction phase at t= 6 (before the settling phase). Samples were collected every 15 mins and filtered instantly to prepare the soluble fraction, and analyzed during feeding, anaerobic, and aerobic phases. Soluble phosphorus, soluble COD, ammonia, nitrate, and nitrite were analyzed for each sample of the three cyclic tests using Hach Methods.

For the sludge samples which include the PS feed, RBF feed, fermented PS, fermented RBF, PS supernatant and RBF supernatant. Total COD, soluble COD, total nitrogen, soluble nitrogen, ammonium, nitrate, nitrite, total phosphorus, soluble phosphorus, volatile fatty acids (VFA) were analyzed twice a week (same analysis day of the influent and effluent samples) according to Hach Methods and suspended solids and alkalinity according to Standard Methods (APHA, 1998). Influent and sludge characteristics are summarized in table 3.12.

Chapter 4.

Aerobic Cellulose Degradation in Sequencing Batch Reactors results

4.1 SBR performance

The influent and effluent water qualities during the steady-state operational periods in phases 1 and 2 are summarized in Table 4.1. Average influent TSS, COD, TN, and TP levels in phases 1 and 2 were 208-361 mg/L, 359-456 mg/L, 37-45 mg/L, and 7.6-7 mg/L, respectively. Average effluent SCOD of R1-R4 were 28-35 mg/L in phase 1 and 36-45 mg/L in phase 2. Generally, effluent SCOD increased at lower temperature and shorter SRT. COD removal efficiencies were 92%-94% in phase 1 and 88%-90% in phase 2, slightly increasing with higher temperature.

Effluent soluble nitrogen concentrations were 8-13 mg/L in phase 1 and 19-27 mg/L in phase 2, decreasing with higher temperature and longer SRT. Particularly, nitrification was hampered at low temperature and short SRT. Nitrogen removal efficiencies calculated based on influent TN and effluent SN increased with higher temperature from 65% (R1) to 78% (R4) in phase 1 and from 41% (R1) to 63% (R4) in phase 2.

As evident from Table 4.1, effluent SP concentrations generally increased with temperature and ranged between 0.2-0.8 mg/L in phase 1 and 0.2-0.4 mg/L in phase 2. Phosphorus removal efficiency decreased with increasing temperature from 97% (R1) to 89% (R4) in phase 1 with similar observations of 94%-96% in phase 2. This trend was related to P uptake for cell synthesis, which decreased for the reactors at higher temperature due to the lower sludge yield. However, the trend was not pronounced in phase 2 possibly because operation at SRT of 3 days showed low biomass concentrations.

Table 4.1 Summary of wastewater characteristics during steady-state conditions in SBRs

	Phase 1 (Day 37-100) (n=19)					Phase 2 (Day 110-160) (n=14)				
		R1 (10°C)	R2 (17°C)	R3 (25°C)	R4 (33°C)		R1 (10°C)	R2 (17°C)	R3 (25°C)	R4 (33°C)
	Influent	Effluent	Effluent	Effluent	Effluent	Influent	Effluent	Effluent	Effluent	Effluent
pH	7.5±0.3	8.0±0.3	8.1±0.3	8.2±0.2	8.2±0.2	7.4±0.3	7.9±0.3	8.1±0.3	8.2±0.3	8.2±0.2
Alkalinity (mgCaCO3/L)	375±35	243±29	247±33	249±25	261±31	368±32	275±33	287±31	286±29	277±35
TSS (mg/L)	208±72	24±10	21±10	19±10	18±10	346±79	23±11	29±6	21±5	17±10
VSS (mg/L)	144±47	16±8	11±7	9±7	9±6	233±55	11±12	16±13	12±10	8±8
TCOD (mg/L)	359±104	35±11	34±9	28±7	29±6	447±132	75±26	64±16	61±18	54±16
SCOD (mg/L)	142±41	28±9	26±8	23±7	26±7	138±36	54±17	44±12	44±12	44±16
TN (mgN/L)	37±8	-	-	-	-	45±8	-	-	-	-
SN (mgN/L)	28±4	13±4	12±3	10±3	8±4	34±5	26±9	25±8	22±13	17±10
Amm-N (mgN/L)	25±4.3	1.3±2.0	1.0±3.3	0.6±1.4	0.2±0.2	25±5	20±8	18±6	15±10	11±7
NO3 (mgN/L)	0.4±0.1	10.7±2.3	10.0±3.0	9.4±3.1	7.8±3.1	0.5±0	1.6±1	1.9±1	2.5±2	3.1±1
NO2 (mgN/L)	0.0±0.0	0.1±0.1	0.1±0.1	0.1±0.2	0.2±0.1	0.1±0	4.8±7	0.9±0	0.9±1	0.9±0.3
TP (mgP/L)	7.6±4.1	-	-	-	-	7.4±2	-	-	-	-
SP (mgP/L)	2.5±1.3	0.2±0.2	0.4±0.8	0.5±0.5	0.8±0.3	1.2±1	0.3±0.2	0.3±0.2	0.4±0.3	0.4±0.3
Reactor										
MLSS (mg/L)		4100±790	3800±1300	3200±1400	2800±1100		1400±610	1400±600	1600±850	1500±860
MLVSS (mg/L)		2900±400	2500±800	2000±800	1700±600		810±260	800±240	850±320	800±330
Sludge yield (gVSS/gCOD)		0.26	0.23	0.21	0.16		0.21	0.18	0.18	0.18

The overall removal efficiencies of COD, total nitrogen (TN) and total phosphorus (TP) are summarized in table 4.2. For the COD and TN removal, the removal efficiencies increase with the temperature increase due to the higher maximum growth rate (μ_{Hmax} at (T)= μ_{max} at T(20).Θ^{T-20}). Hence, with the increase of the temperature, the microorganism's activities rate increase which by turn raise the removal efficiency. However, for the phosphorus removal, decreasing the operation temperature increase the removal efficiency for the reason of the higher formation of biomass in lower temperature reactors which increase the phosphorus removed during cell synthesis (Tchobanoglous et al., 2003b).

In phase 2, the reactors SRT decreased to 3 days. For the COD and total Nitrogen (TN) removal efficiencies decreased compared to phase 1 due to the drop that occurred in all SBRs in the biomass concentration. Between the four SBRs, the removal efficiencies followed the same trend of increasing with the temperature increase for COD and TN, and decreasing for the TP removal.

Table 4.2 SBRs removal performances

	Average Removal (%)	R1	R2	R3	R4
Days 37-100 SRT 15 days		(10 °C)	(17 °C)	(25 °C)	(33 °C)
	COD	92	93	94	93
	TN	65	69	72	78
	TP	97	95	93	89
	Average Removal (%)	R1	R2	R3	R4
Days 110-135 SRT 3 days		(10 °C)	(17 °C)	(25 °C)	(33 °C)
	COD	90	92	92	92
	TN	40	44	50	57
	TP	97	98	95	95

Temperature and SRT effects on the volatile fraction of mixed liquor were pronounced, with the volatile fraction decreasing with higher temperature and shorter SRT. The heterotrophic decay rate is temperature dependent ($b_H = b_{H,20}\theta_{bH}^{T-20}$), which indicates that with the increase of temperature, the decay rate increases. Figure 4.1 presents the mixed liquor suspended solid profiles of R1-R4 during the two phases of the experiment (SRT 15&3 days). As shown the biomass profiles below, it indicates the higher biomass concentration with the lower temperature of R1 at 10°C and the lower biomass concentration took place in R4 operated at the highest temperature of 33°C. Moreover, as indicated in the same figure below that all the reactor biomass (VSS) concentrations dropped scientifically with reducing operation SRT of the SBRs from 15 days to 3 days. The net biomass yield (Ynet) expressed as biomass yield (Y) /(1+b_HSRT) also demonstrates that a higher decay rate reduced net biomass yield in the reactors.

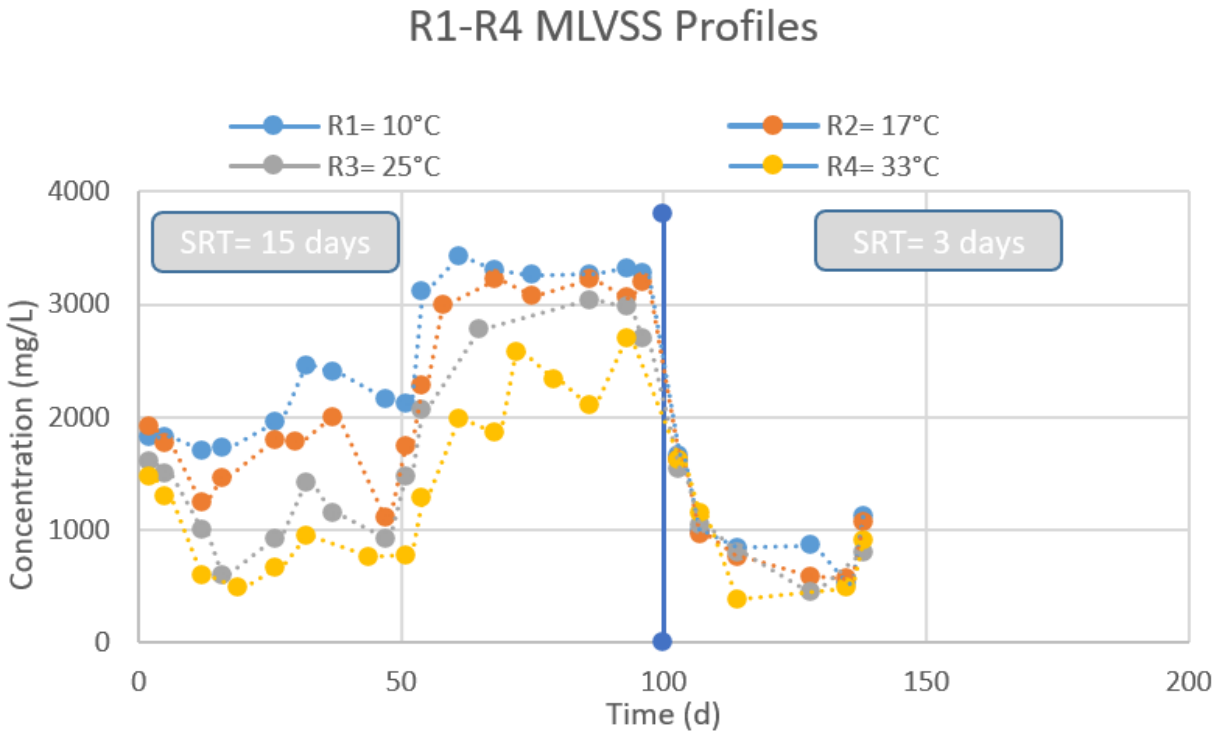

Figure 4.1 Mixed liquor suspended solids profiles

4.2 Fate of cellulose in SBRs and hydrolysis rates

Cellulose concentrations in the influent, effluent, and sludge are summarized in Table 4.3. Average influent cellulose concentrations in phases 1 and 2 were 36 and 66 mg/L, accounting for 17%-20% of the influent TSS. Similarly, average effluent cellulose concentrations in both phases were mostly 2-3 mg/L, accounting for 4%-15% of the effluent TSS, similar to the effluent qualities of two full-scale WWTPs (Ahmed et al., 2019b). Cellulose concentrations in the sludge were 18-81 mg/L for both phases, accounting for 1%-2% of MLSS in phase 1 and 2%-5% of MLSS in phase 2, similar to 1%-2% of MLSS at SRT 7 &14 days reported by Ahmed et al., (2019).

Table 4.3 Cellulose concentrations and degradation

		Effluent (mg/L)				**Sludge (mg/L)**			
	Influent (mg/L)	R1 (10°C)	R2 (17°C)	R3 (25°C)	R4 (33°C)	R1 (10°C)	R2 (17°C)	R3 (25°C)	R4 (33°C)
Phase 1 SRT 15 (d)	36±20 (13)	2±1 (13)	2±1 (13)	3±2 (13)	2±1 (13)	81±26 (10)	51±30 (10)	36±23 (10)	18±11 (10)
Phase 2 SRT 3 (d)	66±49 (7)	2±3 (7)	2±2 (7)	2±1 (7)	4±3 (7)	57±37 (7)	56±22 (7)	44±17 (7)	31±17 (7)
		Degradation efficiency (%)							
		R1 (10°C)	R2 (17°C)	R3 (25°C)	R4 (33°C)				
Phase 1 SRT 15 (d)		80	83	84	90				
Phase 2 SRT 3 (d)		78	80	83	85				

The fate of cellulose was examined using cellulose mass balances on a cumulative basis (equation 4.1).

$$Biodegradtion\ effeciency\ = \frac{Inf\ cellulose-(Eff\ cellulose+Waste\ cellulose+Bioreactor\ cellulose)}{Inf\ cellulose}\ x\ 100$$

(4.1)

Based on the cellulose mass balance, the estimated cellulose biodegradation efficiency was 80%-90% during phase 1 and 78%-85% in phase 2. The estimated degradation efficiencies (table 4.3) during phase 1 indicated the effect of increasing the temperature in increasing the cellulose biodegradation efficiencies.

Figure 4.2 present the four reactors cellulose degradation efficiencies (%) with respect to temperature. The mentioned figure proved the higher the temperature the higher the cellulose degradation efficiency for the same SRT. It also shows the effect of decreasing the SRT on decreasing the hydrolysis efficiency to 3 days compared to the degradation efficiencies at the SRT of 15 days.

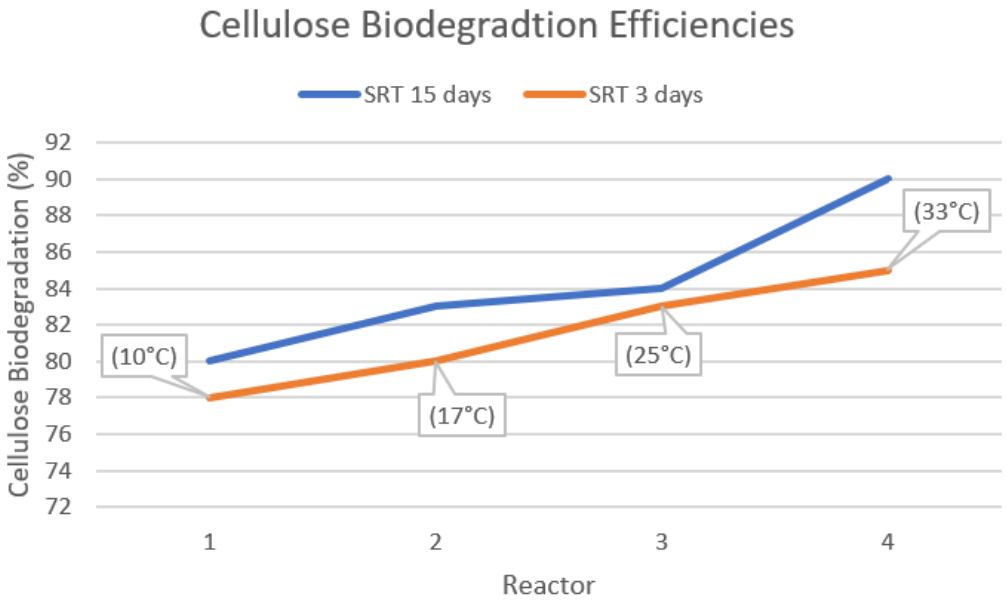

Figure 4.2 Cellulose Biodegradation efficiency with temperature

The cumulative mass balance shown in figure 4.3 was used to estimate cellulose biodegradation by subtracting the sum of effluent, waste sludge, reactor cellulose from influent.

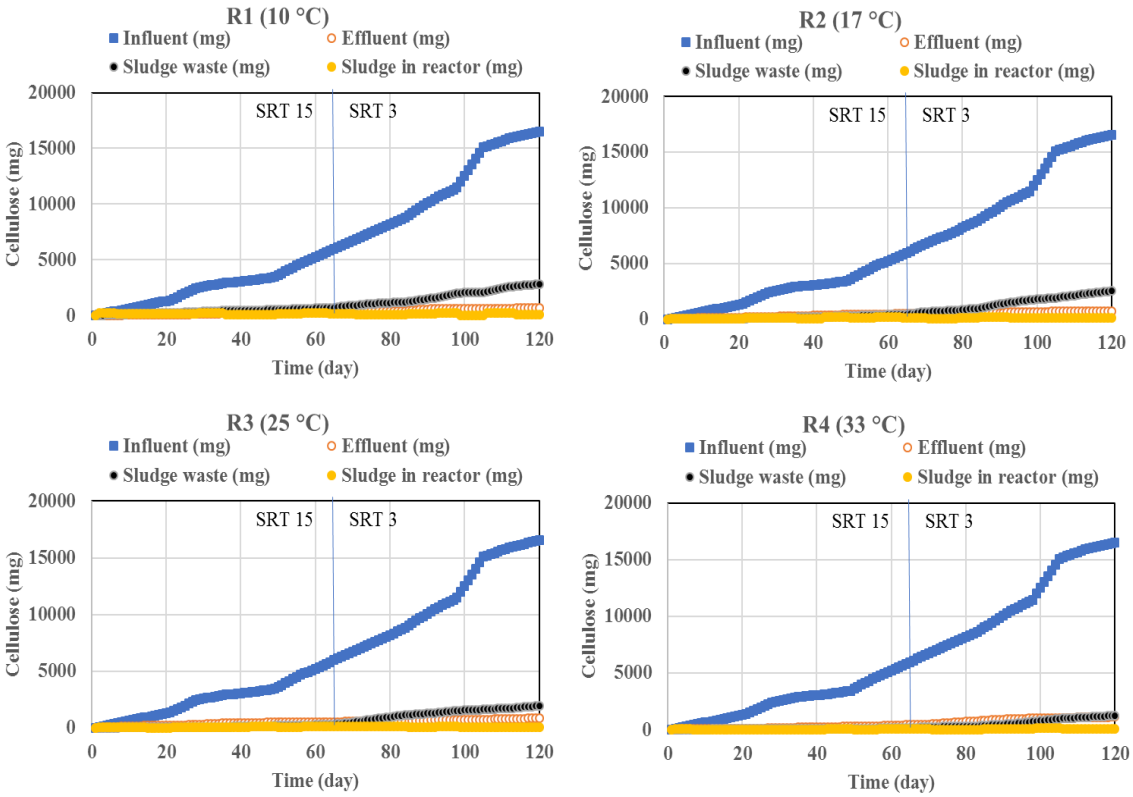

Figure 4.3 Cumulative mass of cellulose in influent, effluent, sludge, and bioreactor

As shown in figure 4.3, the cumulative cellulose mass balance indicated that cellulose in effluent, waste sludge, and reactor cellulose were 6%-9%, 2%-12%, <2% of influent for phase 1 and 2%-7%, 11%-20%, <0.1% for phase 2, respectively. It should be noted that the distribution of cellulose between biomass and effluent was dependent on SRT and temperature. At an SRT of 15 days, the abundance of cellulose in biomass, relative to the effluent increased with lower temperature. At the shorter SRT of 3 days, cellulose was more abundant in waste sludge than the effluent regardless of temperature. The cellulose distribution values (%) in the influent, biomass and effluent are summarized in table 4.4.

Table 4.4 Cellulose distribution in effluent and sludge waste relative to influent based on cumulative mass

		R1	R2	R3	R4
Phase 1 (SRT 15 day)	Effluent (%)	5.8	8.0	8.9	6.9
	Sludge waste (%)	11.9	7.2	4.8	2.3
	Reactor (%)	2.1	2.1	2.1	1.0
Phase 2 (SRT 3 day)	Effluent (%)	3.4	2.4	3.1	6.8
	Sludge waste (%)	19.9	19.5	15.5	10.5
	Reactor (%)	<0.1	<0.1	<0.1	<0.1

Summarizing the cellulose concentrations at the two different operation SRTs of 15 and 3 days in figure 4.4, it shows that cellulose degradation efficiency is dependent on temperature (increasing with the temperature increase) and on SRTs showing lower degradation efficiency when in phase 2 when SRT decreased to 3 days. It also shows the cellulose concentration relatively to mixed liquor (MLVSS) concentration of 1%-2% and 2%-5% at SRT of 15 and 3 days, relatively which indicated that cellulose concentration in the SBRs increase with the SRTs decrease.

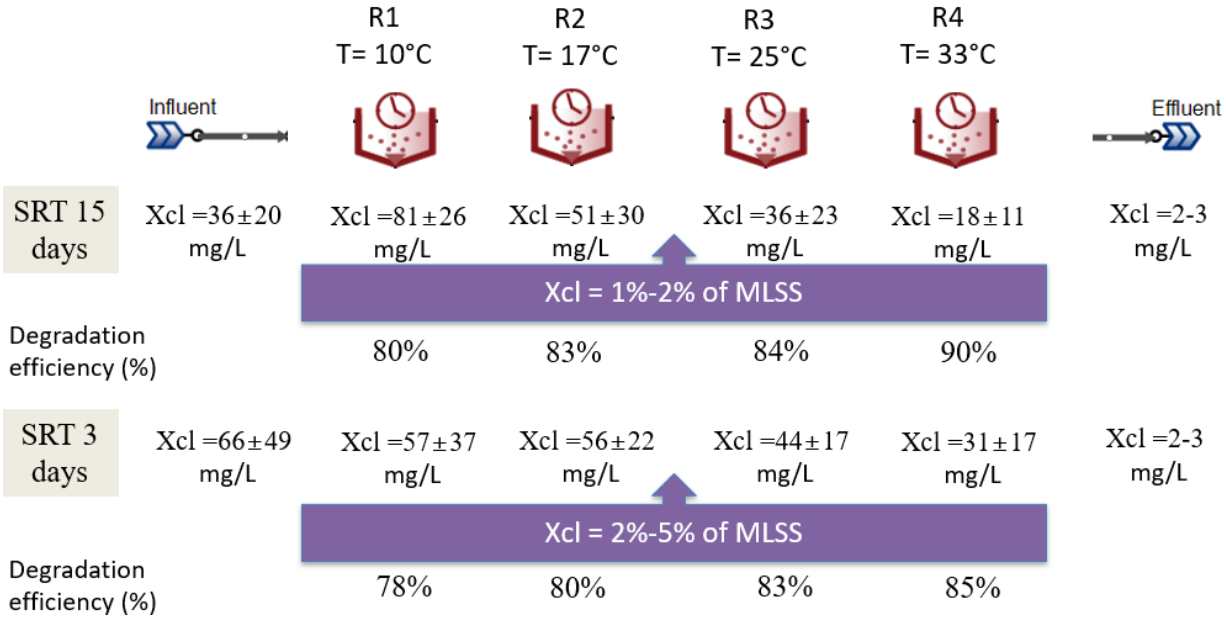

Figure 4.4 Cellulose distribution between reactors (influent, reactors and effluent) at the different SRT values

Cellulose Biodegradation Study Results Summary

From the previous study of cellulose biodegradation, based on the experiment results it can be concluded that:

1. From the influent, biomass and effluent cellulose concentrations, cellulose degradation is mainly dependent on temperature and biological reactors SRTs.

2. Cellulose concentrations in the bioreactors increase with lowering the SRT (1%-2% at SRT of 15 days increased to 2%-5% of the bioreactors MLVSS at SRT of 3 days).

Chapter 5.

Respirometry Results

5.1 Respirometry tests

Calculating OUR curves through oxygen uptake data

Respirometry tests mechanism is simply to monitor the dissolved oxygen (DO) consumption and compute the oxygen mass balance over the liquid phase (Rossi et al., 2020). The respirometer records oxygen uptake data (OU) every 10 mins for the whole running period of the experiment until the OU curve reach a plateau. Oxygen uptake rate is the slope of OU versus time. Based on the oxygen uptake data outputs from the respirometry tests, oxygen uptake rates are basically obtained through calculating the derivative of DO curve (OUR= dO2/dt). Oxygen uptake rates time profiles were plotted for all respirometry runs.

An example of oxygen uptake output curve of one of the respirometry tests of R1 at an S/X of 4 gCellulose_COD/gVSS operated at a temperature of 27 ºC, after the addition of 120 mg/L of α-cellulose to R1 sludge reporting dissolved oxygen readings (mgO_2/L) throughout the experiment time (6.8 days) is shown in figure 5.1a. Then, in figure 5.1b, the OUR curved was derived by the differentiation of oxygen data with time. The same procedures were completed for all respirometric runs.

a)

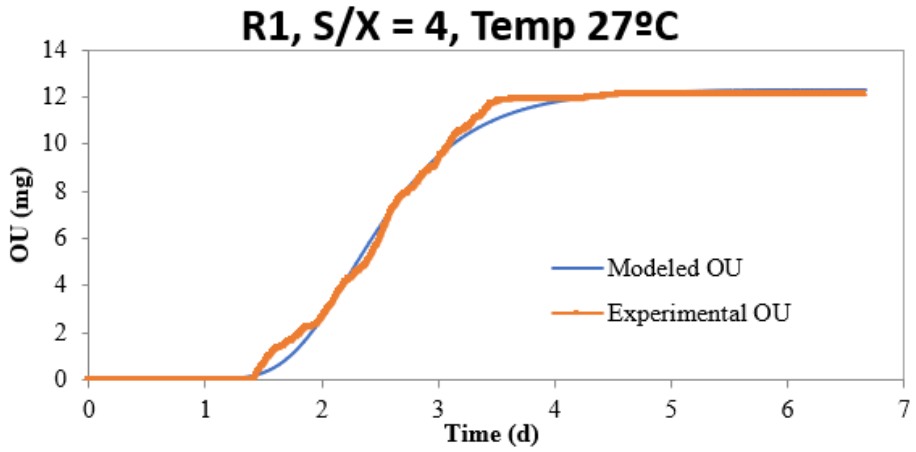

b)

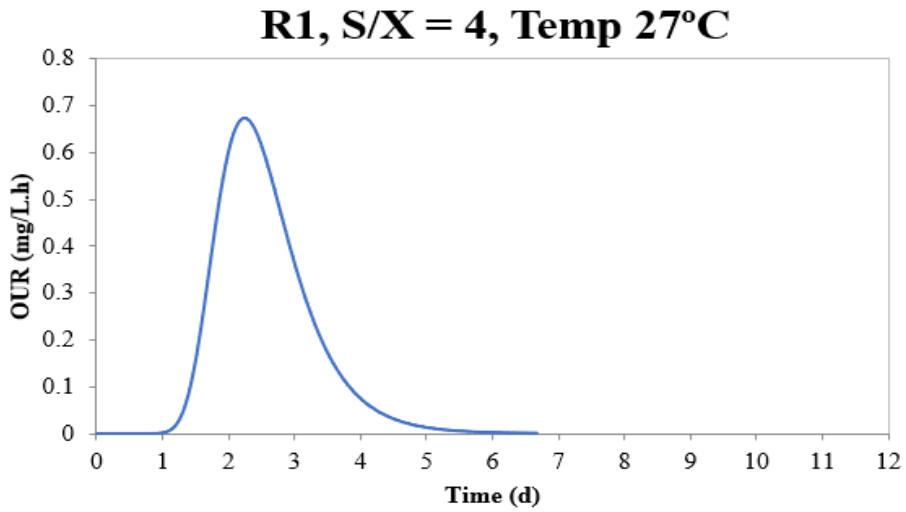

Figure 5.1 Obtaining OUR time profile from OU data, a) OU output of respirometer, b) OUR curve for the same respirometric run

5.2 Simulation results

5.2.1 Models calibration parameters

The μmax controlled the peak level of OUR on the y-axis ($mgO_2/L.h$) with time (d) on the x-axis. Figure 5.2 shows the effect of decreasing μmax value from 6 1/d to 3 1/d, which decreased the peak OUR value from 1.1 to 0.65 mg/L.h.

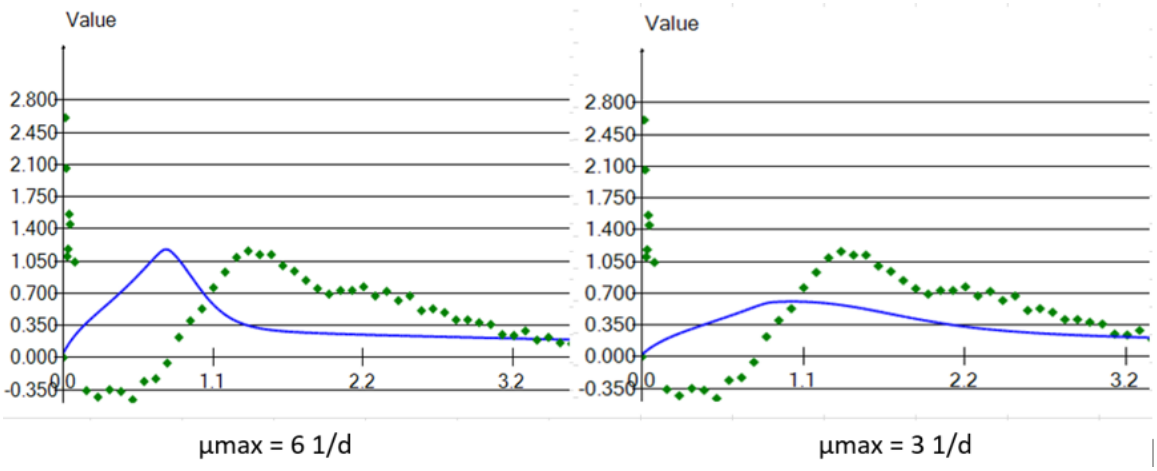

Figure 5.2 Effect of μmax on OUR profiles

For the cellulose hydrolysis factor, it affected the OUR profiles since it controls the availability of food. Figure 5.3 presents an example of an OUR profile of one respirometry run (OUR values on y-axis with time (days) on the x-axis). It shows that decreasing the Khcl decreased the curves slopes which indicates how fast the cellulose is being hydrolyzed and converted to soluble substrate (SS) ready to be utilized by the microorganisms. The y-axis presents the OUR levels ($mgO_2/L.h$) and the x-axis presents the experiment time (d). The effect of decreasing the Khcl from 3 1/d to 1 1/d increased the time to reach peak OUR to 1.5 days from 0.8 days.

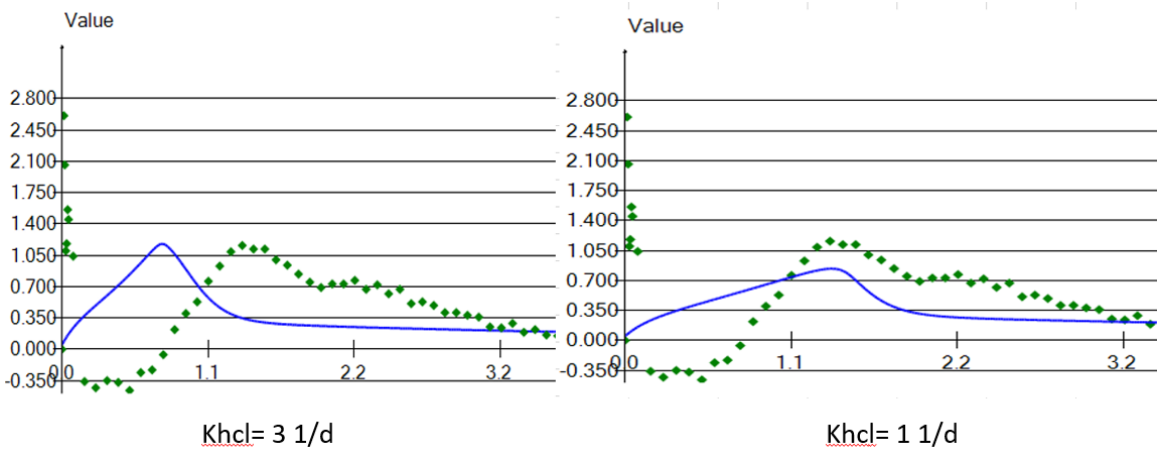

Figure 5.3 Effect of cellulose hydrolysis factor on OUR profiles

It should be noted that the experimental OUR profiles had a lag phase at the start of the experiments which is considered as an adaptation phase for the microorganisms in the new systems. The models did not estimate that lag phase.

5.2.2 Alpha Alpha Cellulose High S/X models

Six respirometric models for high F/M with the addition of α-cellulose were developed on samples from R1 and R4 from the SBR system. The six runs of R1 and R4 were conducted at a temperature of 27°C. The respirometry tests of α-cellulose for both high and low S/X are summarized in figure 5.4. The substrate (S) represents the initial cellulose concentration and the biomass (X) are the initial heterotrophs microorganism concentration.

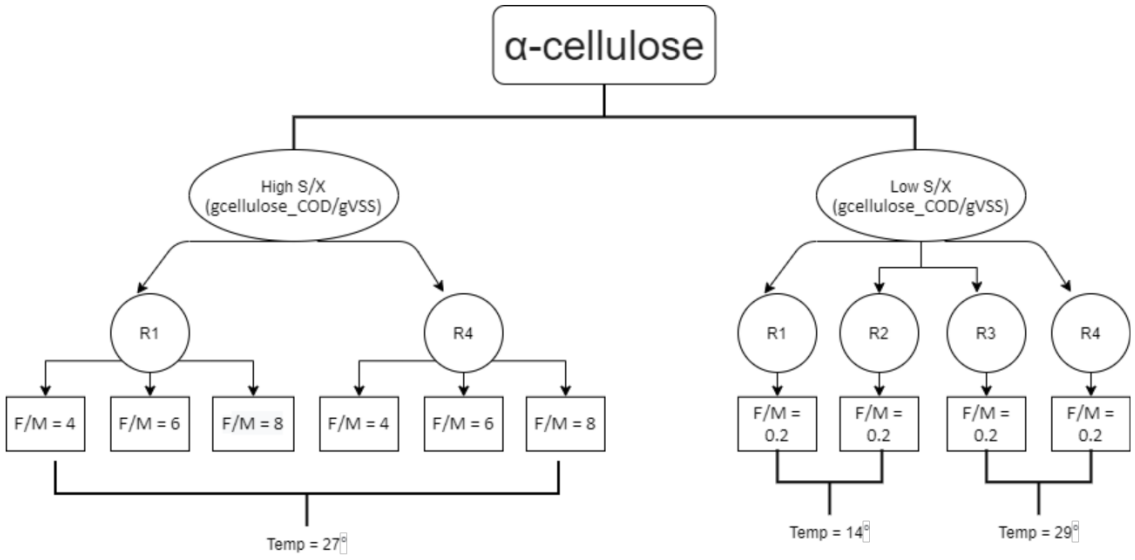

Figure 5.4 α-cellulose high and low S/X models

The hydrolysis rate coefficients of α-cellulose were estimated using SUMO software. Different oxygen uptake rate profiles were monitored at high S/X and were compared with simulated OURs. In this comparison, OUR of mixture of substrate and biomass, biomass alone, and net OUR (substrate alone) were fitted. This comparison was necessitated by the fact that the seed biomass for the respirometry originated from the SBRs and still contained fibrous cellulose, albeit at very low concentrations (2%-8% of the concentration of the α-cellulose added). The parameters maximum growth rate (μ_{max}), Half saturation factor (K_S), and the cellulose hydrolysis rate coefficient (khcl) were changed to match the measured OUR and simulated OUR profiles. It must be asserted that while some of the experimental data showed a lag of 1-2 days, as expected, the model did not predict any lag phase.

The models simulated the experimental conditions including the temperature. Kinetics were recalculated at 20 ºC. The temperature correction factor used for µmax and b_H was 1.07 and 1.04, respectively (Tchobanoglous et al., 2003b). Moreover, theta value of 1.072 was used to correct the cellulose hydrolysis rate (Table A2).

5.2.2.1 Experimental versus simulated OUR profiles

5.2.2.1.1 Reactor 1 S/X = 4,6,8 gCOD/gVSS

Experimental and simulated oxygen uptake rates profiles (OUR) of R1 with different S/X of 4,6 and 8 gCOD/gVSS are shown in figures 5.5.

(a)

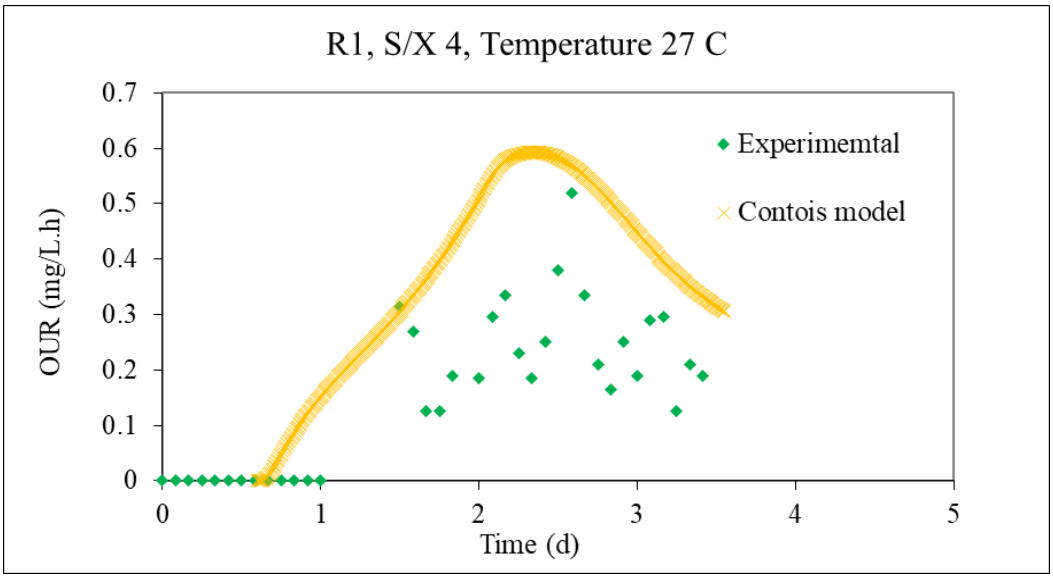

(b)

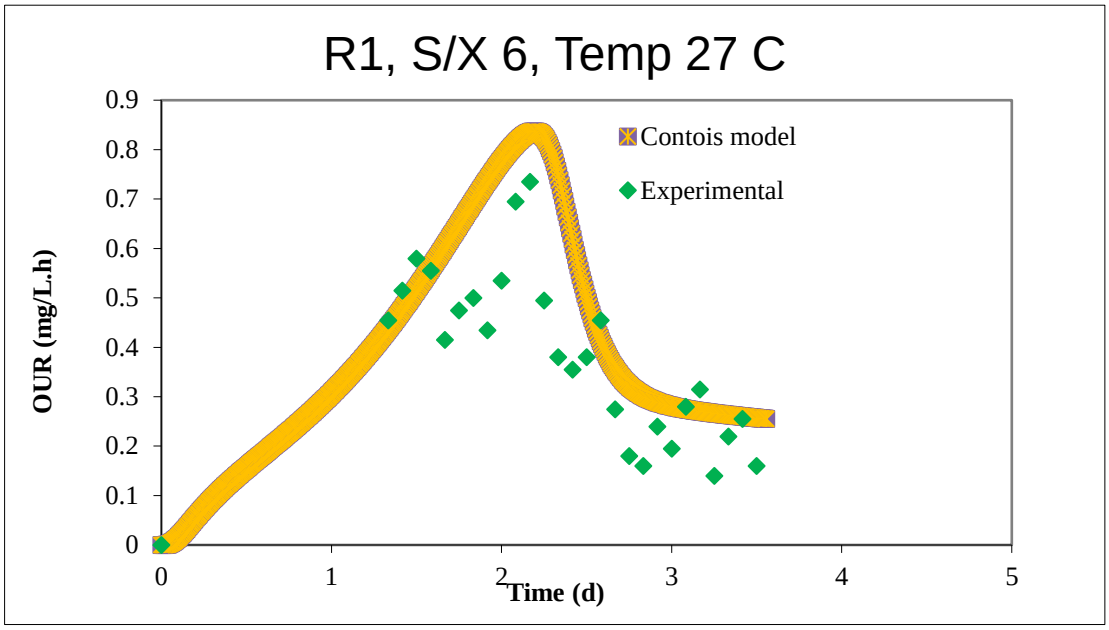

(c)

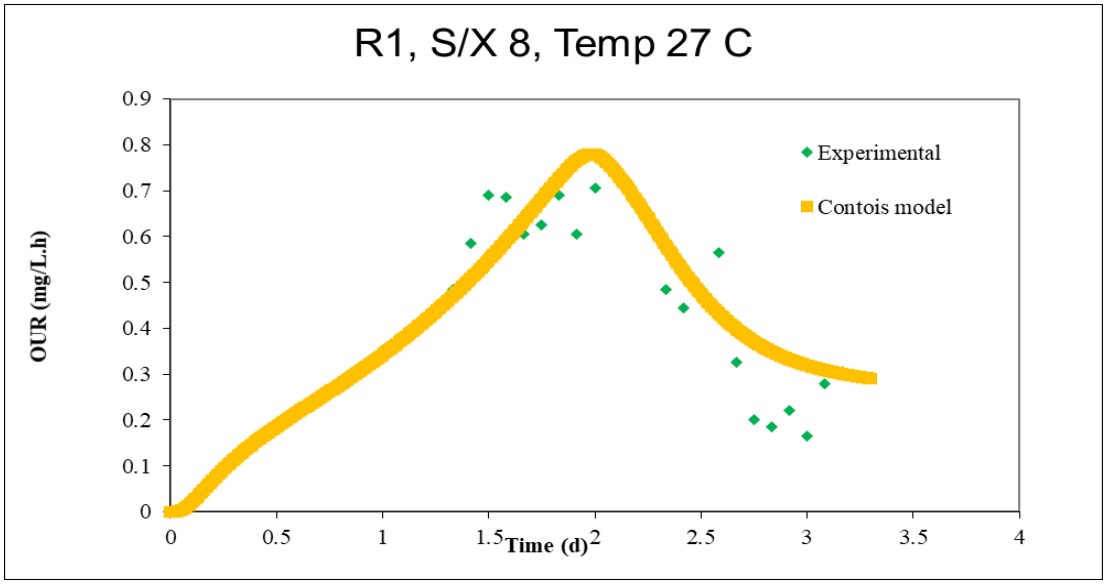

Figure 5.5 α-cellulose, R1 High S/X matching OUR profiles, a) S/X = 4, b) S/X = 6, c) S/X = 8

5.2.2.1.1 Reactor 4, S/X = 4,6,8 gCOD/gVSS

Experimental and simulated oxygen uptake rates profiles (OUR) of R4 with different S/X of 4,6 and 8 gCOD/gVSS are shown in figures 5.6.

(a)

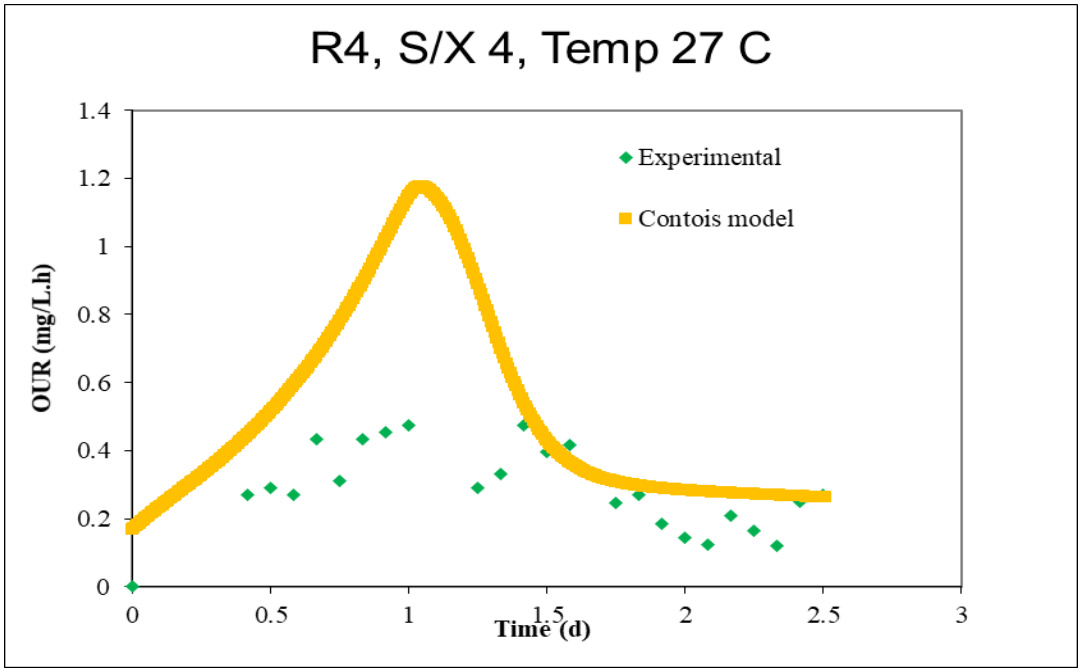

(b)

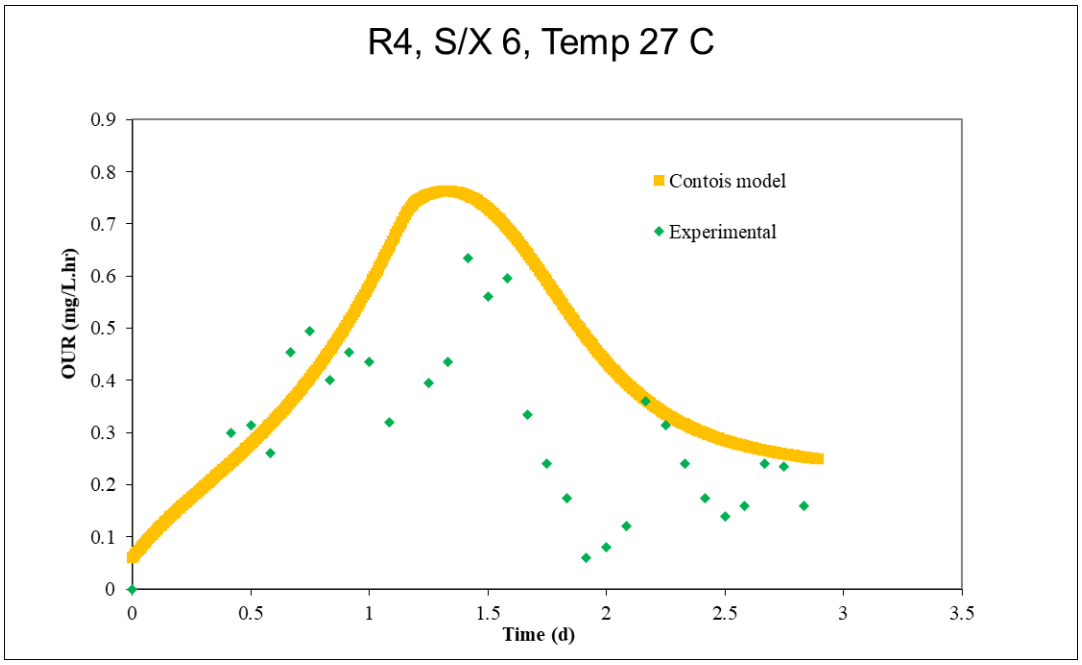

(c)

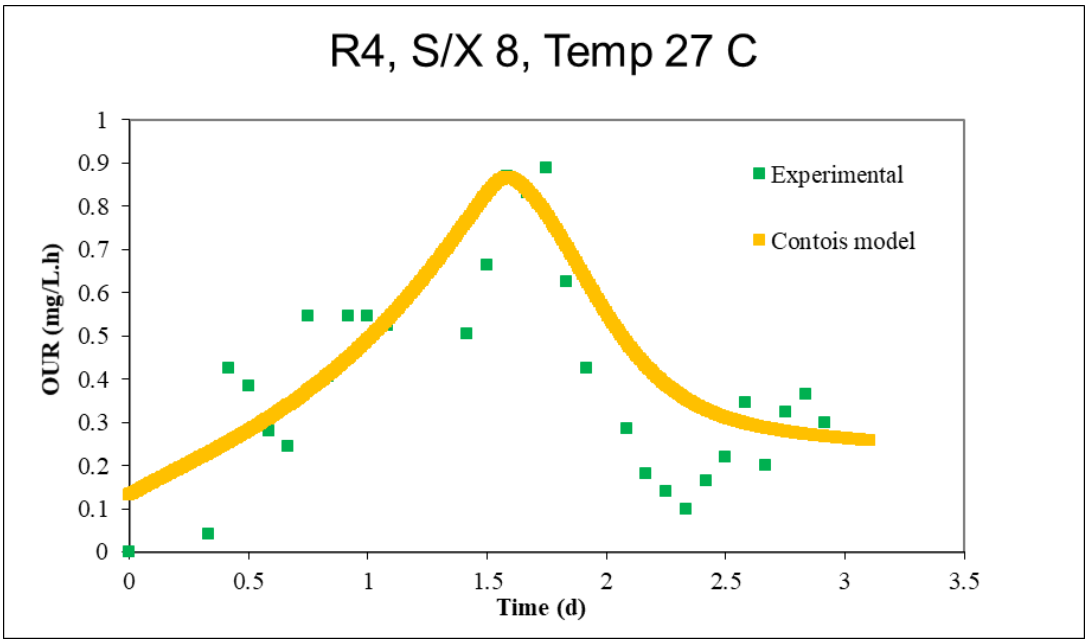

Figure 5.6 α-cellulose, R4 High S/X matching OUR profiles, a) S/X = 4, b) S/X = 6, c) S/X = 8

5.2.2.2 Goodness of fits

5.2.2.2.1 Reactor 1 S/X = 4,6,8 gCOD/gVSS

The simulated output data from the models were compared to the experimental data to evaluate how goodness of fit. Figure 5.7 shows the three cases of high S/X of R1 fits of experimental OUR profiles to the Contois simulated data.

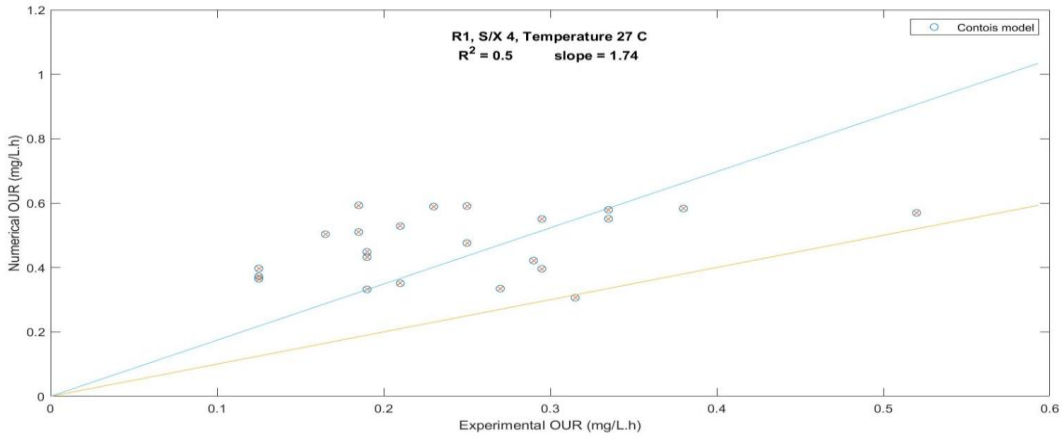

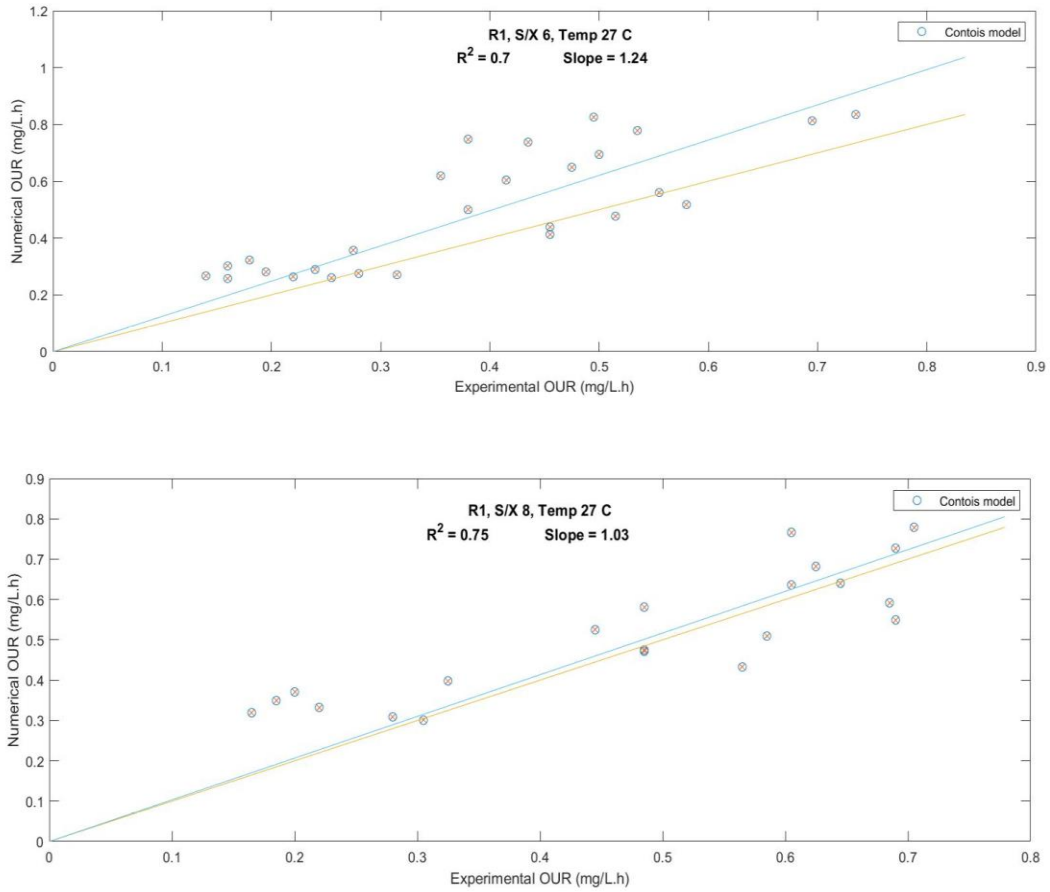

Figure 5.7 High α-cellulose of R1 comparison between experimental and Contois models a) S/X=4, b) S/X = 6, c) S/X= 8

5.2.2.2.1 Reactor 4 S/X = 4,6,8 gCOD/gVSS

Figure 5.8 presents the experimental versus simulated curves as compared above to evaluate the goodness of fit between experimental and simulated data of the three cases of R4 at S/X of 4,6 and 8 operated at a temperature of 27°C.

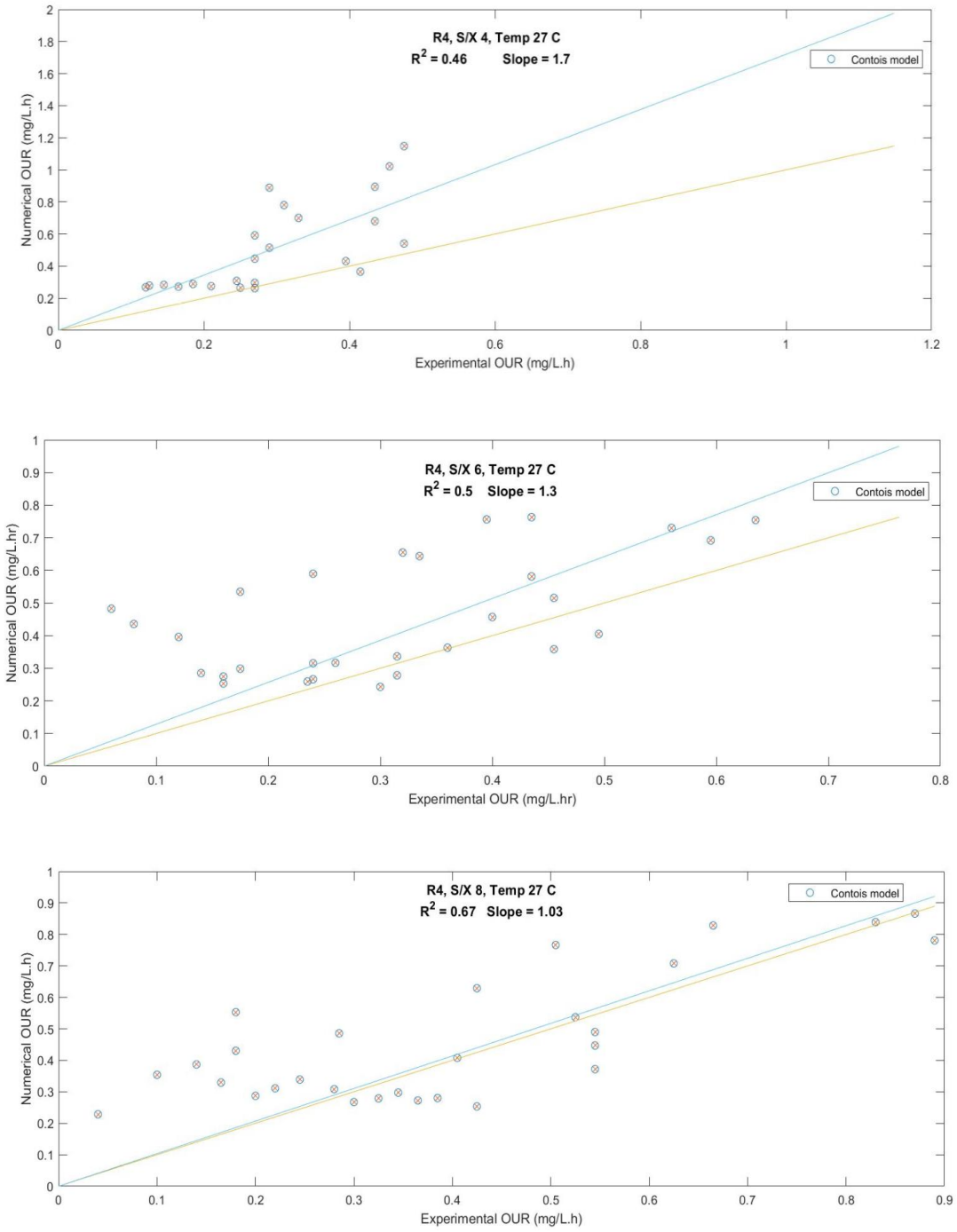

Figure 5.8 High α-cellulose of R4 comparison between experimental and Contois model

The closer the slope of the line presenting the modelled data to the value of 1.0, the more it is representative of the experimental data. The high S/X scenarios showed poor correlations with average slopes of 1.42 and 1.34 for R1 and R4, respectively which indicates that the model does not fit the experimental data (compared to the low S/X cases). In these cases, the models were active biomass limited with high concentrations of substrate (α-cellulose). Hence the hydrolysis factors estimated were more descriptive to the α-cellulose which was the dominant in the high S/X cases (where α-cellulose concentration in the biomass is much greater than the biomass cellulose). Simulation using respirometry tests with α-cellulose showed higher hydrolysis rates of 3 d^{-1} at 20 °C. It was concluded that the Contois model was not well descriptive of the α-cellulose at high S/X cases and the estimated high Kxcl values described the hydrolysis rate of α-cellulose not the cellulose in the biomass.

Table 5.1 presents the summary of kinetics used in the simulation of the six high S/X cases. At the high S/X ratio with α-cellulose, the average hydrolysis rate (Khcl) of cellulose were 3.0 d-1 which represents the hydrolysis factor of α-cellulose. A half saturation concentration of Xcl/Xb,H value of 1 was used in all modelling scenarios based on ASM3 model (Henze et al., 2000b). Active biomass estimation was in the range of 46%-66% of the MLVSS concentrations.

Table 5.1 High S/X models estimated kinetics

	High S/X					
Seed source		R1			R4	
Temperature (°C)	27	27	27	27	27	27
F/M (gCOD/gVSS)	4	6	8	4	6	8
Active cell (mgCOD/L)	13	13	13	10	10	10
PCOD (mg/L)	0.1	0.1	0.1	0.1	0.1	0.1
μmax (d^{-1}) at 20°C	2.4	3	3	2.2	3	3
Ks (mg/L) at 20°C	40	20	40	20	40	35
b_H (d^{-1}) at 20°C	0.4	0.4	0.4	0.3	0.4	0.4
kh (d^{-1}) at 20°C	3	1.9	2.2	3.4	3	2
Khcl at 20°C	3	3	3	3	3	3
Kxcl at 20°C	1	1	1	1	1	1

Where μmax is the maximum growth rate of heterotrophic microorganisms, ks is the half-saturation factor of organics, b_H is the decay rate, kh is the hydrolysis rate of particulates, khcl is the hydrolysis rate of cellulose and kxcl is the half-saturation factor of Xcl/Xh.

5.2.3 Aplha Cellulose Low S/X models

5.2.3.1 Experimental versus simulated OUR profiles

Experimental and simulated oxygen uptake rates profiles (OUR) of R1-R4 with different S/X of 0.2 gcellulose_COD/gVSS are shown in figure 5.9. To more accurately estimate kinetics related to substrate degradation alone at low S/X condition, net OUR (mixture -biomass alone) was simulated.

(a)

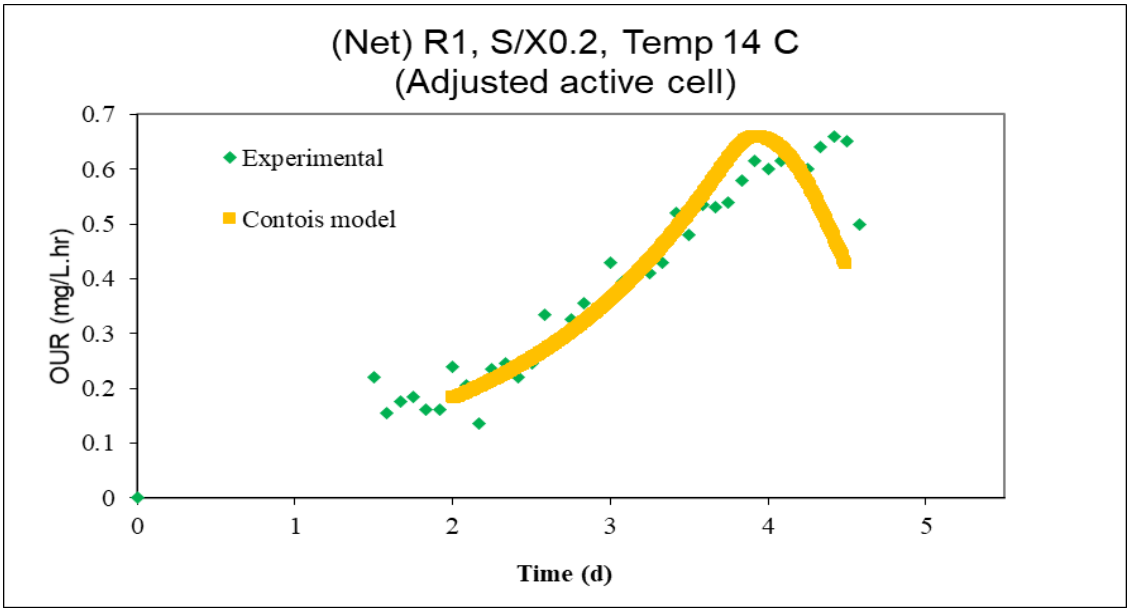

(b)

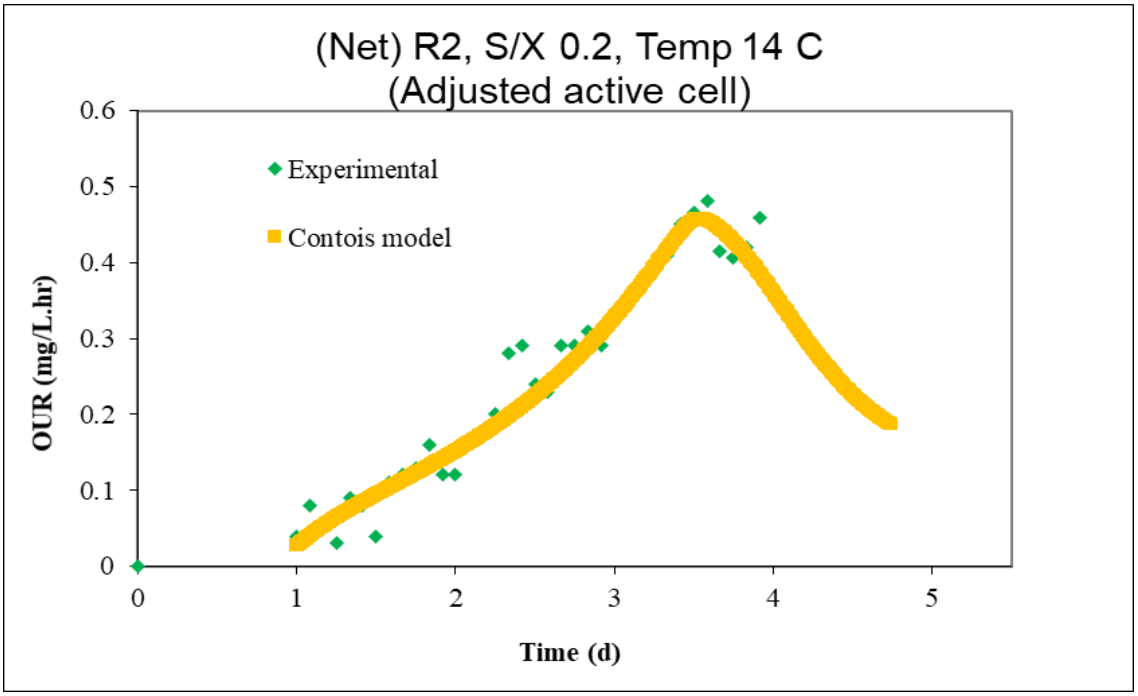
(Net) R2, S/X 0.2, Temp 14 C
(Adjusted active cell)
Experimental
Contois model
OUR (mg/L.hr)
Time (d)
0
0.1
0.2
0.3
0.4
0.5
0.6
0
1
2
3
4
5

(c)

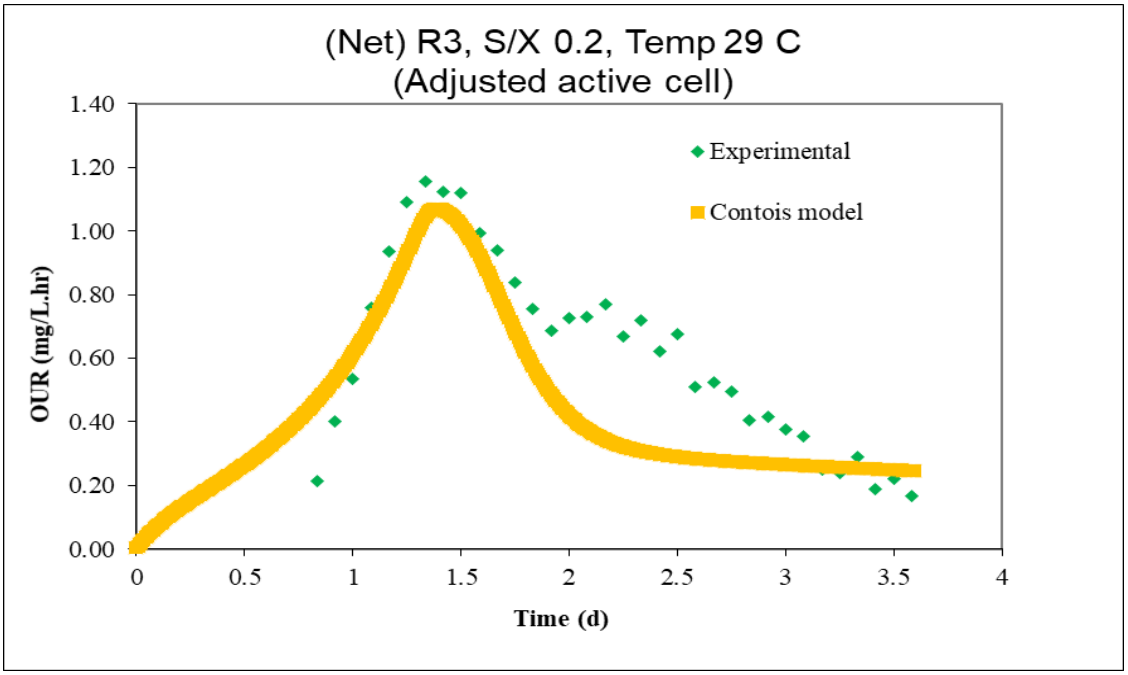
(Net) R3, S/X 0.2, Temp 29 C
(Adjusted active cell)
Experimental
Contois model
OUR (mg/L.hr)
Time (d)
0.00
0.20
0.40
0.60
0.80
1.00
1.20
1.40
0
0.5
1
1.5
2
2.5
3
3.5
4

(d)

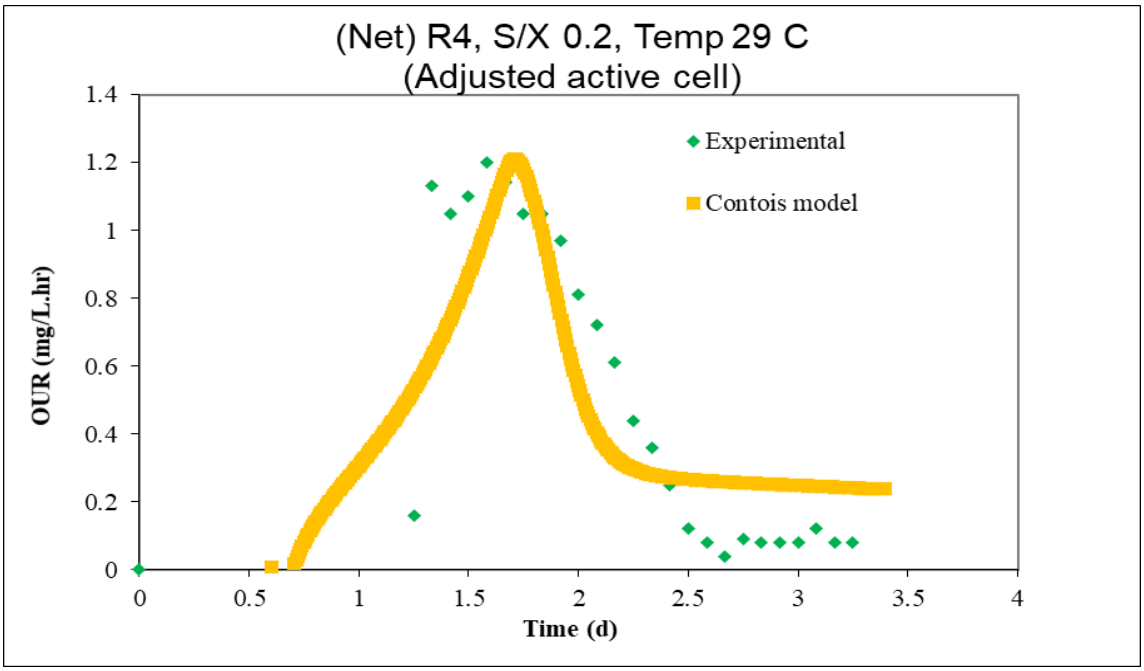

Figure 5.9 α-cellulose, R1-R4 Low S/X matching OUR profiles, a) R1 S/X = 0.2, b) R2 S/X = 0.2, c) R3 S/X = 0.2, d) R4 S/X = 0.2

5.2.3.2 Goodness of fits

Figure 5.10 presents the experimental versus simulated curves as compared above to evaluate the goodness of fit between experimental and simulated data of the four cases of R1-R4 at S/X of 0.2 gcellulose_COD/gVSS operated at a temperature of 14°C and 29°C for R1&R2 and R3&R4, respectively.

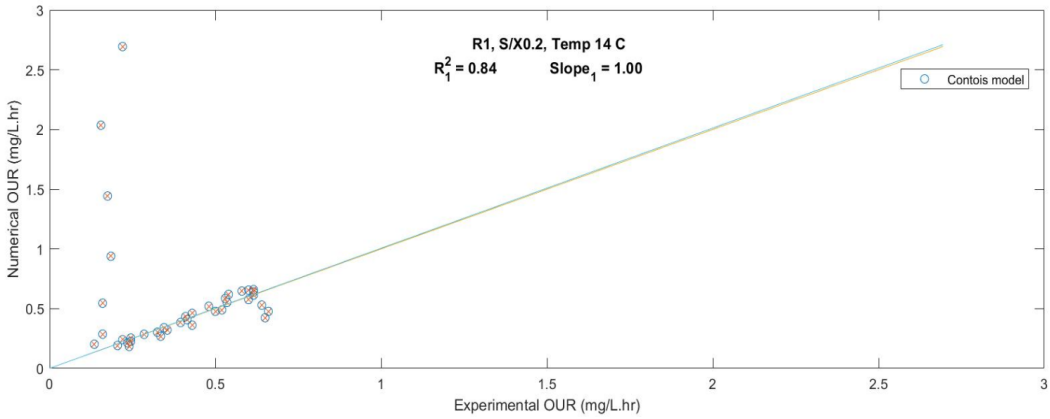

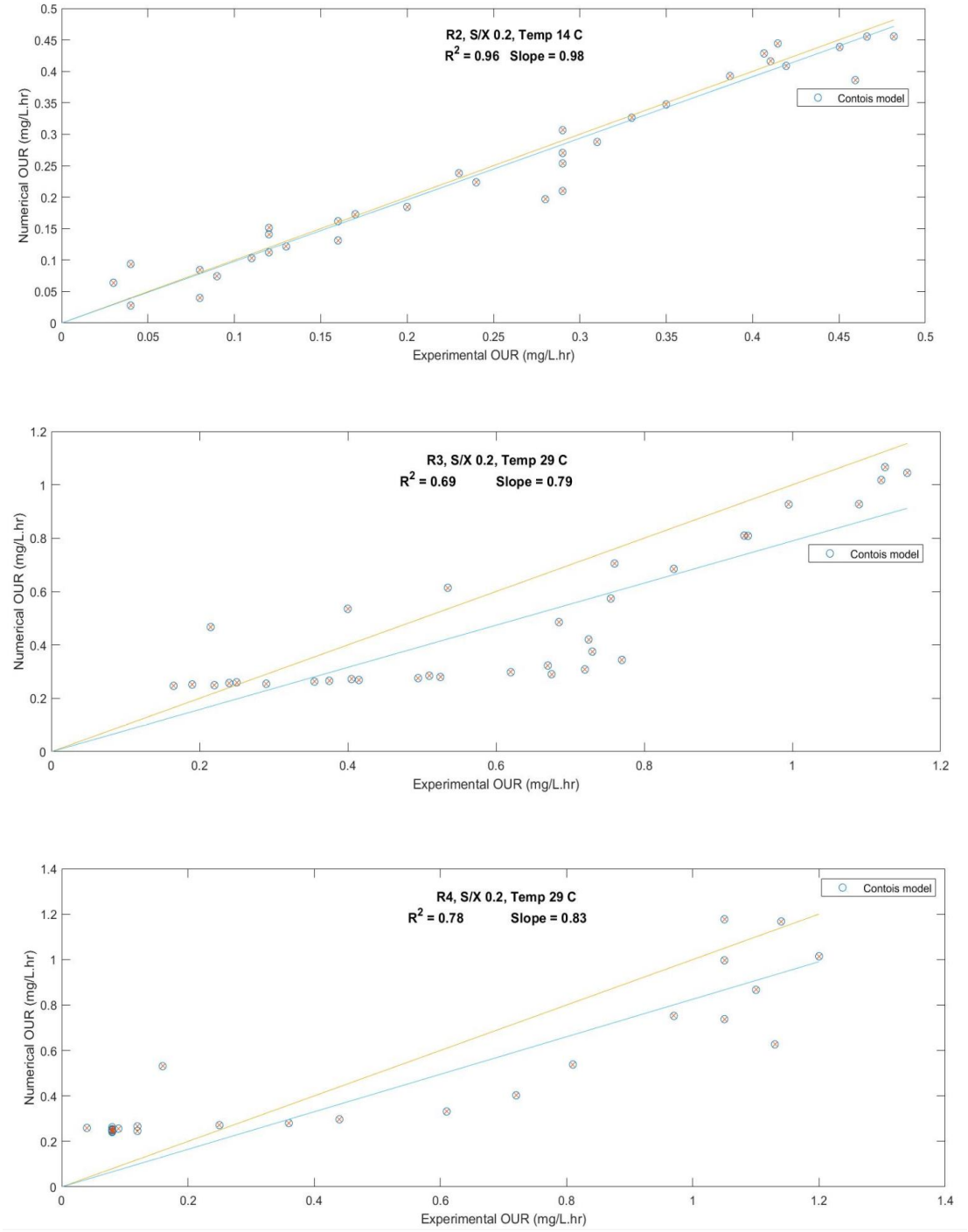

Figure 5.10 Low α-cellulose of R1 to R4 comparison between experimental and Contois Model

For the low S/X cases, scrutiny of the data and change of operational conditions indicated that the simulated curves showed good correlations to the experimental data with average slope of 0.9 which indicates the goodness of fit to the experimental data with the slope of 1 (Figure 5.8). The models were substrate (α-cellulose) limited in these cases; the hydrolysis factors estimated were low compared to high S/X models. The hydrolysis factors estimated for the four cases presented in Table 5.2 were close to the decay constant (b_H) of activated sludge of Henze et al.(2000). In these cases, the cellulose that was dominant the cellulose in the seed sludge.

Hence, the active cells were adjusted from 513-621mgCOD/L to 10 mgCOD/L (table 5.2). This adjustment was necessary to determine the amount of active biomass which actually biodegraded the dominant fibrous cellulose as the simulated curves using the original active cell concentrations did not match the experimental data. Benneouala et al., (2017) also reported that not all the active biomass was involved in the degradation of particulates. The 10 mgCOD/L of active cell concentration was estimated based on trial and error approach by changing active cell concentration and comparing the simulated curves with experimental OUR data. It indicates that although active biomass was abundant, the biomass actually involved in the fibrous cellulose degradation was a small fraction i.e. 2% of the active biomass. This observation agreed with the finding of Benneouala et al., (2017) that cellulose degradation was predominantly done by the colonizing biomass rather than the whole biomass.

Table 5.3 represents the kinetics summary used in modelling the low S/X experimental cases. The average khcl of samples at low S/X ratios was 0.525 d^{-1}. The distinct difference between high S/X and low S/X conditions was related to khcl, which dramatically decreased at low S/X ratios due to influence of active biomass, as the hydrolysis rate of fibrous cellulose alone was estimated as 0.35-0.7 d^{-1} (Table 5.2). At the low S/X ratios, the biomass concentration used was 36-46 times higher than the amount at high S/X ratio, and the influence of biomass levels on OUR curves was significantly higher at low S/X condition.

Table 5.2 Kinetics inputs for R1-R4 Low S/X models

	Low S/X			
Seed source	R1	R2	R3	R4
Temperature (ºC)	14	14	29	29
F/M (gCOD/gVSS)	0.2	0.2	0.2	0.2
Active cell (mgCOD/L)	10	10	10	10
PCOD (mg/L)	0.2	0.2	0.1	0.2
μmax (d^{-1}) at 20ºC	3.0	4.5	3.0	3.0
Ks (mg/L) at 20ºC	20	40	40	20
b_H (d^{-1}) at 20ºC	0.4	0.4	0.4	0.4
kh (d^{-1}) at 20ºC	2.3	2.3	2.7	2.8
Khcl at 20ºC	0.70	0.45	0.60	0.35
Kxcl at 20ºC	1	1	1	1

High and low S/X goodness of fit of α-cellulose are compared in Table 5.3. Low S/X were more describing the experimental data as mentioned earlier by having an average slope of 0.9 (higher than high S/X cases), which indicates the better fits of the OUR experimental and simulated profiles.

Table 5.3 α-cellulose high and low F/M comparison between experimental and Contois model.

	High S/X	High S/X	Low S/X			
Seed source	R1	R4	R1	R2	R3	R4
Temperature (ºC)	2 2 27 7 7	2 2 27 7 7	14	14	29	29
F/M (gCOD/gVSS)	4 6 8	4 6 8	0.2	0.2	0.2	0.2
Khcl at 20ºC	3 3 3.0 . . 0 0	3 3 3.0 . . 0 0	0.7	0.45	0.6	0.3 5
Kxcl at 20ºC	1 1 1	1 1 1	1	1	1	1
b_H (d^{-1}) at 20ºC	0 0 0.4 . . 4 4	0 0 0.4 . . 3 4	0.4	0.4	0.4	0.4
Slope of experimental vs simulated	1 1 1.03 . . 7 2 4 4	1 1 1.03 . . 7 3	1.0	0.98	0.79	0.8 3
R^2	0 0 0.75 . . 5 7	0 0 0.67 . . 4 5 6	0.84	0.96	0.69	0.7 8

5.2.4 Fibrous Cellulose (RBF) high and low S/X models

Two respirometric models for high and low S/X with the addition of RBF were developed on mixture of biomass from reactors 1 and 4 as mentioned earlier. As shown in Figure 5.11, the two runs of R1 and R4 were conducted at a temperature of 20°C. The experimental conditions of the two fibrous cellulose runs are summarized in table A2.

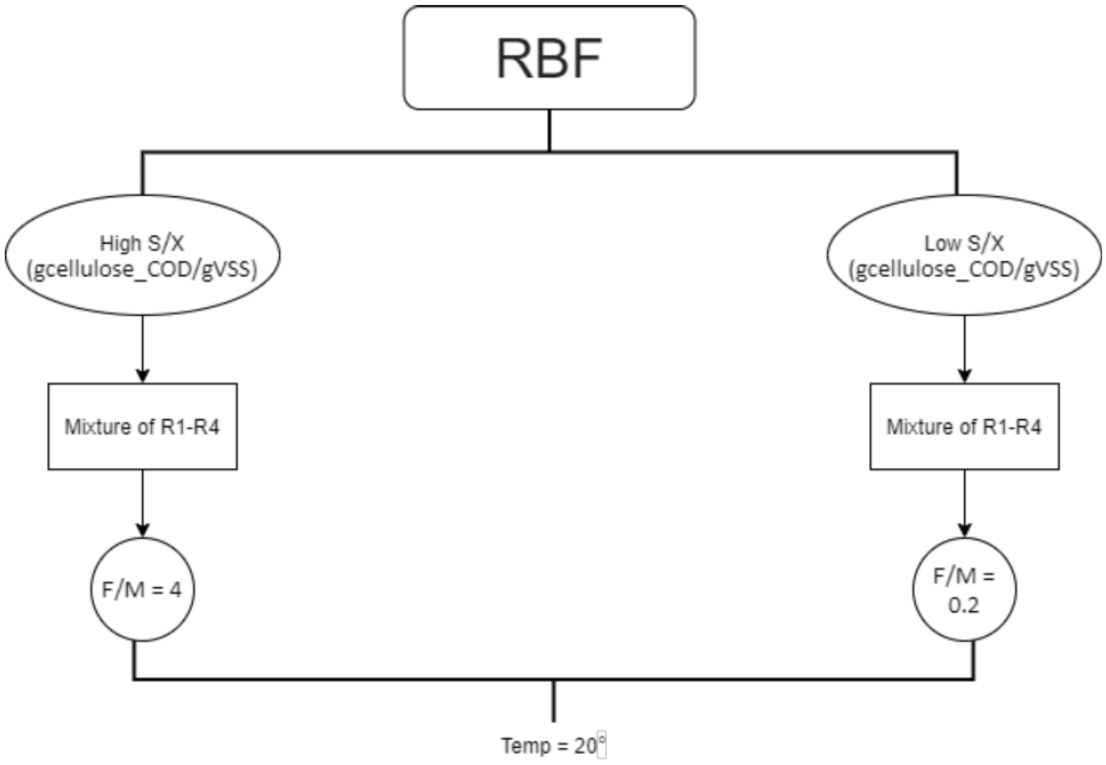

Figure 5.11 RBF models

5.2.4.1 Experimental versus simulated OUR profiles

Experimental and simulated oxygen uptake rates profiles (OUR) of R1-R4 with different S/X of 4 and 0.2 gcellulose_COD/gVSS are shown in figure 5.12.

(a)

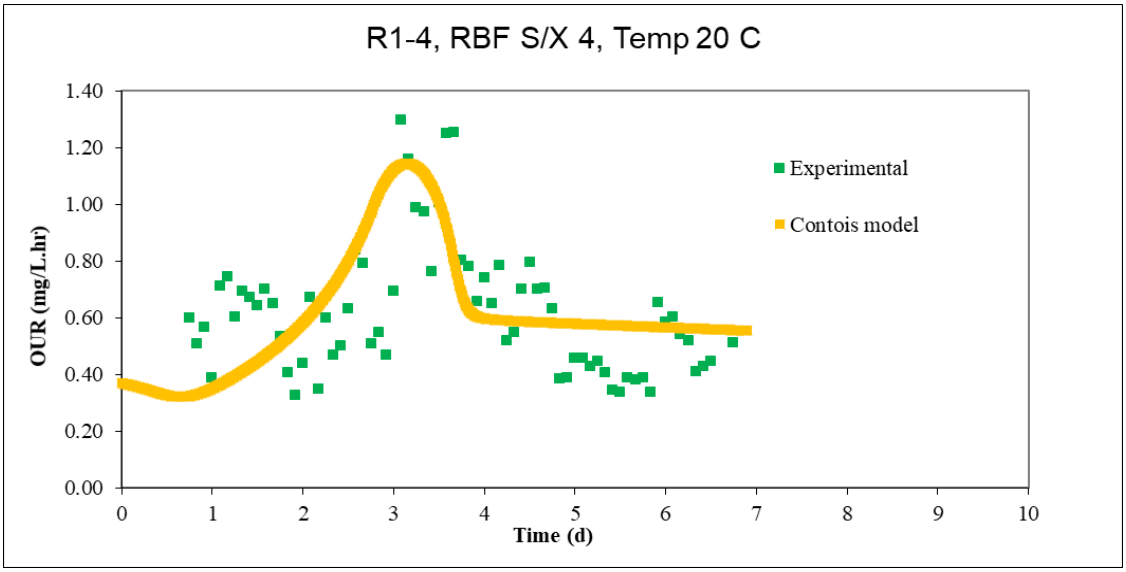

(b)

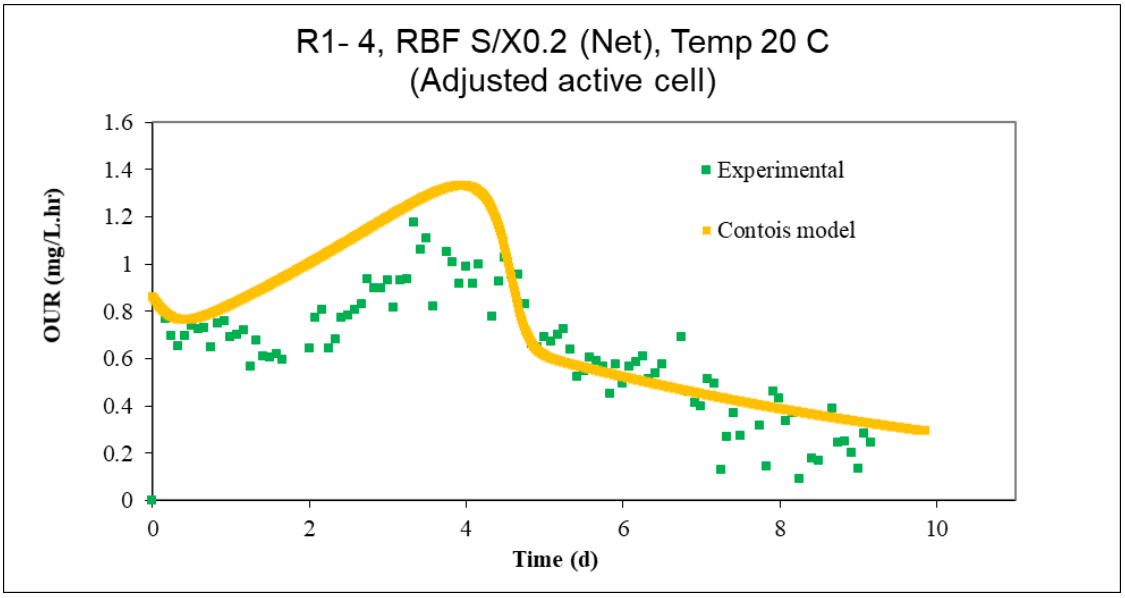

Figure 5.12 RBF Mixture of R1-R4 High and Low S/X matching OUR profiles, a) R1-R4 S/X = 4, b) R1-R4 S/X = 0.2

5.2.4.2 Goodness of fits

Figure 5.13 presents the experimental versus simulated curves as compared above to evaluate the goodness of fit between experimental and simulated data of the two cases of R1-R4 at S/X of 4 and 0.2 operated at a temperature of 20°C.

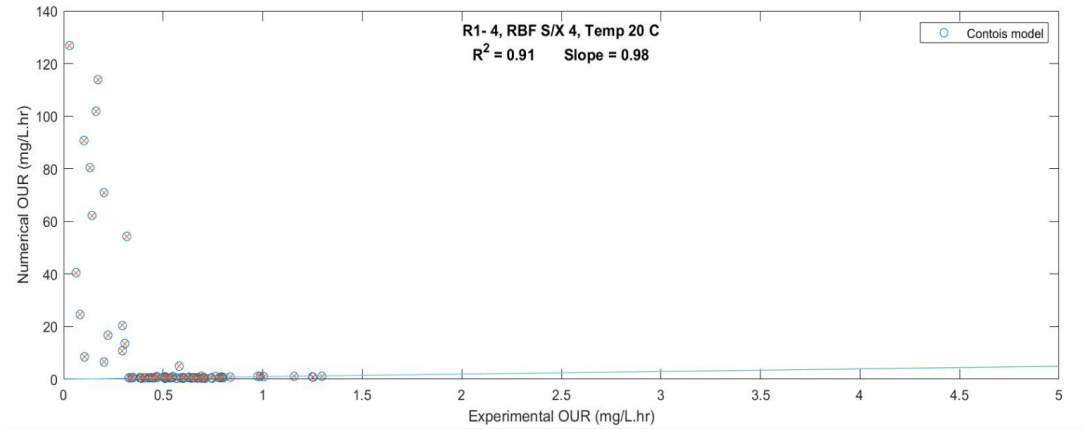

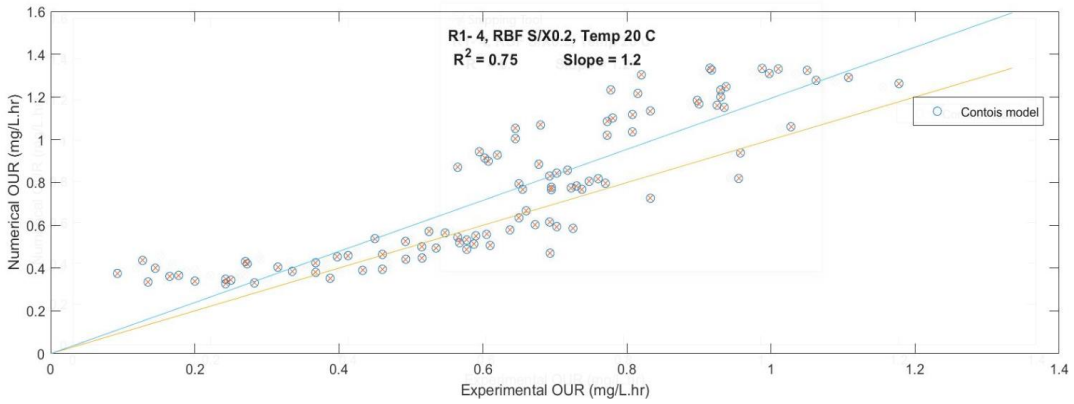

Figure 5.13 High and low RBF comparison between experimental and Contois model

Both models showed good fits to the experimental data with slopes of 1 and 1.2 for high and low S/X respectively.

Table 5.4 is the summary of the high and low RBF models kinetics and inputs used to match the experimental OUR profiles. Similarly, respirometric tests with mixture of RBF sludge and biomass at high and low S/X showed khcl values of 1 and 0.6 d-1, respectively. In matching the experimental net OUR at the low S/X, initial active biomass was adjusted from 466 mgCOD/L to 35 mgCOD/L and initial PCOD concentration was decreased by 72% from 530 mg/L to 150 mg/L similar to the aforementioned with the low S/X α-cellulose cases, and the estimated hydrolysis rate was 0.6 d^{-1}. The adjustment indicated that only 8% of active biomass actually (466 mg/L) degraded 28% of the initial PCOD during the test. PCOD degradation was slower than α-cellulose. The cellulose content of the PCOD in the RBF sludge was 19%. Thus, since the cellulose content of the RBF sludge of 19% was lower than the degraded 28% of PCOD, it is evident that other non-cellulosic PCOD was also biodegraded. The overall values of khcl for the α-cellulose were higher than for the RBF fibrous cellulose-rich sludge, implying that the hydrolysis rate of cellulose is slower than α-cellulose. In addition, the microcrystalline α-cellulose used in this study is partially depolymerized cellulose which can degrade faster than cellulose in wastewater.

Table 5.4 Kinetics inputs for RBF High and low S/X models

RBF sludge		
Seed source	Mixture of R1-R4	
Temperature (ºC)	20	20
F/M (gCOD/gVSS)	4	0.2
Active cell (mgCOD/L)	22	35
PCOD (mg/L)	150	150
µmax (d-1) at 20ºC	6	3
Ks (mg/L) at 20ºC	40	40
kd (d-1) at 20ºC	0.4	0.4
kh (d-1) at 20ºC	3	1.2
Khcl at 20ºC	1	0.6
Kxcl at 20ºC	1	1

Chapter 6.

Enhancing Phosphorus Removal Using Fermentation Results

6.1 Phase 1 (day 1-42)

6.1.1 SBR Performance

Steady-state influent and effluent characteristics for phase 1 are summarized in Table 6.1. Both PE-SBR and RBF-SBR were fed with primary effluent (PE) for the first and the second phase due to delays in running the RBF pilot located in Greenway WWTP related to the Covid-19 situation.

Table 6.1 Phase 1 influent and effluent characteristics

August 1st- September 10th			
Phase 1 (day 1- 42) (n=5)			
		PE-SBR	RBF-SBR
	P.E (influent)	Effluent	Effluent
pH	7.5 ± 0.1	7.9 ± 0.2	8.1 ± 0.1
Alkalinity (mgCaCO3/L)	377 ± 42	253 ± 39	253 ± 41
TSS (mg/L)	91 ± 11	15 ± 7	11 ± 2
VSS (mg/L)	70 ± 8	11 ± 6	5 ± 3
TCOD (mg/L)	258 ± 66	32 ± 16	23 ± 9
SCOD (mg/L)	167 ± 27	21 ± 11	18 ± 10
TN (mgN/L)	33 ± 8	18 ± 4	18 ± 4
SN (mgN/L)	28 ± 6	16 ± 4	15 ± 3
Amm-N (mgN/L)	23 ± 5.4	0 ± 0.2	0 ± 0.2
NO3 (mgN/L)	0.4 ± 0.2	12.2 ± 1.7	12.1 ± 1.1
NO2 (mgN/L)	0.01 ± 0.01	0.06 ± 0.02	0.05 ± 0.03
TP (mgP/L)	4.3 ± 0.6	2 ± 0.5	1.9 ± 0.6
SP (mgP/L)	2.6 ± 0.4	1.5 ± 0.4	1.5 ± 0.4
Reactor			
MLSS (mg/L)	NA	1308 ± 380	1174 ± 492
MLVSS (mg/L)	NA	967 ± 275	881 ± 359

.

The average influent (Greenway primary effluent) TSS, TCOD, TN and TP concentrations were 80-102 mg/L, 192-324 mg/L, 25-41 mg/L and 3.7-4.9 mg/L, respectively. Removal efficiencies for stage 1 are shown in Table 6.2. Based on the influent and effluent data of phase 1, the high effluent TN (14-22 mg/L) and TP (1.9-2.0 mg/L) concentrations confirm that both reactors were deficient in readily biodegradable COD (rbCOD). Effluent SCOD were mostly in the range of 10-32 mg/L and 10-28 mg/L with removal efficiency 86% and 87% for PE-SBR and RBF-SBR, respectively. Full nitrification was achieved, and ammonia was completely removed in both reactors. Effluent TP concentrations were mostly above 1.5 mg/L corresponding to a poor average removal of 55% (Table 6.2) for both reactors, which shows the carbon limitation in the SBRs and the competition between the denitrification and biological phosphorus removal processes over the organic carbon.

Table 6.2 Removal efficiencies of SBRs in phase 1

Phase 1 Removal efficiencies (%)		
	PE-SBR	**RBF-SBR**
TSS	84 ± 6	88 ± 2
VSS	85 ± 8	92 ± 4
TCOD	87 ± 9	90 ± 4
SCOD	86 ± 8	87 ± 7
TN	43 ± 11	44 ± 11
SN	40 ± 12	42 ± 6
Amm-N	99 ± 1	100 ± 1
TP	52 ± 13	55 ± 16
SP	39 ± 20	39 ± 22

6.1.2 Mass balance

Nitrogen Mass Balance

Nitrogen mass balance in the both SBRs were performed. The mass balance used Eqs. (6.1)-(6.5) was used to determine the nitrogen input (mg/L) to the reactor:

$$Influent\text{-}N = Q^{*}\,(C_{Inf\text{-}TKN} + C_{Inf\text{-}NOx}) \quad (6.1)$$

Where, Q (L/d), and C (mg/L) represent the flow and concentrations, respectively.

Nitrification, denitrification and cell synthesis were considered in the nitrogen mass balance and the transformation of nitrogen (mg/L) in the influent. The nitrogen in the effluent (mg/L) was calculated using Eq. (6.2):

$$Effluent\text{-}N = N_{CE} + N_{DN} + N_{WAS} \quad (6.2)$$

$$N_{CE} = Q^{*}\,(C_{Eff\text{-}TKN} + C_{Eff\text{-}NOx} + f_{N^{*}}\, C_{Eff\text{-}VSS}) \quad (6.3)$$

$$N_{DN} = Q^{*}\,(C_{Inf\text{-}TKN} - C_{Eff\text{-}TKN} - C_{N\text{-}cell\ synthesis} - C_{Eff\text{-}NOx}) \quad (6.4)$$

$$N_{WAS} = (C_{MLVSS^{*}}\, V_R/\Theta_C - Q^{*}\, C_{Eff\text{-}VSS})^{*} f_N \quad (6.5)$$

Where N_{CE} (mg/d), N_{DN} (mg/d), N_{WAS} (mg/d), represent the nitrogen in the clarified effluent, denitrification, and waste activated sludge streams, respectively. f_N, V_R (L), and Θ_C, represent N-content of the biomass, reactor volume, and solid retention time of the reactor (10 days), respectively. f_N values vary between 0.10-0.12 (Tchobanoglous et al., 2003b).

Phosphorus Mass Balance

For the phosphorus mass balance, the phosphorus concentration in the influent in the effluent was calculated using Eqs (6.6)-(6.7).

$$Influent\text{-}P = Q^{*}\, C_{Inf\text{-}TP} \quad (6.6)$$

$$Effluent\text{-}P = P_{CE} + P_{WAS} \quad (6.7)$$

$$P_{CE} = Q^{*}\,(C_{Eff\text{-}SP} + f_{P^{*}}\, C_{Eff\text{-}VSS}) \quad (6.8)$$

$$P_{WAS} = (C_{MLVSS^{*}}\, V_R/\Theta_C - Q^{*}\, C_{Eff\text{-}VSS})^{*} f_P \quad (6.9)$$

Where P_{CE} (mg/d), P_{WAS} (mg/d), and F_P represent the phosphorus in the clarified effluent, and waste activated sludge streams, and the P-content of the biomass, respectively. F_P was reported to be in the range of 5%-7% (Tchobanoglous et al., 2003b).

Nitrogen and phosphorus mass balance results in Phase 1 are shown in Table 6.3.

Table 6.3 Nitrogen and Phosphorus mass balance for phase 1

	Nirogen mass balance			**Phosphorus mass balance**	
	PE-SBR	RBF-SBR		PE-SBR	RBF-SBR
Influent-N (%)	100	100	P (influent)	100	100
N (WAS) (%)	20	19	P (WAS)	42	41
N (Effluent) (%)	64	62	P (Effluent)	47	43
N (Denitrified) (%)	18	18	P-balance	11	16
N-balance (%)	-2.1	0.6			

Based on the nitrogen mass balance calculated for phase 1, the nitrogen that was removed via cell synthesis is about 20% of the influent for both reactors with the remaining 80% oxidized with an overall average nitrogen removal efficiency of 51%.

The phosphorus mass balance results for phase 1 presented in Table 6.3, indicate good closure with discrepancies of 11% and 16%; 45% of the phosphorus in both reactors was used in the

biomass cell synthesis and 7% of the phosphorus concentration remained in the effluent, with an overall average phosphorus removal of 52% and 55% for PE-SBR and RBF-SBR, respectively.

6.2 Phase 2 (day 43-53)

By the end of phase 1 and at day 37, the system started to be fed with ATU at a dose of 20 mg/L. This addition contributed to the system with an additional COD of 80 mg/L, based on the wastewater flow of 1 L/cycle. Nitrification and hence denitrification were inhibited in the two reactors. Ammonia concentration in the effluent of both reactors jumped to an average of 25 mg/L which was the result of the influent. Total phosphorus removal efficiencies increased to 69% and 72% for PE-SBR and RBF-SBR, respectively due to the presence of extra organic carbon provided with denitrification inhibition. Effluent concentrations of NH_4-N and NO_X-N through the operation period are shown in figure 6.1a and 6.1b.

a)

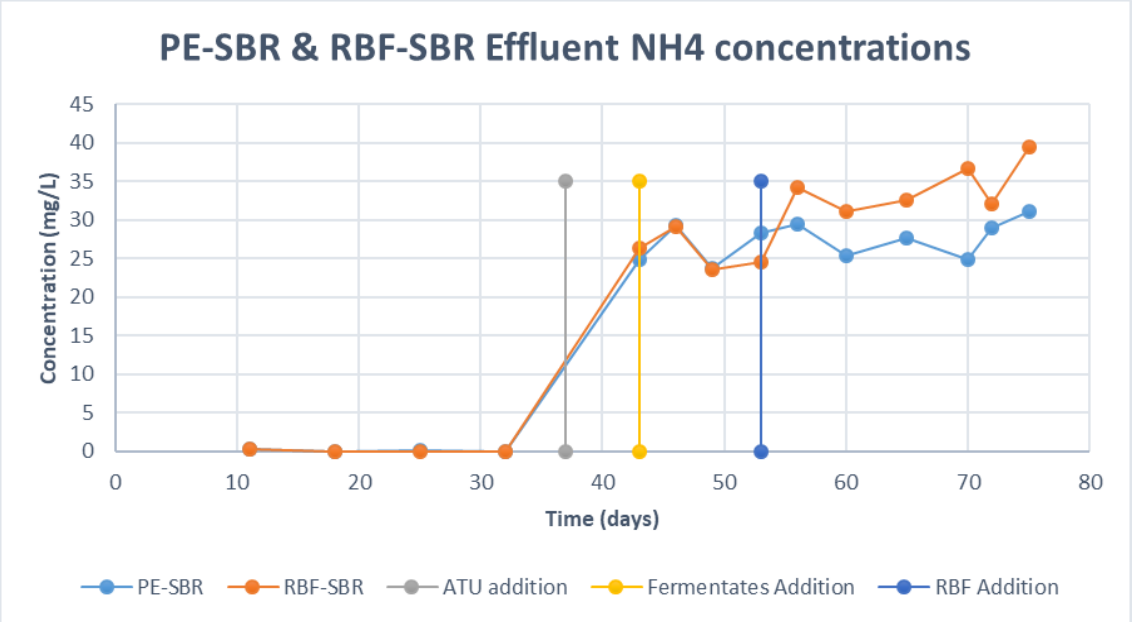

b)

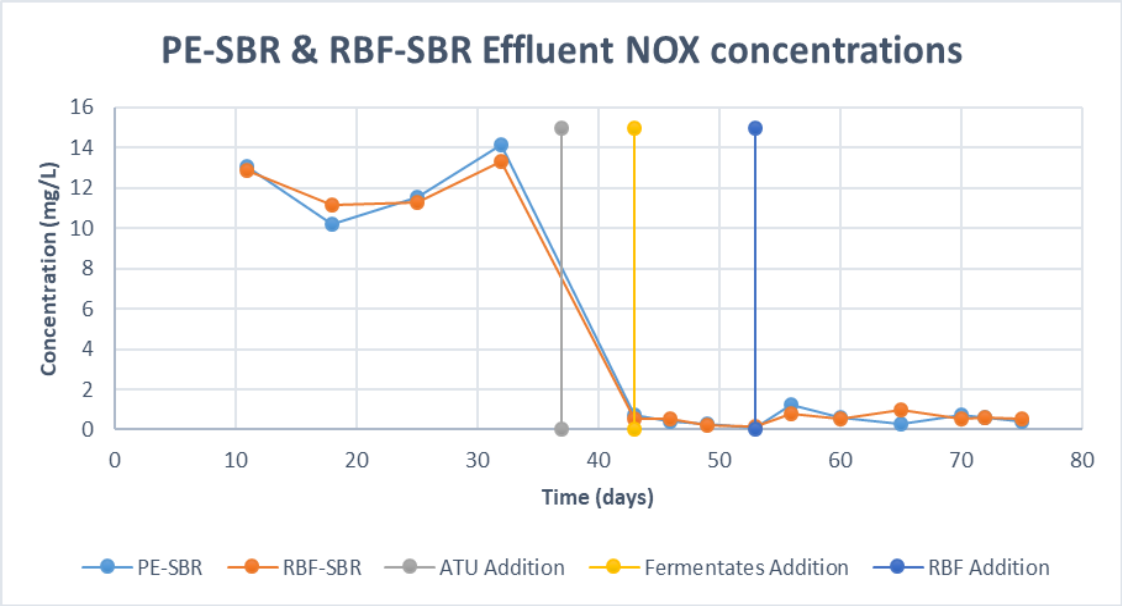

Figure 6.1 Effect of addition of ATU to both PE-SBR and RBF-SBR effluent concentrations a) NH4 effluent time profile, b) NOX effluent time profile

Phase 2 was considered to be a preparation phase for switching RBF-SBR feed to RBF effluent and fermented RBF sludge. In this phase, both reactors were identical with the addition of 120 mg/L of fermented primary sludge to each reactor at the start of each cycle. The addition of fermented primary sludge for the two reactors was from day 43-53. Influent and effluent characteristics are included in Table 6.4. Soluble COD concentrations increased in the effluent of the two reactors to an average of 107 mg/L and 74 mg/L for PE-SBR and RBF-SBR, respectively. This increase is due to two reasons for the addition of the fermentates to the reactors and also the ATU addition which contributes 80-90 mg/L of SCOD. Hence, an accumulation of SCOD started in this phase for both reactors.

Table 6.4 Phase 2 influent and effluent characteristics

September 10th- September 21st			
Phase 2 (43-53) (n=3)			
		PE-SBR	RBF-SBR
	P.E	Effluent	Effluent
pH	7.7 ± 0.2	8.1 ± 0.1	8.2 ± 0.1
Alkalinity (mgCaCO3/L)	375 ± 25	405 ± 14	403 ± 23
TSS (mg/L)	93 ± 13	18 ± 5	15 ± 8
VSS (mg/L)	69 ± 9	11 ± 3	5 ± 2
TCOD (mg/L)	304 ± 68	124 ± 47	83 ± 26
SCOD (mg/L)	106 ± 14	107 ± 45	74 ± 23
TN (mgN/L)	30 ± 3	42 ± 9	41 ± 9
SN (mgN/L)	23 ± 2	40 ± 10	37 ± 9
Amm-N (mgN/L)	21 ± 2.6	27 ± 2.9	26 ± 3
NO3 (mgN/L)	0.4 ± 0.2	0.3 ± 0.2	0.3 ± 0.2
NO2 (mgN/L)	0.01 ± 0	0.01 ± 0	0.01 ± 0.01
TP (mgP/L)	4 ± 0.2	0.5 ± 0.1	0.5 ± 0
SP (mgP/L)	2.1 ± 0.2	0.1 ± 0.1	0.1 ± 0.1
Reactor			
MLSS (mg/L)	NA	2381 ± 447	3067 ± 1356
MLVSS (mg/L)	NA	1654 ± 387	2203 ± 1021

Total phosphorus removal increased from 69% to 85%-91% for PE-SBR and from 72% to 87%-89% in RBF-SBR, which showed the effectiveness of adding the fermentates in providing an extra carbon source for the biological phosphorus removal process. Effluent total phosphorus concentrations were in the range of 0.5-0.6 mg/L in the two reactors while effluent SP hovered around of 0-0.2 mg/L for both reactors, corresponding to a removal efficiency of 91-98% (Table 6.5).

Table 6.5 Removal efficiencies of SBRs in phase 2

Phase 2 Removal efficiencies (%)		
	PE-SBR	**RBF-SBR**
TSS	81 ± 4	84 ± 6
VSS	84 ± 2	92 ± 3
TCOD	81 ± 9	94 ± 7
SCOD	59 ± 30	93 ± 17
TP	88 ± 3	88 ± 1
SP	95 ± 3	95 ± 4

Total nitrogen removal was neglected as the study focused on biological phosphorus removal, Soluble effluent nitrogen profile through the operation period is depicted in figure A5.2.

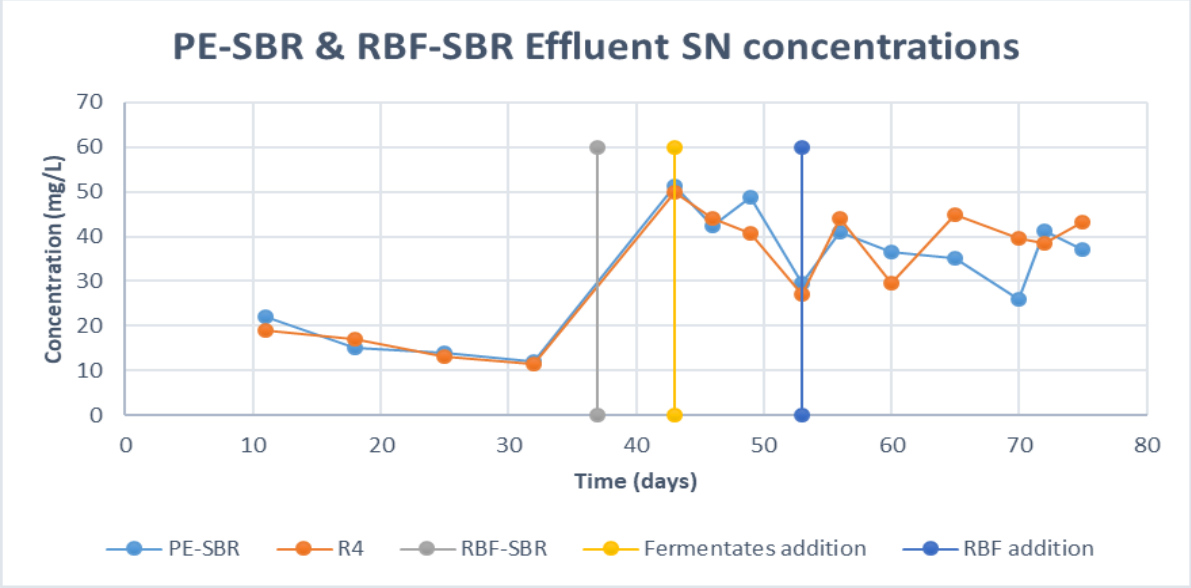

Figure 6.2 Soluble Nitrogen effluent time profile

6.3 Phase 3 (day 54-75)

6.3.1 SBRs Performance

Phase 3 was from day 53-75 when RBF-SBR feed was switched to RBF effluent (RBFE) and the fermented sludge added in each cycle was switched to RBF sludge. Table 6.6 shows the influent and the effluent concentrations in each reactor as well as the combined influent characteristics with the addition of the fermentates supernatant and the ATU addition.

Table 6.6 Phase 3 influent and effluent characteristics

September 21st- October 13th-20th						
Phase 3 (54-75) (n=6)						
	P.E influent	Combined influent (PE + supernatant)	RBF influent	Combined influent (RBF + supernatant)	PE-SBR Effluent	RBF-SBR Effluent
pH	7.6 ± 0.3	-	7.6 ± 0.2	-	8.1 ± 0.1	8.2 ± 0.1
Alkalinity (mgCaCO3/L)	353 ± 23	405	364 ± 19	431	381 ± 13	404 ± 12
TSS (mg/L)	87 ± 11	-	257 ± 63	-	20 ± 8	17 ± 8
VSS (mg/L)	64 ± 9	-	159 ± 42	-	11 ± 7	10 ± 5
TCOD (mg/L)	230 ± 40	569	382 ± 46	678	150 ± 20	126 ± 9
SCOD (mg/L)	129 ± 33	385	149 ± 44	414	143 ± 18	120 ± 7
TN (mgN/L)	29 ± 5	53	38 ± 5	65	38 ± 4	44 ± 3
SN (mgN/L)	23 ± 3	43	27 ± 5	50	36 ± 6	40 ± 6
Amm-N (mgN/L)	21 ± 1	33	25 ± 3.1	38	28 ± 2.4	34 ± 3.2
NO3 (mgN/L)	0.7 ± 0.3	-	0.6 ± 0.3	-	0.6 ± 0.3	0.7 ± 0.2
NO2 (mgN/L)	0.02 ± 0.01	-	0.02 ± 0.01	-	0.01 ± 0.01	0.01 ± 0.01
TP (mgP/L)	4.7 ± 1.5	11	9.1 ± 3.2	14	0.6 ± 0.1	0.7 ± 0.2
SP (mgP/L)	2.8 ± 0.7	8	4.1 ± 0.7	9	0.1 ± 0.1	0.3 ± 0.2

However, despite the phosphorus added with the supernatant to each reactor, P.E-SBR achieved an average SP removal of 98.2% (Table 6.7), with effluent concentrations of 0-0.2 mg/L. RBF-SBR achieved an average SP removal efficiency of 96.1% with effluent concentrations in the range of 0.1-0.5 mg/L. Soluble COD accumulation continued in this phase as well, SCOD in the effluent was in the range of 125-161 mg/L and 113-127 mg/L for PE-SBR and RBF-SBR. This increase in SCOD is mainly from the supernatant addition and also the ATU contribution. ATU contributed with 80 mg/L which was added to the influent in phase 3.

Table 6.7 Removal efficiencies of the SBRs in phase 3

	PE-SBR	RBF-SBR
TSS (%)	77 ± 8	93 ± 4
VSS (%)	84 ± 9	93 ± 4
TCOD (%)	67 ± 11	88 ± 3
SCOD (%)	51 ± 13	70 ± 9
TP (%)	92 ± 5	95 ± 3
SP (%)	98 ± 2	97 ± 3

The phosphorus removal efficiencies for PE-SBR and RBF-SBR during the operation period are shown in figure 6.3.

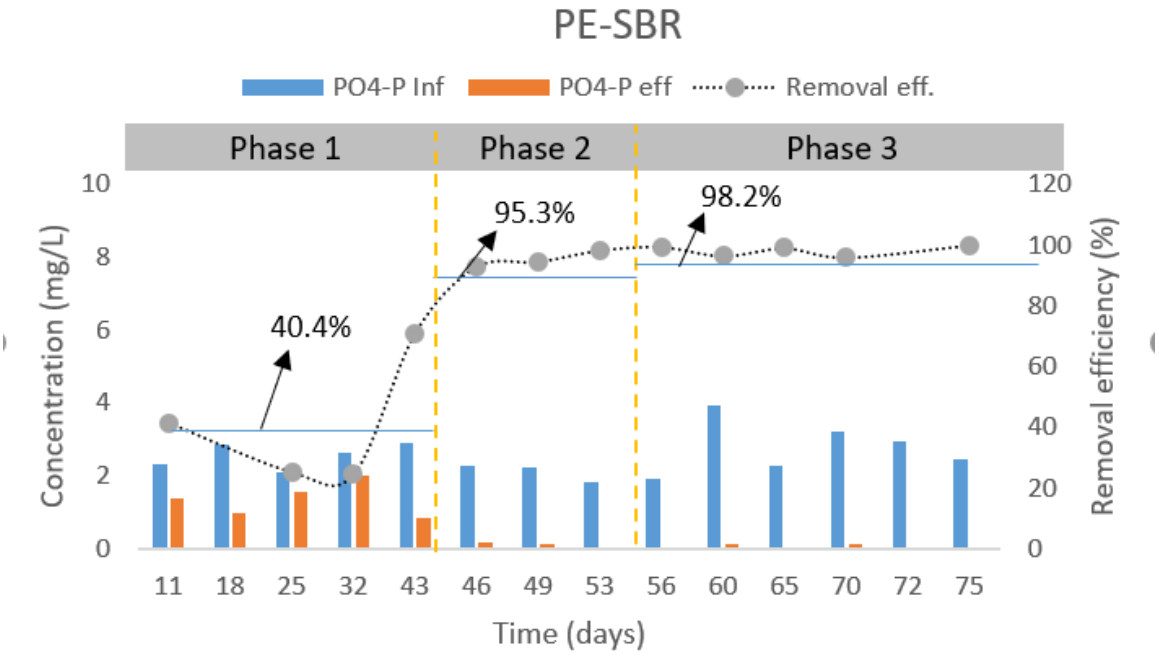

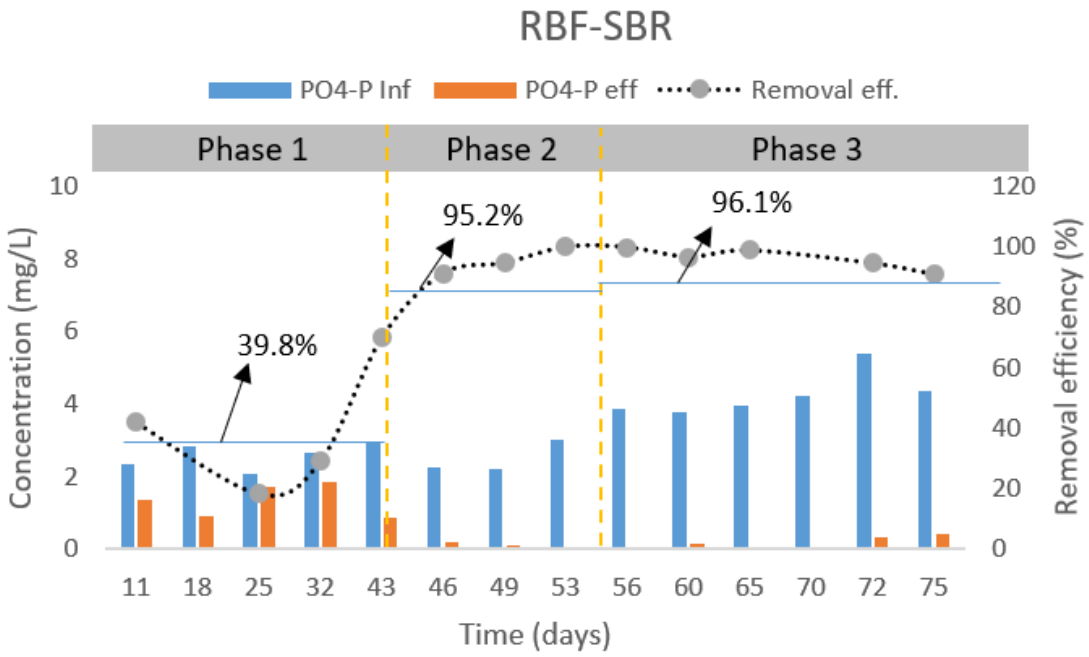

Figure 6.3 Phosphorus influent, effluent and removal efficiencies

Plans for optimization of fermentation liquid dose were derailed due to COVID-19, and the experiment was shut down after 75 days of operation.

6.3.2 Fermentation Supernatant Characteristics

The fermentation supernatant characteristics are included in Table 6.8. The hydrolysis and acidification yields were calculated for both sludge types. The calculated hydrolysis of the fermented sludges was 13.5±2% and 12±5.8% for PS and RBF sludge respectively. The supernatant added 3068-4496 mg/L and 3120-4632 mg/L of VFA to PE-SBR and RBF-SBR, respectively. The addition of the PS and RBF supernatants to both reactors contributed also 134-182 mg/L and 111-163 mg/L of total phosphorus to PE-SBR and RBF-SBR, respectively. It has also added 114-158 mg/L and 112-159 mg/L of soluble phosphorus to PE-SBR and RBF-SBR, respectively. Moreover, the acidification yields were 54±8% and 54±9.8% for PS and RBF sludge, respectively.

Table 6.8 Feed, fermentates sludges and supernatants characteristics

	Feed Sludge		Fermentates		Supernatants	
	Primary sludge	**RBF Sludge**	**PS Fermentate**	**RBF Fermentate**	**PS Supernatant**	**RBF Supernatant**
PH	6.2 ±0.3	6.2 ±0.4	5.2 ±0.2	5.2 ±0.2	5.2 ±0.2	5.2 ±0.2
Alk (mg/L)	1826 ±266	1397 ±210	2186 ±896	2267 ±689	2186 ±896	2267 ±689
VFA (mg/L)	945 ±513	974 ±470	3372 ±842	3508 ±898	3782 ±714	3876 ±756
TCOD (mg/L)	33331 ±5512	39225 ±14022	32493 ±4467	34940 ±7583	9127 ±2032	9298 ±2364
SCOD (mg/L)	1861 ±925	2042 ±602	6609 ±1178	6873 ±1110	7169 ±1028	7321 ±874
TN (mg/L)	880 ±275	1383 ±472	1455 ±619	1347 ±471	669 ±127	691 ±162
SN (mg/L)	190 ±108	163 ±79	577 ±124	625 ±161	585 ±117	731 ±302
NH4 (mg/L)	59 ±62	139 ±100	338 ±62	350 ±74	338 ±62	350 ±74
NO3 (mg/L)	16 ±9	17 ±6	21 ±18	19 ±8	21 ±18	18 ±9
NO2 (mg/L)	0.31 ±0.18	0.28 ±0.17	0.29 ±0.18	0.21 ±0.09	0.29 ±0.18	0.21 ±0.09
TP (mg/L)	460 ±202	474 ±170	483 ±129	451 ±138	158 ±24	137 ±26
SP (mg/L)	38 ±14	50 ±15	139 ±22	135 ±19	136 ±22	135 ±23
NOX (mg/L)	15.3 ±8.7	16.9 ±6	20.9 ±18.1	19 ±7.9	20.9 ±18.1	18.3 ±9.2
TS (mg/L)	26302 ±4601	50612 ±10841	18672 ±3125	24533 ±7896	554 ±177	614 ±254
VS (mg/L)	19173 ±2869	33083 ±11182	13295 ±2206	18396 ±6219	426 ±185	466 ±204

6.3.3 Phosphorus mass balance of phase 3

Following the same equations of phosphorus mass balance in phase 1 based on the combined influent characteristics with the addition of fermentates, a mass balance for phase 3 was conducted as shown in Table 6.9.

Table 6.9 Phosphorus mass balance for PE-SBR and RBF-SBR in phase 3

	PE-SBR	**RBF-SBR**
P (Influent) (%)	100	100
P (WAS) (%)	81	87
P (Effluent) (%)	7	7
P-balance (%)	12	6

The mass balance results show that after the addition of fermentates, despite significantly increasing influent phosphorus, about 84% of the phosphorus in the reactors was incorporated in biomass and only 7% escaped in the SBR effluent, with an overall average phosphorus removal of 91% and 93% for PE-SBR and RBF-SBR, respectively. This increase in the phosphorus removed biologically is due to the VFA added from the fermented sludge which increased the phosphorus uptake and release rates, and promoted the growth of phosphorous accumulating organisms (PAOs). The comparison between phase 1 and phase 3 mass balance is shown in figure 6.4.

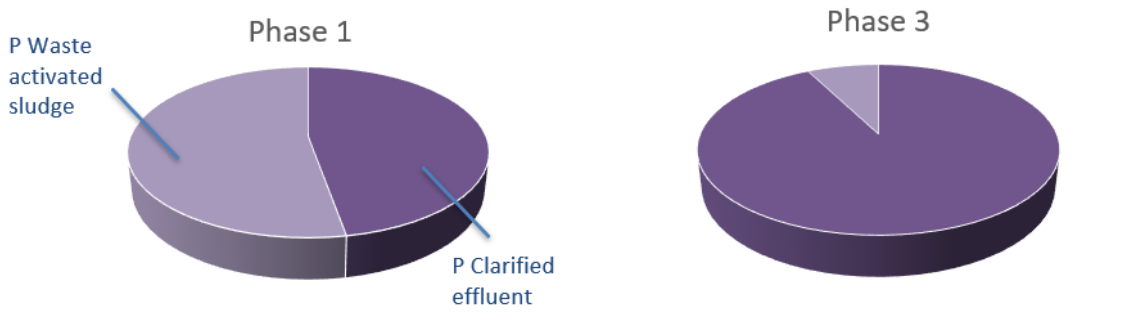

Figure 6.4 Comparison of the phosphorus mass balance between phase 1 and phase 3

6.3.4 Reactors Biomass profiles

The biomass concentrations in the two reactors increased with the fermentates addition. For PE-SBR, MLSS and MLVSS concentrations increased with a ratio of 2.1 times the initial concentration at the beginning of phase 2 to reach 2813 mg/L and 2033 mg/L, respectively. Furthermore, RBF-SBR biomass increased significantly as well, MLSS and MLVSS increased with a ratio of 3 times the initial concentration before the start of this phase to reach 4590 mg/L and 3360 mg/L, respectively. Biomass time profiles for both reactors are shown in figure 6.3a and 6.3b.

(a)

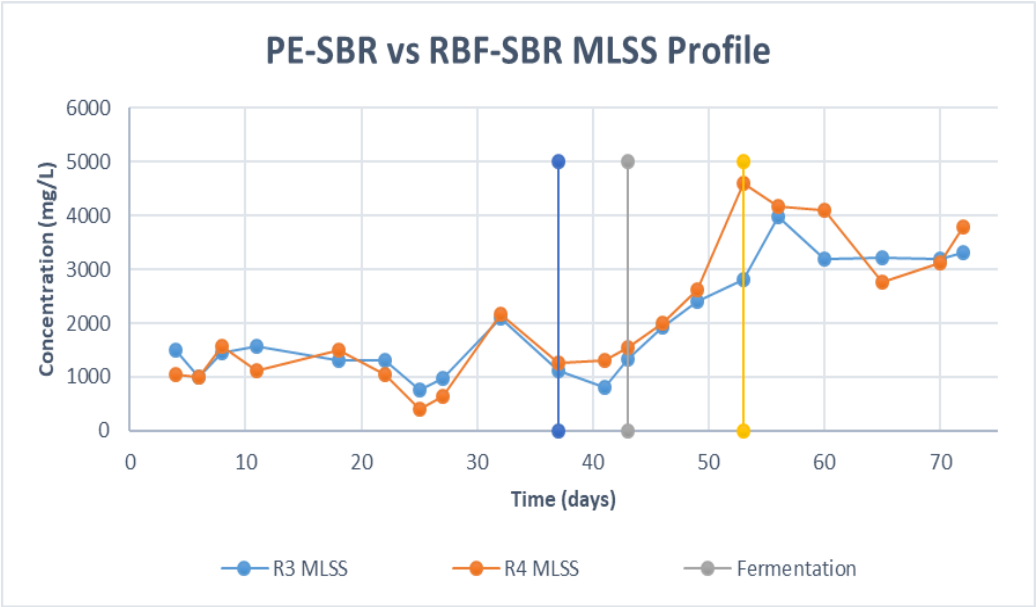

(b)

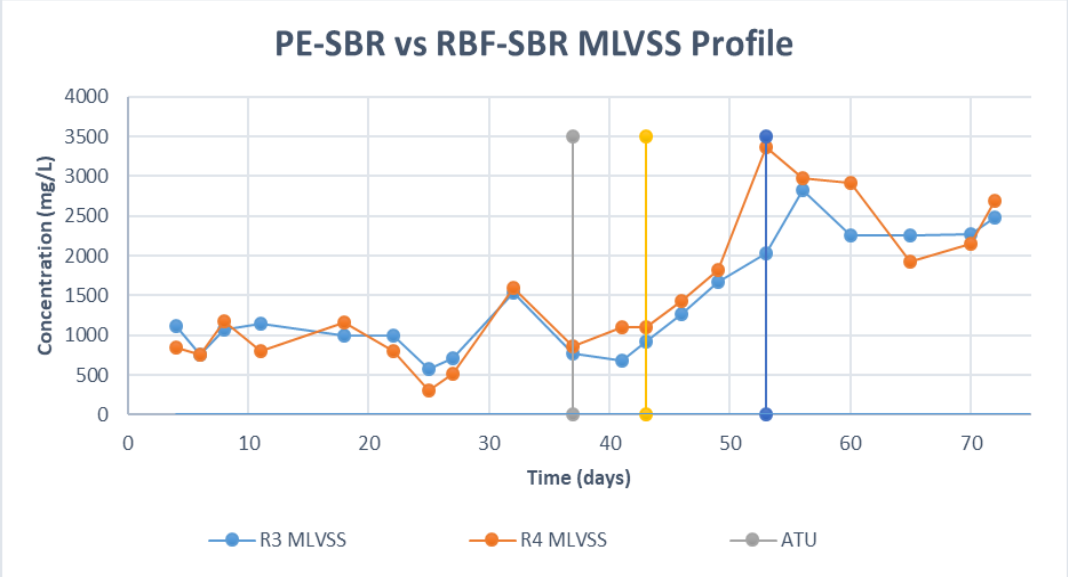

Figure 6.5 PE-SBR and RBF-SBR biomass profiles

Biomass concentration in both reactors in the two reactors were in the range of 3034-3718 mg/L of MLSS and 2172-2668 mg/L of MLVSS for PE-SBR. For RBF-SBR the range of MLSS was in the range of 2968-4200 mg/L and for the MLVSS 2064-3018 mg/L.

6.3.5 Cyclic tests

One cyclic test was conducted during phase 1 to monitor the SCOD usage during the reaction time (anoxic and aerobic). The results showed that due to the lack of carbon source, nitrate concentration decreased slightly from 3.8 mg/L at the start of the anoxic phase to 2.6 mg/L at the end of the anoxic phase. Moreover, effluent phosphorus concentrations showed the lack of carbon source to remove the soluble phosphorus during the phosphorus uptake phase (aerobic phase). The low effluent SCOD concentrations were mostly influent soluble inert COD.

An average of three cyclic tests results were conducted in phase 3. Soluble phosphorus (SP) profiles from the start of the feeding at t=0 till the end of the reaction time t=6.5 for PE-SBR and RBF-SBR are plotted in Figure 6.3. Initial SP concentrations at the beginning of the anaerobic phase in both reactors started at 1.7 and 3.5 mg/L for PE-SBR and RBF-SBR, respectively. For PE-SBR, during the anaerobic phase, SP reached a peak level of 18.6 mg/L with an average phosphorus release rate of 5.5 mg PO4-P/g VSS·h. Moreover, by the end of the aerobic phase SP concentration ended with an average of 0.1 mg/L with a phosphorus uptake rate of 3.8 mg PO4-P/g VSS·h. Soluble phosphorus and COD profiles for the cyclic tests is shown in figures 6.6-6.7.

On the other hand, SP shown figure 6.6 in the RBF-SBR during the anaerobic phase reached a peak of 22.94 mg/L at an average phosphorus release rate of 6 mg PO4-P/g VSS·h to. By the end of the aerobic phase, with an average phosphorus uptake rate of 3.9 mg PO4-P/g VSS·h, SP reached 0.15 mg/L.

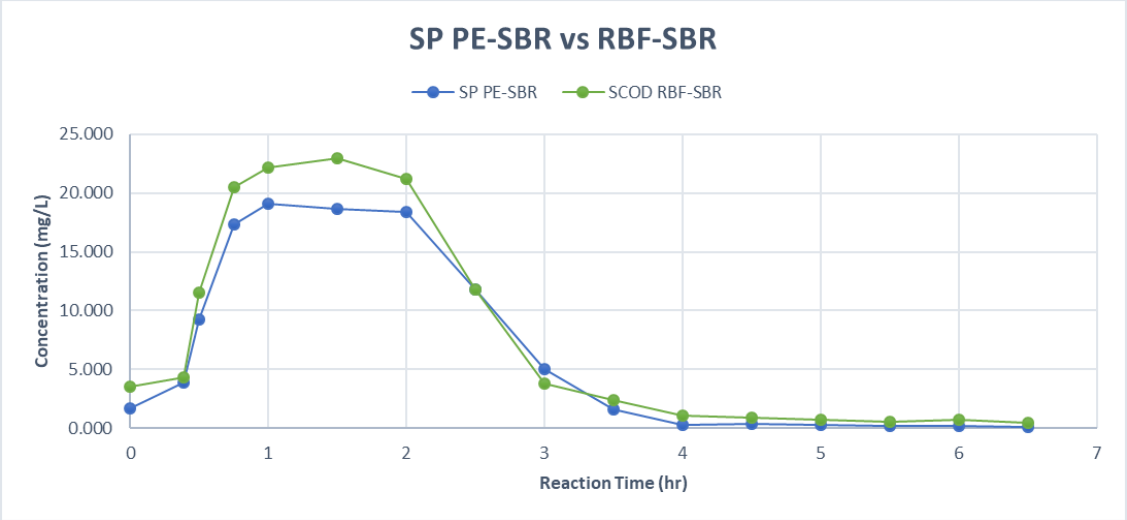

Figure 6.6 SP profiles for PE-SBR and RBF-SBR during one cycle.

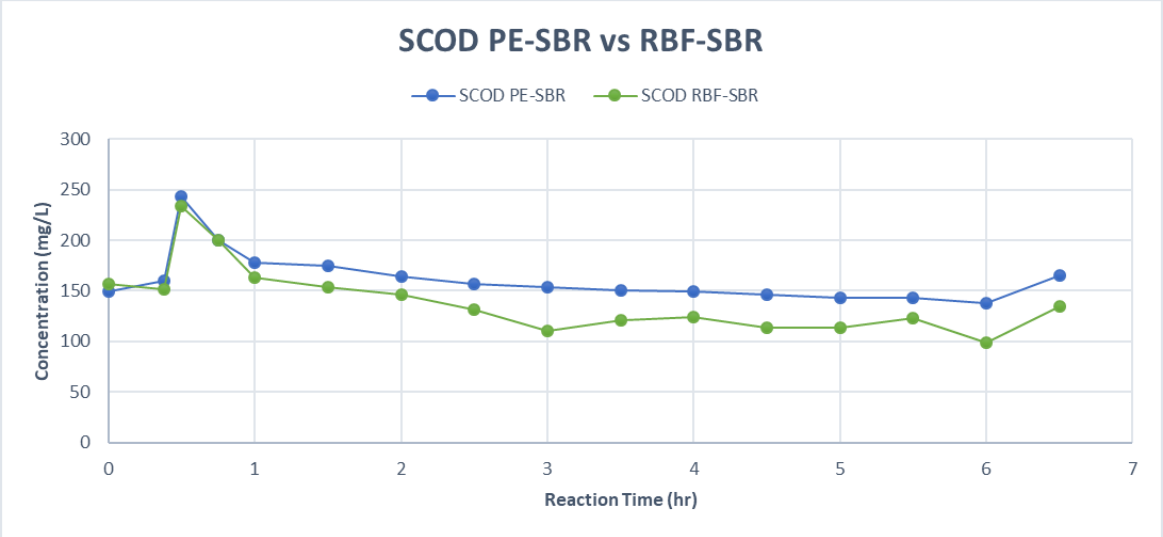

Figure 6.7 SCOD profiles for PE-SBR and RBF-SBR during one cycle.

Both reactors showed consistent ammonia, nitrate, and nitrite profiles. The cyclic tests average results shown in figure 6.8 indicated the inhibitory effect of ATU added at the start of each phase in both reactors during one cycle.

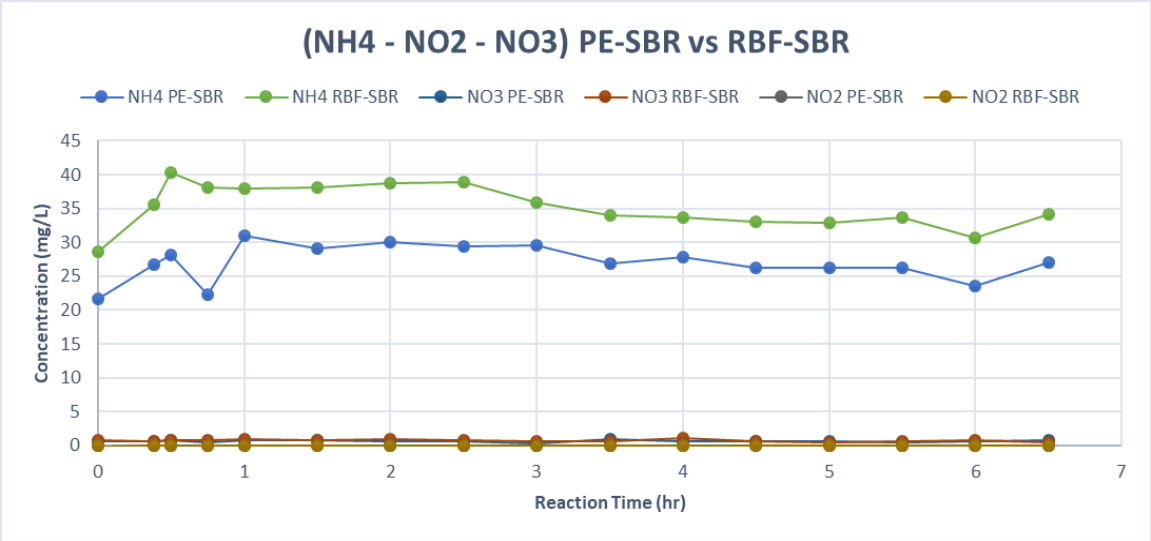

Figure 6.8 NH4 and NOX profile for PE-SBR and RBF-SBR during one cycle in phase 3.

Both reactors showed consistent removal by the addition of fermentates as an extra carbon source reaching the phosphorus concentrations desired of below 0.5 mg/L without any chemical treatment.

Chapter 7.

Conclusions and Recommendations

7.1 Conclusions

Based on the first study of the four SBRs operated at four different temperatures and two different SRT, cellulose average concentration in the influent and accounted 17%-20% of the SBR system influent TSS with an average concentration of 36 mg/L and 66 mg/L for phase 1 and 2, respectively. Cellulose ended up with an average concentration of 2-3 mg/L in the system effluent. Based on cellulose mass balance on the experimental data, the biodegradation efficiency of cellulose was 80%-90% at SRT of 15 days and 78%-85% at SRT of 3 days. The results indicated that cellulose biodegradation is dependent on temperature and SRT. Hence, during the cold seasons, increasing the biological reactors SRT can balance the lower temperatures regarding the cellulose recovery and hence the biomass volume. Cellulose concentrations in the bioreactor's biomass increase with lowering the SRT (1%-2% at SRT of 15 days increased to 2%-5% of the bioreactors MLVSS at SRT of 3 days).

Data from the respirometry runs were collected to calibrate the ASM1 modified models. The cellulose simulation study showed higher hydrolysis rates when system reactors was fibrous cellulose limited (cellulose concentration in the biomass) at high availability of food to microogranims concentration (S/X ratios), where the dominant cellulose content was the alpha cellulose added to the respirometry bottles compared to the low S/X cases where the hydrolysis rates estimated by the models represents the fibrous cellulose hydrolysis kinetics. Incorporating cellulose into ASM1 model to simulate the respirometric runs and estimating cellulose hydrolysis rates at different temperatures using Contois model estimated cellulose hydrolysis rate of 3 d^{-1} at 20 °C based on α-cellulose at high S/X ratios in the range of 4,6 and 8 gcellulose_COD/gVSS while hydrolysis rate of PCOD of RBF sludge was estimated 0.6-1 d^{-1}. For the low S/X of 0.2 gcellulose_COD/gVSS, the model estimated a hydrolysis rate of cellulose of 0.5 d^{-1}.

Cellulose can either be removed by primary treatment technologies and hence can be fermented with the primary treatment solids and added to the biological reactors as an extra source of carbon to enhance biological phosphorus removal (EBPR), or through degradation in the biological reactions. Fermentation is effective in providing external carbon for enhancing biological phosphorus removal and achieving high phosphorus removal efficiencies of above 95% biologically without chemical addition. However, this may increase SCOD in the effluent, the fractionation of which was beyond the scope of this work. Moreover, simultaneous optimization of effluent phosphorous and COD, would be dictated by regulatory requirements, and hence choosing the optimum fermentate dose to the biological reactors requires further investigation.

Due to the high concentration of solids in the fermnented sludges which increase by turn the SBRs effluent solids concentration. Hence, including proper solids separation after the fermentation process using centrifugation and filtration helped reduce the inert solids accumulation in the bioreactors and reduce by turn the biosolids yield.

7.2 Recommendations

Based on the major findings of the thesis projects, future research should address the following topics:

- Validation of the modified activated sludge model to simulate cellulose using a Contois model for a full-scale treatment plant in order to check its effectiveness and its capability to predict cellulose fate in WWTPs.

- The fractionation of COD, N, and P in the fermentate according to ASIM models is needed for optimization of the required fermentate dose to meet specific effluent requirements.

- Whole plant modeling is required to assess the impact of fermentate solids separation and liquid diversion to BNR processes on overall aeration energy consumption, waste activated sludge production, anaerobic bioenergy generation, and solids processing and disposal.

References

AENOR, 2003. Evaluación de la biodegradabilidad aeróbica última y de la desintegración de los materiales de envase y de embalaje mediante el análisis del dioxido de carbono liberado (Evaluating the Final Aerobic Biodegradability and the Disintegration of Packaging and Wrapping Materials though the Analysis of the Carbon Dioxide Released). p. 24. Standard UNE 14046.

Ahmed, A.S., Bahreini, G., Ho, D., Sridhar, G., Gupta, M., Wessels, C., Marcelis, P., Elbeshbishy, E., Rosso, D., Santoro, D., Nakhla, G., 2019a. Fate of cellulose in primary and secondary treatment at municipal water resource recovery facilities. Water Environ. Res. 91, 1479–1489. https://doi.org/10.1002/wer.1145

Ahmed, A.S., Bahreini, G., Ho, D., Sridhar, G., Gupta, M., Wessels, C., Marcelis, P., Elbeshbishy, E., Rosso, D., Santoro, D., Nakhla, G., 2019b. Fate of cellulose in primary and secondary treatment at municipal water resource recovery facilities. Water Environ. Res. 91, 1479–1489. https://doi.org/10.1002/wer.1145

Ahn, Y.H., Speece, R.E., 2006. Elutriated acid fermentation of municipal primary sludge. Water Res. 40, 2210–2220. https://doi.org/10.1016/j.watres.2006.03.022

Alvarez, J.V.L., Larrucea, M.A., Bermúdez, P.A., Chicote, B.L., 2009. Biodegradation of paper waste under controlled composting conditions. Waste Manag. 29, 1514–1519. https://doi.org/10.1016/j.wasman.2008.11.025

APHA, 1998. Standard Methods for the Examination of Water and Wastewater, twentieth ed. American Public Health Association, Washington, DC, USA.

Bauer, S., Ibáñez, A.B., 2014. Rapid determination of cellulose: Rapid Determination of Cellulose. Biotechnol. Bioeng. 111, 2355–2357. https://doi.org/10.1002/bit.25276

Behera, C.R., Santoro, D., Gernaey, K.V., Sin, G., 2018. Organic carbon recovery modeling for a rotating belt filter and its impact assessment on a plant-wide scale. Chem. Eng. J. 334, 1965–1976. https://doi.org/10.1016/j.cej.2017.11.091

Benneouala, M., Bareha, Y., Mengelle, E., Bounouba, M., Sperandio, M., Bessiere, Y., Paul, E., 2017a. Hydrolysis of particulate settleable solids (PSS) in activated sludge is determined by the bacteria initially adsorbed in the sewage. Water Res. 125, 400–409. https://doi.org/10.1016/j.watres.2017.08.058

Benneouala, M., Bareha, Y., Mengelle, E., Bounouba, M., Sperandio, M., Bessiere, Y., Paul, E., 2017b. Hydrolysis of particulate settleable solids (PSS) in activated sludge is determined by the bacteria initially adsorbed in the sewage. Water Res. 125, 400–409. https://doi.org/10.1016/j.watres.2017.08.058

Boztas, S., 2017. The ick factor: Dutch project making bike lanes and bottles from used loo roll. The Guardian.

Chakraborty, T., 2015. Evaluation of Filtration Performance of a Rotating Belt Filter for Different Primary Wastewater Influents.

Comeau, Y., Hall, K., Hancock, R., Oldham, W., 1986. Biochemical model for enhanced biological phosphorus removal. Water Res. 20, 1511–1521. https://doi.org/10.1016/0043-1354(86)90115-6

Cuevas-Rodríguez, G., González-Barceló, Ó., González-Martínez, S., 1998. Wastewater fermentation and nutrient removal in sequencing batch reactors 10.

Cydzik-Kwiatkowska, A., Zielińska, M., 2016. Bacterial communities in full-scale wastewater treatment systems. World J. Microbiol. Biotechnol. 32, 66. https://doi.org/10.1007/s11274-016-2012-9

D., F.T., A., G., L., H.L., T., E.C., 1979. Enhanced Biological Phosphorus Removal in Activated Sludge Systems. AMIE, volume 11.

DuBois, Michel., Gilles, K.A., Hamilton, J.K., Rebers, P.A., Smith, Fred., 1956. Colorimetric Method for Determination of Sugars and Related Substances. Anal. Chem. 28, 350–356. https://doi.org/10.1021/ac60111a017

Ghasimi, D.S.M., Zandvoort, M.H., Adriaanse, M., van Lier, J.B., de Kreuk, M., 2016a. Comparative analysis of the digestibility of sewage fine sieved fraction and hygiene paper produced from virgin fibers and recycled fibers. Waste Manag. 53, 156–164. https://doi.org/10.1016/j.wasman.2016.04.034

Ghasimi, D.S.M., Zandvoort, M.H., Adriaanse, M., van Lier, J.B., de Kreuk, M., 2016b. Comparative analysis of the digestibility of sewage fine sieved fraction and hygiene paper produced from virgin fibers and recycled fibers. Waste Manag. 53, 156–164. https://doi.org/10.1016/j.wasman.2016.04.034

Gupta, M., Giaccherini, F., Sridhar, G.R.D., Batstone, D., Santoro, D., Nakhla, G., 2018a. Application of Respirometric Techniques to Determine COD Fractionation and Biokinetic Parameters of Sieved Wastewater. Proc. Water Environ. Fed. 2018, 106–121. https://doi.org/10.2175/193864718825138079

Gupta, M., Ho, D., Santoro, D., Torfs, E., Doucet, J., Vanrolleghem, P.A., Nakhla, G., 2018b. Experimental assessment and validation of quantification methods for cellulose content in municipal wastewater and sludge. Environ. Sci. Pollut. Res. 25, 16743–16753. https://doi.org/10.1007/s11356-018-1807-7

Gupta, M., Ho, D., Santoro, D., Torfs, E., Doucet, J., Vanrolleghem, P.A., Nakhla, G., 2018c. Experimental assessment and validation of quantification methods for cellulose content in municipal wastewater and sludge. Environ. Sci. Pollut. Res. 25, 16743–16753. https://doi.org/10.1007/s11356-018-1807-7

Harris, D., Bulone, V., Ding, S.-Y., DeBolt, S., 2010. Tools for Cellulose Analysis in Plant Cell Walls: Figure 1. Plant Physiol. 153, 420–426. https://doi.org/10.1104/pp.110.154203

Henze, M., Gujer, W., Mino, T., Loosdrecht, M.C.M. van, 2000a. Activated sludge models ASM1, ASM2, ASM2d and ASM3. IWA Publishing.

Henze, M., Gujer, W., Mino, T., Loosdrecht, M.C.M. van, 2000b. Activated sludge models ASM1, ASM2, ASM2d and ASM3. IWA Publishing.

Henze, M., van Loosdrecht, M.C.M., Ekama, G.A., Brdjanovic, D., 2008. Biological Wastewater Treatment, Principles, Modelling and Design. IWA Publishing, London, UK.

Hofsten, B.V., Edberg, N., 1972. Estimating the Rate of Degradation of Cellulose Fibers in Water. Oikos 23, 29. https://doi.org/10.2307/3543924

Honda, S., Miyata, N., Iwahori, K., 2002. Recovery of biomass cellulose from waste sewage sludge 5.

Honda, S., Miyata, N., Iwahori, K., 2000a. A Survey of Cellulose Profiles in Actual Wastewater Treatment Plants. Jpn. J. Water Treat. Biol. 36, 9–14. https://doi.org/10.2521/jswtb.36.9

Honda, S., Miyata, N., Iwahori, K., 2000b. A Survey of Cellulose Profiles in Actual Wastewater Treatment Plants. Jpn. J. Water Treat. Biol. 36, 9–14. https://doi.org/10.2521/jswtb.36.9

Hurwitz, E., Beck, A.J., Sakellariou, E., Krup, M., 1961a. Degradation of Cellulose by Activated Sludge Treatment. J. Water Pollut. Control Fed. 33, 1070–1075.

Hurwitz, E., Beck, A.J., Sakellariou, E., Krup, M., 1961b. Degradation of Cellulose by Activated Sludge Treatment. J. Water Pollut. Control Fed. 33, 1070–1075.

Ji, Z., Chen, Y., 2010. Using Sludge Fermentation Liquid To Improve Wastewater Short-Cut Nitrification-Denitrification and Denitrifying Phosphorus Removal via Nitrite. Environ. Sci. Technol. 44, 8957–8963. https://doi.org/10.1021/es102547n

Jiang, S., Chen, Y., Zhou, Q., Gu, G., 2007. Biological short-chain fatty acids (SCFAs) production from waste-activated sludge affected by surfactant. Water Res. 41, 3112–3120. https://doi.org/10.1016/j.watres.2007.03.039

Lema, J.M., Suarez, S., 2017. Innovative Wastewater Treatment & Resource Recovery Technologies: Impacts on Energy, Economy and Environment. IWA Publishing.

Li, Dr.N.N., Fane, Dr.A.G., Ho, W.S.W., Matsuura, T., 2011. Advanced Membrane Technology and Applications. John Wiley & Sons, Inc.

Li, S., Wu, Z., Liu, G., 2019a. Degradation kinetics of toilet paper fiber during wastewater treatment: Effects of solid retention time and microbial community. Chemosphere 225, 915–926. https://doi.org/10.1016/j.chemosphere.2019.03.097

Li, S., Wu, Z., Liu, G., 2019b. Degradation kinetics of toilet paper fiber during wastewater treatment: Effects of solid retention time and microbial community. Chemosphere 225, 915–926. https://doi.org/10.1016/j.chemosphere.2019.03.097

Liu, J., Yuan, Y., Li, B., Zhang, Q., Wu, L., Li, X., Peng, Y., 2017. Enhanced nitrogen and phosphorus removal from municipal wastewater in an anaerobic-aerobic-anoxic sequencing batch reactor with sludge fermentation products as carbon source. Bioresour. Technol. 244, 1158–1165. https://doi.org/10.1016/j.biortech.2017.08.055

Mansouri, S.S., Udugama, I.A., Cignitti, S., Mitic, A., Flores-Alsina, X., Gernaey, K.V., 2017. Resource recovery from bio-based production processes: a future necessity? Curr. Opin. Chem. Eng. 18, 1–9. https://doi.org/10.1016/j.coche.2017.06.002

Mino, T., Gujer, W., Henze, M., van Loosdrecht, M.C.M., 1995. Activated sludge models ASM1, ASM2, ASM2d and ASM3.

Nowak, O., Svardal, K., Franz, A., Kuhn, V., 1999. Degradation of particulate organic matter ? A comparison of different model concepts. Water Sci. Technol. 39. https://doi.org/10.1016/S0273-1223(98)00781-1

Olsson, C., Westm, G., 2013. Direct Dissolution of Cellulose: Background, Means and Applications, in: Van De Ven, T.G.M. (Ed.), Cellulose - Fundamental Aspects. InTech. https://doi.org/10.5772/52144

Reijken, C., Giorgi, S., Hurkmans, C., Pérez, J., van Loosdrecht, M.C.M., 2018a. Incorporating the influent cellulose fraction in activated sludge modelling. Water Res. 144, 104–111. https://doi.org/10.1016/j.watres.2018.07.013

Reijken, C., Giorgi, S., Hurkmans, C., Pérez, J., van Loosdrecht, M.C.M., 2018b. Incorporating the influent cellulose fraction in activated sludge modelling. Water Res. 144, 104–111. https://doi.org/10.1016/j.watres.2018.07.013

Revilla, M., Galán, B., Viguri, J.R., 2016. An integrated mathematical model for chemical oxygen demand (COD) removal in moving bed biofilm reactors (MBBR) including predation and hydrolysis. Water Res. 98, 84–97. https://doi.org/10.1016/j.watres.2016.04.003

Rossi, S., Sforza, E., Pastore, M., Bellucci, M., Casagli, F., Marazzi, F., Ficara, E., 2020. Photo-respirometry to shed light on microalgae-bacteria consortia—a review. Rev. Environ. Sci. Biotechnol. 19, 43–72. https://doi.org/10.1007/s11157-020-09524-2

Ruiken, C.J., Breuer, G., Klaversma, E., Santiago, T., van Loosdrecht, M.C.M., 2013a. Sieving wastewater – Cellulose recovery, economic and energy evaluation. Water Res. 47, 43–48. https://doi.org/10.1016/j.watres.2012.08.023

Ruiken, C.J., Breuer, G., Klaversma, E., Santiago, T., van Loosdrecht, M.C.M., 2013b. Sieving wastewater – Cellulose recovery, economic and energy evaluation. Water Res. 47, 43–48. https://doi.org/10.1016/j.watres.2012.08.023

Seviour, R.J., Mino, T., Onuki, M., 2003. The microbiology of biological phosphorus removal in activated sludge systems. FEMS Microbiol. Rev. 27, 99–127. https://doi.org/10.1016/S0168-6445(03)00021-4

SUMO, Dynamita, Nyons, France, 2019. . Dynamita Process Modeling, Nyons, France.

Tas, D.O., Karahan, Ö., I˙nsel, G., Övez, S., Orhon, D., Spanjers, H., 2009. Biodegradability and Denitrification Potential of Settleable Chemical Oxygen Demand in Domestic Wastewater. Water Environ. Res. 81, 715–727. https://doi.org/10.2175/106143009X425942

Tchobanoglous, G., Burton, F.L., Stensel, H.D., 2003a. Wastewater Engineering: Treatment and Reuse. 4th Edition. Metcalf and Eddy, McGraw Hill Education.

Tchobanoglous, G., Burton, F.L., Stensel, H.D., 2003b. Wastewater Engineering: Treatment and Reuse. 4th Edition. Metcalf and Eddy, McGraw Hill Education.

Thomas, M., Wright, P., Blackall, L., Urbain, V., Keller, J., 2003. Optimisation of Noosa BNR plant to improve performance and reduce operating costs. Water Sci Technol.

Thoorens, G., Krier, F., Leclercq, B., Carlin, B., Evrard, B., 2014. Microcrystalline cellulose, a direct compression binder in a quality by design environment—A review. Int. J. Pharm. 473, 64–72. https://doi.org/10.1016/j.ijpharm.2014.06.055

Tong, J., Chen, Y., 2009. Recovery of nitrogen and phosphorus from alkaline fermentation liquid of waste activated sludge and application of the fermentation liquid to promote biological municipal wastewater treatment. Water Res. 43, 2969–2976. https://doi.org/10.1016/j.watres.2009.04.015

Tong, J., Chen, Y., 2007a. Enhanced Biological Phosphorus Removal Driven by Short-Chain Fatty Acids Produced from Waste Activated Sludge Alkaline Fermentation. Environ. Sci. Technol. 41, 7126–7130. https://doi.org/10.1021/es071002n

Tong, J., Chen, Y., 2007b. Enhanced Biological Phosphorus Removal Driven by Short-Chain Fatty Acids Produced from Waste Activated Sludge Alkaline Fermentation. Environ. Sci. Technol. 41, 7126–7130. https://doi.org/10.1021/es071002n

Verachtertk, H., Bevers, J., 1982. Investigations on cellulose biodegradation in activated sludge plants 6.

Weimer, P.J., 1992. Cellulose Degradation by Ruminal Microorganisms. Crit. Rev. Biotechnol. 12, 189–223. https://doi.org/10.3109/07388559209069192

Yuan, H., Chen, Y., Zhang, H., Jiang, S., Zhou, Q., Gu, G., 2006. Improved Bioproduction of Short-Chain Fatty Acids (SCFAs) from Excess Sludge under Alkaline Conditions. Environ. Sci. Technol. 40, 2025–2029. https://doi.org/10.1021/es052252b

Zhao, Y., 2017. Pollution Control and Resource Recovery: Municipal Solid Wastes Incineration.

Zheng, X., Tong, J., Li, H., Chen, Y., 2009. The investigation of effect of organic carbon sources addition in anaerobic–aerobic (low dissolved oxygen) sequencing batch reactor for

nutrients removal from wastewaters. Bioresour. Technol. 100, 2515–2520. https://doi.org/10.1016/j.biortech.2008.12.003

Appendix

Table A.1 Respirometry setup conditions of α-cellulose using an 8-cell Challenge Respirometer

	α-cellulose									
	High S/X						Low S/X			
Seed source	R1			R4			R1	R2	R3	R4
Temperature (ºC)	27	27	27	27	27	27	14	14	29	29
S/X (g cellulose_COD/gVSS)	4	6	8	4	6	8	0.2	0.2	0.2	0.2
Biomass (mgVSS/L)	15	15	15	15	15	15	539	539	592	692
Cellulose in bottle										
Cellulose of biomass in bottle (mgCOD/L)							61	60	9	10
α-cellulose or RBF cellulose in bottle (mgCOD/L)	58	88	120	58	88	120	120	120	120	120
RBF Cellulose in bottle										
PCOD in bottle (mg/L)										
PCOD excluding cellulose in bottle (mg/L)										

Table A.2 Respirometry setup conditions of fibrous cellulose using an 8-cell Challenge respirometer

	RBF cellulose	
	High S/X	Low S/X
Seed source	mixture of R1-R4	mixture of R1-R4
Temperature (ºC)	20	20
S/X (g cellulose_COD/gVSS)	4	0.2
Biomass (mgVSS/L)	24	498
Cellulose in bottle		
Cellulose of biomass in bottle (mgCOD/L)	2	43
α-cellulose or RBF cellulose in bottle (mgCOD/L)	100	100
RBF Cellulose in bottle		
PCOD in bottle (mg/L)	530	530
PCOD excluding cellulose in bottle (mg/L)	430	430

Table A.3 Temperature correction factors for model kinetics

Symbol	Name	Default at 20°C	Unit	θ
μ_H	Maximum specific growth rate of heterotrophs	6	d^{-1}	1.07
η_g	Reduction factor for anoxic growth of heterotrophs	0.8	unitless	-
K_S	Half-saturation of SB	20	g COD m^{-3}	1
b_H	Decay rate of heterotrophs	0.62	d^{-1}	1.04
$K_{O,H}$	Half-saturation of oxygen	0.2	g $O_2.m^{-3}$	-
K_{NO}	Half-saturation of nitrate	0.5	g $N.m^{-3}$	1
$K_{NH,H}$	Half-saturation of ammonia	0.05	g $N.m^{-3}$	1
	Hydrolysis	Type (Kinetic)		
Symbol	Name	Default	Unit	θ
k_h	Maximum specific hydrolysis rate	3	g X_S.g $X_{B,H}^{-1}.d^{-1}$	1.041
K_X	Half-saturation of $X_B/X_{B,H}$	0.03	g X_S.g $X_{B,H}^{-1}$	-
η_h	Correction factor for hydrolysis under anoxic conditions	0.4	unitless	-
K_{cl}	Hydrolysis of cellulose	0.4	g X_{cl}.g $X_{B,H}^{-1}.d^{-1}$	1.072
K_{Xcl}	Half-saturation of $X_{cl}/X_{B,H}$	20	g X_{cl}.g $X_{B,H}^{-1}$	-

Curriculum Vitae

Name: Moustafa Elbahrawi

Education

Master of Science – Civil and Environmental 2021
University of Western Ontario
London, Ontario, Canada
Thesis: Cellulose biodegradability and its impact on Enhanced biological phosphorus removal.
Supervisor: Dr. George Nakhla

Bachelor of Science – Civil Engineering 2011-2016
Faculty of Engineering, Alexandria University
Alexandria, Egypt

Honors and Awards:

Western Graduate Research Scholarship 2018-2020

Related Work Experience

Graduate Teaching Assistant
The University of Western Ontario
2019-2020
Research intern in Trojan technologies
September 2019 – January 2020